2017

Neuroinflammation in Alzheimer's Disease and Vascular Cognitive Impairment

Erica M. Weekman
University of Kentucky, erica.weekman@icloud.com
Digital Object Identifier: https://doi.org/10.13023/ETD.2017.051

STUDENT AGREEMENT:

I represent that my thesis or dissertation and abstract are my original work. Proper attribution has been given to all outside sources. I understand that I am solely responsible for obtaining any needed copyright permissions. I have obtained needed written permission statement(s) from the owner(s) of each third-party copyrighted matter to be included in my work, allowing electronic distribution (if such use is not permitted by the fair use doctrine) which will be submitted to UKnowledge as Additional File.

I hereby grant to The University of Kentucky and its agents the irrevocable, non-exclusive, and royalty-free license to archive and make accessible my work in whole or in part in all forms of media, now or hereafter known. I agree that the document mentioned above may be made available immediately for worldwide access unless an embargo applies.

I retain all other ownership rights to the copyright of my work. I also retain the right to use in future works (such as articles or books) all or part of my work. I understand that I am free to register the copyright to my work.

REVIEW, APPROVAL AND ACCEPTANCE

The document mentioned above has been reviewed and accepted by the student's advisor, on behalf of the advisory committee, and by the Director of Graduate Studies (DGS), on behalf of the program; we verify that this is the final, approved version of the student's thesis including all changes required by the advisory committee. The undersigned agree to abide by the statements above.

Erica M. Weekman, Student

Dr. Donna M. Wilcock, Major Professor

Dr. Kenneth S. Campbell, Director of Graduate Studies

NEUROINFLAMMATION IN ALZHEIMER'S DISEASE AND VASCULAR COGNITIVE IMPAIRMENT

DISSERTATION

A dissertation submitted in partial fulfillment of the
requirements for the degree of Doctor of Philosophy in the
College of Medicine
at the University of Kentucky

By
Erica Marie Weekman

Lexington, Kentucky

Director: Dr. Donna M Wilcock, Associate Professor of Physiology

Lexington, Kentucky

2017

ABSTRACT OF DISSERTATION

NEUROINFLAMMATION IN ALZHEIMER'S DISEASE AND VASCULAR COGNITIVE IMPAIRMENT

It was once believed that the brain was immunologically privileged with no resident or infiltrating immune cells; however, now it is understood that the cells of the brain are capable of a wide range of inflammatory processes and phenotypes. Inflammation in the brain has been implicated in several disease processes such as Alzheimer's disease (AD) and vascular cognitive impairment and dementia (VCID); however, the role of inflammation in these two dementias is poorly understood.

When we stimulated a pro-inflammatory phenotype with an adeno-associated viral vector in a transgenic mouse model of AD that develops Aβ plaques, we saw a pro-inflammatory response at 4 months that transitioned to a mixed phenotype by 6 months. This transition also appeared with an increase in Aβ burden suggesting that anti-inflammatory markers contribute to disease progression.

Treatment of astrocytes, microglia, endothelial cells and neurons with high levels of homocysteine, a risk factor for VCID, resulted in a wide range of gene expression changes. Astrocytes showed decreased levels of several potassium channels and aquaporin 4 and increased matrix metalloproteinase 9. Microglia showed an initial pro-inflammatory response that transitioned to an anti-inflammatory phenotype. Endothelial cells showed a disruption in several tight junction proteins and neurons had changes in kinases and phosphatases known to affect tau phosphorylation.

Finally, while AD and VCID are the two most common forms of dementia, they are not mutually exclusive and it is estimated that 60% of AD patients also have cerebrovascular pathology contributing to the clinical syndrome. To determine the effect of co-morbid AD and VCID on the effectiveness of therapies that target AD pathologies, we placed APP/PS1 mice on a diet that induces hyperhomocysteinemia and consequently VCID. These mice were then placed on an anti-Aβ immunotherapy. While the co-morbidity mice had a

significant reduction in Aβ, there was no cognitive benefit of the immunotherapy in these mice. Interestingly, these co-morbidity mice also had a reduction in inflammatory markers and microglial staining, suggesting a suppressed inflammatory response. From these studies, it is clear that inflammation plays a complex role in AD, VCID and during treatment when both AD and VCID are present.

KEYWORDS: Alzheimer's disease, neuroinflammation, vascular cognitive impairment and dementia, hyperhomocysteinemia, anti-Aβ immunotherapy, matrix metalloproteinase

Erica Marie Weekman

February 6, 2017

NEUROINFLAMMATION IN ALZHEIMER'S DISEASE AND VASCULAR COGNITIVE IMPAIRMENT

By

Erica Marie Weekman

Donna M Wilcock, Ph.D.

Director of Dissertation

Kenneth S Campbell, Ph.D.

Director of Graduate Studies

February 6, 2017

Dedicated to my mom, dad and sisters

for their love, support and encouragement

ACKNOWLEDGEMENTS

While the following dissertation may seem like an individual work, I received assistance and support from several people who I'd like to thank.

Donna, I couldn't have asked for a better mentor and role model. Over the last 5 years, you constantly made time to meet with me and answer any and all questions I had – even the dumb ones. Thank you for letting me follow you around at conferences and hover at social events so that I could be introduced to people, for letting me take way too many Friday's off to visit my family, and for grounding me from lab work so that I would be forced to finish my first paper. Your guidance, patience and support have helped shape me into the scientist I am today. You've shown me how to be a successful woman in science and I hope that one day I can be half as good of a mentor as you have been for me. Also, sorry we made you the evil stepmother when we were assigning lab members to the characters from Cinderella.

Tiffany, we both know this dissertation would not have happened without you. It's unbelievable and slightly unfair how amazing you are – you put the rest of us to shame. I can't thank you enough for everything you've done over the last 5 years to help me reach this point. Thank you for putting up with the millions of questions I've asked, for listening to me rant about my problems, for showing me pretty much every technique in the lab, and for coming down to the animal facility to inject a rogue mouse on more than one occasion. And thank you for providing me with distractions when I needed them – and when I didn't. I'm definitely going to miss sharing a desk with you.

Mom, I know I give you a hard time about it, but thank you for making me read and do workbooks during the summer before I could go swimming. You've always pushed me to do my best and to put all my effort into everything that I do. Without your encouragement, support and understanding I would not be where I am today. Thank you for guilt tripping me into visiting you and dad more often. You constantly remind me that it's important to make time for family and to not get lost in my work. Also, thank you for patiently listening to me talk about my projects even though you had no idea what I was talking about.

Dad, thank you for making sure that I had enough alcohol to get through grad school, for coming to Lexington to fix my car several times and for making margaritas for around the pool during the summer. And thank you for making me do home improvement projects every time I came home – it always reminds me that I may know a lot about science, but I'm still clueless when it comes to anything else.

Elizabeth and Rachel, you guys have always been my best friends and I don't know how I could have made it through grad school – or life – without you. Elizabeth, thank you for reminding me that there's more to life than science and school and for not getting too mad when Annie and I got into trouble. Rachel, thank you for always laughing at my jokes, for making me constantly laugh at yours and for acting like children every time we're together.

TABLE OF CONTENTS

LIST OF TABLES

LIST OF FIGURES

Chapter 1

Introduction

Dementia

According to the Diagnostic and Statistical Manual of Mental Disorders, dementia is classified as a neurocognitive disorder that affects both cognitive function, such as memory, speech, language, judgment and reasoning, and the performance of everyday living activities, such as making a meal, paying bills or getting dressed. While young-onset cases of dementia are increasingly recognized, dementia is typically a disorder that affects the older population, age 65 and up. In 2015, it was estimated that 46.8 million people worldwide were living with dementia (1). With the number of people aged over 60 expected to increase worldwide by 1.25 billion by 2050, accounting for 22% of the world's population, it is crucial to understand the causes of dementia and develop treatments (2).

***Alzheimer's disease*:** First described by Alois Alzheimer in 1906, Alzheimer's disease (AD) is the most common form of dementia, accounting for around 60% of all dementia cases (3). Clinically, AD is characterized by a worsening ability to remember new information, difficulty solving problems and completing familiar tasks at home, confusion with time or place, and trouble understanding visual images. Pathologically, AD is characterized by extracellular amyloid plaques made up of the amyloid-beta (Aβ) protein, neurofibrillary tangles that are comprised of intraneuronal inclusions of hyperphosphorylated tau, and neuronal loss (4). Aβ is produced when the larger amyloid precursor protein

(APP) is cleaved by both β and γ secretase. β secretase cleavage of APP occurs at amino acid 671 while γ secretase cleaves at either amino acid 711 or 713. This results in either $A\beta_{1-40}$ or $A\beta_{1-42}$. $A\beta_{1-42}$ is the main Aβ species found in the amyloid plaques that characterize AD. $A\beta_{1-40}$ associates mainly with the vessels in the brain, known as cerebral amyloid angiopathy (CAA); however, it can also be found in Aβ plaques. Cleavage of APP by α and γ secretase does not result in Aβ production since α secretase cleaves within the Aβ sequence of APP, resulting in a shorter and non-amyloidogenic fragment. Tau, the component of neurofibrillary tangles, modulates the stability of axonal microtubules and can be phosphorylated at several different sites in order to regulate its function. Hyperphosphorylation of tau, which occurs in AD, promotes aggregation of tau and eventual tangle formation and neuronal death.

Research into the cause of AD has revealed several genetic links and mutations associated with the disease. In 1993, apolipoprotein E (ApoE), a plasma protein that transports cholesterol in the brain, was identified as the most common significant genetic risk factor for AD (5-8). There are three alleles for the ApoE gene (ApoE 2, ApoE 3, and ApoE 4) and each person has two alleles. ApoE 3 accounts for about 70-80% of the ApoE gene pool, while ApoE 4 accounts for 10-15% and ApoE 2 only accounts for 5-10% (9). ApoE 2, the least common allele, may be protective against AD compared to both ApoE 3 and ApoE 4. While ApoE 3 is the most common allele, it reduces the risk of developing AD compared to ApoE 4, suggesting a role for ApoE 4 in the pathogenesis of AD. Studies elucidating the mechanism of ApoE 4 in AD

revealed ApoE 4 had a decreased ability to clear Aβ compared to ApoE 3 and ApoE 2 (10, 11). ApoE 4 is also associated with an earlier age of onset. While having two ApoE 4 alleles further increases the risk of developing AD, it does not guarantee that the person will develop the disease. Some people with the ApoE 4 allele never develop AD. Around the same time that ApoE 4 was identified as a genetic risk factor for AD, it was also discovered that certain mutations in either APP or in the core proteins of the γ secretase complex, known as presenilin 1 (PS1) or PS2, cause early onset familial AD (12-16). Several mutations around the β and γ secretase cleavage sites and within the Aβ region on APP that increase Aβ production or aggregation have been identified in families with early onset AD where symptoms can appear as early as a person's thirties. Missense mutations in PS1 and PS2 have also been identified in early onset cases and are the most common cause of familial AD. These rare, dominantly inherited mutations (seen in <5% of AD cases) either increase the rate of Aβ production or increase the cleavage of APP into the amyloidogenic $A\beta_{1-42}$. Overall, both ApoE 4 and the mutations in APP, PS1 and PS2 increase Aβ aggregation.

In 1992, it was hypothesized that Aβ aggregation was the initiating factor in AD progression since the genetic links to AD all lead to an increase in Aβ rather than tangles (17-19). This amyloid hypothesis states that an increase in Aβ aggregation either from decreased clearance or increased production, leads to microglial and astrocytic activation, altered neuronal ionic homeostasis, altered kinase and phosphatase activity which increases phosphorylation of tau leading to tangle formation, neurodegeneration and finally dementia. Other evidence

supporting this hypothesis comes from people with Down's syndrome, frontotemporal dementia patients and several Aβ studies. Since APP is located on chromosome 21, people with Down's with a complete triplication of chromosome 21 harbor three copies of the gene, which leads to early onset Aβ deposition. In fact, by age 40, virtually all adults with Down's syndrome have sufficient levels of plaques and tangles for a pathological diagnosis of AD (20-22). People with translocation who only have triplication of a portion of chromosome 21 without APP show a Down's syndrome phenotype but do not develop AD (23). On the other hand, individuals who have the APP gene duplicated but not rest of chromosome 21 do not have Down's syndrome but they do develop AD in their mid-50s (24). In frontotemporal dementia patients, mutations in the tau protein cause neurofibrillary tangle formation in the brain leading to dementia (25). However, the mutations that lead to neurofibrillary tangles do not induce Aβ aggregation and plaque formation, suggesting that neurofibrillary tangles are deposited after changes in Aβ metabolism occur (26). Finally, in cultured rat neurons, human $A\beta_{1-42}$ oligomers induced tau hyperphosphorylation and injection of $A\beta_{1-42}$ isolated from AD patients led to cognitive impairment in healthy rats (27, 28).

Due to the amyloid hypothesis, amyloid deposition and Aβ have become popular targets for AD therapeutics. One of the most promising potential therapeutics is anti-Aβ immunotherapy. In 1999, Schenk et al. reported that active immunization with $A\beta_{1-42}$ prevented the development of Aβ plaques, neuritic dystrophy and astrogliosis in young PDAPP mice (6 weeks old) and

reduced the levels of Aβ in old PDAPP mice (11 months old) (29). Subsequently, it was shown that active immunization in APP/PS1 and TgCRND8 mice improved cognitive function and reduced Aβ deposition (30, 31). Active immunization in beagles and non-human primates also showed reduced Aβ deposition (32, 33).

With the success of active immunization in animal models, a clinical trial in patients with AD using the full length Aβ peptide was initiated. While there were no adverse responses in the phase 1 study, a fraction of the patients in the phase 2a trial developed aseptic meningoencephalitis, which is an inflammatory reaction in the central nervous system (34, 35). The appearance of these adverse events halted the phase 2a trial and spurred the use of monoclonal antibodies to target Aβ and clear it from the brain. Initial studies showed that several different antibodies were able to reduce Aβ levels in mice (36, 37). In a series of studies, intracranial injection of an anti-Aβ antibody led to clearance of diffuse Aβ within 1 day and clearance of congophilic amyloid by 3 days (38, 39). Systemic administration of antibodies led to a significant decrease in congophilic plaques by 3 months; however, it was reported that passive immunotherapy caused microhemorrhages in mice (40). Further studies into the appearance of microhemorrhages showed a time dependent increase in the number of microhemorrhages and an increase in vascular amyloid deposition as well as association of the microhemorrhages with these vascular deposits (41-43).

Again, due to the success of these antibodies in animal models, several clinical trials have been initiated. One of the most promising antibodies to enter clinical trials was bapineuzumab. In the phase 1 trial, patients received a single

administration of 0.5, 1.5 or 5 mg/kg of bapineuzumab and were tested cognitively before administration and again 16 weeks later (44). In this trial, 3 out of 10 patients in the highest dose group developed vasogenic edema, also termed an amyloid related imaging abnormality (ARIA-E). While the phase 1 trial wasn't designed to measure effects on cognition, it was found that bapineuzumab improved mini mental state examination (MMSE) scores in the 0.5 and 1.5 mg/kg groups. Bapineuzumab moved to a phase 2 clinical trial that included 234 patients, four doses (0.15, 0.5, 1 or 2 mg/kg) and six infusions of the drug 13 weeks apart (45). While there were no significant differences found in the primary efficacy analysis (MMSE scores only showed a trend, no change in cerebrospinal fluid (CSF) biomarkers, or brain or ventricular volume), 9.7% of the bapineuzumab treated patients developed reversible vasogenic edema. The MRI detected edema (ARIA-E) was more common in the higher dose groups and in patients with the ApoE 4 allele. In a phase 3 clinical trial of bapineuzumab treatment in ApoE 4 carriers, there were, again, no improvements in clinical outcomes and 14.2% of the highest dose group (2 mg/kg) developed ARIA-E (46).

There are several proposed mechanisms for how anti-Aβ antibodies clear Aβ from the brain. The first involves the traditional role of an antibody to opsonize antigens leading to complement activation and phagocytosis (36). For this mechanism, anti-Aβ antibodies bind to Aβ and then the Fc portion of the antibody binds to the Fcγ receptor (FcγR) on microglia leading to phagocytosis. While this mechanism assumes that the antibody crosses the blood brain barrier (BBB), the

“peripheral sink” mechanism does not make this assumption (37). In this proposed mechanism, antibodies clear Aβ from the blood, creating an Aβ concentration gradient between the brain and the blood. This causes Aβ to then be transported down its concentration gradient from the brain to the blood. Finally, the last proposed mechanism is that the antibody modifies the secondary structure of the Aβ monomers so that they are less likely to aggregate into oligomeric or fibrillar forms (47). It is important to note, however, that these three mechanisms are not mutually exclusive. The antibodies can utilize these mechanisms to different degrees and may depend on the specific binding sites of each antibody and the isotype (48, 49). For example, antibodies that do not bind the fibrillar forms of Aβ may not have the ability to activate microglia via the FcγR, but could utilize the peripheral sink method instead.

***Vascular cognitive impairment and dementia*:** Inadequate blood flow to any part of the body can cause damage to cells and since the brain requires a large blood supply and has the most intricate system of blood delivery, it is especially susceptible to damage by changes in blood flow. Changes in blood flow that damage areas of the brain causing cognitive decline is known as vascular cognitive impairment and dementia (VCID) and is the second leading cause of dementia. It is estimated that VCID accounts for 10-40% of dementia cases (50); however, issues with diagnostic criteria and the recent inclusion of cognitive disorders ranging from mild cognitive impairment all the way to dementia make estimating the prevalence of VCID difficult. While recent advances in neuroimaging have made the diagnosis of VCID easier, defining the

pathology underlying the cognitive decline in VCID is still difficult. For instance, infarcts can vary in size as well as location, can occur in patients with and without dementia, and can also be found in patients with AD. Further studies are required to understand the cognitive consequences of cerebrovascular pathologies.

Cerebral small vessel disease (SVD) is a leading cause of cognitive decline in the elderly and the most common form of VCID. SVD is defined as the pathological processes that affect the small vessels of the brain (small arteries, arterioles, capillaries and small veins). The main consequences of SVD include lacunar infarcts, white matter lesions and microhemorrhages. Hypertension, arteriolosclerosis, cerebral autosomal dominant arteriopathy with subcortical ischemic strokes and leukoencephalopathy (CADASIL) and CAA are the most common causes of SVD.

Cerebral amyloid angiopathy is a common pathology found in 80-100% of AD cases, but it can also be found in patients without other AD pathologies (51). This is termed sporadic or spontaneous CAA and appears in 10-30% of the elderly population (51). Advanced CAA can induce loss of smooth muscle cells, microaneurysms and microhemorrhages (52). While CAA is most commonly seen as the cause of spontaneous intracerebral hemorrhage, there is increasing evidence that it is a contributor to cognitive decline and, therefore, VCID. Over 40% of CAA patients who have intracerebral hemorrhages also have some degree of cognitive decline (53). Intracerebral hemorrhages, cerebral microbleeds, white matter hyperintensities and cerebral infarcts could be contributing mechanisms to the cognitive decline seen in CAA patients.

While VCID encompasses a wide range of pathologies, there are also several risk factors for VCID. Some risk factors include hypertension, hypercholesterolemia, diabetes and hyperhomocysteinemia; however, the most common risk factor for VCID is a stroke. Depending upon location and volume of the stroke, degree of related neuronal damage, and the presence of pre-existing cognitive impairment and vascular pathology, cognitive decline after a stroke can occur. In fact, as the risk of death from strokes has declined due to lesser stroke severity and improved management, the number of stroke survivors with cognitive decline has increased. The risk of post-stroke dementia has been estimated to be around 10% after the first stroke, depending on location and size, while cognitive decline after a recurrent stroke rose to 30% (54, 55). Other studies estimate that dementia occurs in about 30% of patients with a history of stroke (56). The risk of post-stroke dementia is more likely when vascular co-morbid conditions are present, such as hypertension, atrial fibrillation or diabetes (57, 58). Modification of risk factors for stroke could, therefore, reduce the risk of stroke and post-stroke dementia.

***Co-morbidity of AD and VCID*:** There is increasing awareness of AD with cerebrovascular pathologies and it is estimated that about 40-50% of AD patients have co-morbid vascular injury (59-61). Vascular co-morbidities are also more commonly found in late stage AD and in the oldest old (62). It is also thought that vascular injuries co-morbid with AD act as an extra “hit” to the brain that lowers the threshold for cognitive impairment in persons with AD pathology (63). It is suggested that patients with both AD and VCID have a shorter time to dementia

and their rate of cognitive decline is faster (64). Other studies have shown that VCID and AD are additive when it comes to cognitive deficits (65-68). While the role that vascular injury plays in the progression of AD remains unknown, it has been hypothesized that vascular dysfunction leads to Aβ accumulation in the parenchyma and blood vessels (69, 70). This high prevalence of co-morbidity patients and the possibility that vascular injury impacts cognition could affect treatments for dementia.

Neuroinflammation

It has long been thought that the brain was immunologically privileged with no resident or infiltrating immune cells; however, it is now understood that the cells of the brain are capable of a wide range of neuroinflammatory responses. The glial cells of the brain (astrocytes, microglia, oligodendrocytes, and pericytes) are all capable of an inflammatory response, but the main regulator of inflammation in the brain is the microglia cell (71). Originally thought to be derived from the macrophage cell line, it is now understood that yolk-sac derived fetal macrophages are the precursors for microglia (72, 73). Depending on the stimuli, macrophages are capable of a variety of inflammatory responses. The presence of tumor necrosis factor alpha (TNFα) or interferon gamma (IFNγ) stimulates macrophages to release several pro-inflammatory cytokines and to produce reactive oxygen species (74-76). This state, termed M1 or pro-inflammatory, has high microbicidal activity and is an important defense mechanism for the body. However, if this state goes unchecked, it can cause

damage to the tissues and it has been implicated in the development of autoimmune disorders (77). On the other end of the spectrum is the M2a or wound healing and repair state. Activated by interleukin-4 (IL-4) or IL-13, this state is generally seen in allergic responses and plays a role in extracellular matrix remodeling and deposition (78, 79). Immune complexes (IgG antibody-antigen complexes), toll-like receptor activation, or IL-1 receptor ligands can all stimulate an M2b or immune complex mediated state (78, 79). This state is a combination of a pro-inflammatory and wound healing and repair state. Finally, the M2c, or acquired deactivation state, is activated by IL-10 and contributes to an environment that is defective in pathogen killing and enhances survival of organisms (78, 79). These states have been used to describe peripheral macrophage inflammatory phenotypes, but it has been shown that microglia are capable of expressing many of these macrophage markers (80). Table 1.1 shows the specific markers used to categorize the inflammatory phenotypes in the brain.

***Alzheimer's disease*:** When Alois Alzheimer first described the pathologies of AD, he also noticed inflammation of the glia. For decades, it was believed that neuroinflammation had a negative influence on the disease progression of AD. Initially, neuroinflammation in AD focused on the "autotoxic loop" which was first described by E.G. McGeer and P.L. McGeer in 1998 (81). In this "vicious cycle," cellular debris caused by AD pathologies activates microglia, this activation of microglia leads to the release of cytotoxic cytokines that causes a more rapid neuronal death which then provides more cellular debris to start the cycle over again. Evidence to support this cycle is the increased IL-1β and TNFα

levels found in the brains and CSF of AD patients; however, these levels are not high enough to cause significant neuronal death (81). Attempts to recreate this "autotoxic loop" often led to clearance of Aβ plaques in transgenic mice, showing that neuroinflammation could be a beneficial process in AD.

To determine the effects of neuroinflammation on AD pathologies, several studies have induced the different neuroinflammatory phenotypes in AD transgenic mice. Lipopolysaccharide (LPS) is a gram-negative bacterial cell surface proteoglycan that stimulates a pro-inflammatory response in wildtype mice that peaks around 3 days (82). When injected into APP/PS1 mice, LPS stimulated Aβ clearance between 0 and 3 days (83). However, when LPS was injected into tau transgenic mice, tau pathology was exacerbated 7 days after the injection (84). Another study using the 3XTg mouse model that has both Aβ deposition and tau pathology showed that LPS injection exacerbated tau hyperphosphorylation (85). This suggests that Aβ and tau have different responses to the inflammatory phenotypes and caution should be used when applying findings in Aβ depositing mice to the overall condition of AD.

Genetic manipulation of individual inflammatory cytokines has yielded similar results to LPS induced neuroinflammation. Overexpression of TGFβ, a marker for the acquired deactivation phenotype, reduced Aβ deposition and increased microglial activation in APP mice; however, in this study, while parenchymal amyloid was reduced, there was a significant increase in CAA (86). Blockage of the pro-inflammatory cytokine TNFα in 3XTg mice resulted in increased Aβ and tau pathology (87). Overexpression of IL-1β, another pro-

inflammatory cytokine, in APP/PS1 mice resulted in decreased Aβ deposition and increased microglial activation (88).

As mentioned previously, one of the mechanisms of anti-Aβ immunotherapy involves activation of the immune system in the brain. When injected either directly into the parenchyma or systemically, anti-Aβ antibodies initiate a switch from an anti-inflammatory phenotype in Aβ depositing mice to a pro-inflammatory phenotype by increasing expression of IL-1β, TNFα, and IL-6 (89). This switch in phenotype occurs before any reduction in Aβ is seen, suggesting that activation of microglia to produce a pro-inflammatory phenotype is a mechanism for Aβ clearance. However, it should be noted that IL-1β has been shown to be neurodegenerative and can cause tau hyperphosphorylation (90, 91).

While there is evidence that a pro-inflammatory phenotype can reduce Aβ, the effect of an anti-inflammatory or wound healing and repair phenotype is less clear. As Aβ depositing mice age and Aβ deposition increases, the inflammatory phenotype becomes increasingly polarized to a wound healing and repair phenotype. Lithium, which decreases pro-inflammatory cytokines and increases wound healing and repair cytokines, is also an inhibitor of glycogen-synthase kinase 3 β, which is known to phosphorylate tau (92, 93). When APPSwDI/NOS2-/- mice were treated with lithium, the wound healing and repair phenotype was enhanced and Aβ deposition was increased (94). This suggests that the wound healing and repair phenotype increases Aβ deposition. Further

studies are required in order to fully understand the effect of the wound healing and repair phenotype on AD pathologies.

Little is also known about the neuroinflammatory phenotype in the human AD brain. Our research group analyzed the frontal cortex of early, mid and late stage AD patients for several neuroinflammatory markers and found that early stage patients were either polarized to a pro-inflammatory or a wound healing and repair phenotype (95). Further analysis of the pathology of early stage AD brains showed that the patients who were polarized to a wound healing and repair phenotype had more CAA and these patients had significantly more cerebrovascular risk factors present. Late stage AD brains were not polarized towards any phenotype but instead had a mix of markers from all the phenotypes. This heterogeneity in neuroinflammation in early stage AD brains could influence responses to therapies.

***Vascular cognitive impairment and dementia*:** Even less is known about neuroinflammation's role in VCID compared to its role in AD. It is hypothesized that neuroinflammation and oxidative stress play a key role in neurovascular dysfunction. Some patients with spontaneous CAA present with CAA related inflammation as well as white matter abnormalities (52). Hypertensive patients show deficits in autoregulation of cerebral perfusion in response to blood pressure changes and this leads to aberrant angiotensin II signaling. Angiotensin II, which mediates vascular remodeling in response to blood pressure dysregulation, has been linked to the stimulation of NADPH oxidase (96, 97). NADPH oxidase, which is also increased in hypoperfusion

models, is an important source of vascular oxidative stress and reactive oxygen species (98). This increase in reactive oxygen species can stimulate inflammatory pathways via toll-like receptors and lead to BBB breakdown. This vascular damage via inflammation most likely interferes with neurovascular coupling and the proliferation, migration and differentiation of oligodendrocytes contributing to white matter damage and VCID (99). Further studies are required to elucidate the connection between inflammation and VCID.

Matrix Metalloproteinases

Matrix metalloproteinases (MMPs) are a family of proteases that regulate many physiological processes including activation of growth factors, cleavage of zymogens and remodeling of the extracellular matrix (100). Due to their large variety of substrates, the majority of MMPs have been linked to the development of several diseases such as cancer metastasis, chronic inflammation, abdominal aortic aneurysms and several neurological disorders (101-104). Recently, the remodeling of the extracellular matrix and disruption of the neurovascular unit via MMPs have been implicated in vascular cognitive impairment. Consisting of astrocytic end feet, neurons, pericytes and endothelial cells, the neurovascular unit plays a key role in maintaining homeostasis in the brain and formation of the BBB. MMPs have been shown to break down the extracellular matrix and the tight junctions that form the BBB, leading to leakage and hemorrhaging into brain tissue (105).

MMPs are a family of 23 proteases in humans (24 in mice) that degrade the extracellular matrix along with other substrates such as contractile proteins, tight junction proteins, and pro-forms of signaling molecules (100). Based on substrate specificity, MMPs are separated into five classes: collagenases, stromelysins, a heterogeneous group, membrane anchored MMPs, and finally, the gelatinases. The gelatinase class, which is present in the brain, includes MMP2, which is also known as Gelatinase A, and MMP9, also known as Gelatinase B. The gelatinase class of MMPs can degrade gelatin, cytokines (100) and even Aβ (106, 107), but they also have roles in axonal growth, synaptic plasticity and vascularization (108-112). Due to their variety of substrates, it is important to maintain control over MMP2 and MMP9 activity; therefore, they are endogenously regulated at several different levels. Similar to other MMPs, gene expression of MMP2 and MMP9 is regulated by cytokines, growth factors and other proteins. The pro-inflammatory cytokines TNFα and IL1β can stimulate transcription of MMP9 (113, 114), while activator protein 2, specificity protein 1, and polyomavirus enhancer-A binding protein 3 can stimulate transcription of MMP2 (115). At the protein level, MMP2 is constitutively expressed in the brain while MMP9 expression is induced by neuroinflammation. However, both are secreted as zymogens that require cleavage via other MMPs. For MMP2 activation, a complex of MMP14, which is also known as membrane type 1 MMP (MT1-MMP), tissue inhibitor of metalloproteinase 2 (TIMP2) and proMMP2 must be formed. MMP14 is one of six enzymes that include a C terminal hydrophobic transmembrane domain that anchors the enzyme to the plasma membrane and

thus restricts its activity to the cell surface (116, 117); this then constrains the action of MMP2 as well (118). Activation of proMMP9 requires cleavage via MMP3 which can also be activated via neuroinflammation (100). Finally, the endogenous inhibitor TIMP1 binds and inhibits MMP9 (100). Active MMP2 can be inhibited by TIMP2, even though TIMP2 is necessary, along with MMP14, for activation of proMMP2 (100). Therefore, TIMP2 participates in activation of proMMP2 and inhibition of active MMP2. Recent studies have also shown that nitric oxide can regulate MMP9 activity and the activity of TIMP1 (119). The MMP2 and MMP9 systems, which are summarized in Figure 1.1, are associated with tight junction breakdown leading to BBB leakage (120).

***Alzheimer's disease*:** Of patients with AD, almost 95% have CAA (121). The main criterion for clinical diagnosis of CAA is the presence of cortical cerebral brain hemorrhage which causes and/or contributes to neurodegeneration and dementia (122). Patients with AD and multiple microhemorrhages had more severe cognitive impairment compared to AD patients without microhemorrhages (123). MMP2 and MMP9 have been widely associated with BBB disruption and microhemorrhages in CAA and AD.

In postmortem AD brains, MMP9 was elevated in neurons, senile plaques, tangles and within the vascular wall (124). MMP9 was also elevated in the plasma, hippocampus and cerebral cortex of AD patients (124-127). Bruno et al demonstrated an increase in MMP9 activity during the progression of AD that correlates with cognitive impairment (128). MMP2 was found in reactive astrocytes around Aβ plaques and near cerebral microvascular fibrillar amyloid

deposits in Tg-SwDI mice (129). MMP9 expression was also shown in CAA vessels in APP transgenic mice (130). This suggests that MMP2 and MMP9 play a role in BBB breakdown and hemorrhaging in CAA.

It has long been known that AD induces a neuroinflammatory response, although the effect of this inflammation remains unknown. During AD, peripheral immune cells, such as lymphocytes, monocytes and neutrophils, can cross the BBB and infiltrate the brain (131). $A\beta_{25-35}$, a truncated form of the $A\beta$ peptide, has been shown to activate invading neutrophils, the most abundant immune cell to infiltrate the brain, and stimulate the release of proMMP9 (132). While this stimulation and release does not activate proMMP9, there are several other proteases, such as MMP3, that can cleave and activate the released proMMP9. This activation of neutrophils and release of proMMP9 indicates that MMP9 may play a role in the inflammatory response during AD.

Tau has also been shown to be a substrate for MMP3 and MMP9 (133). While MMP3 cleavage of tau does not result in tau aggregation, MMP9 cleavage does result in tau oligomer formation. Frost et al. previously demonstrated that extracellular pro-aggregatory tau can be incorporated into neurons and induce neurotoxic intracellular tau aggregation which spreads to other cells (134). This suggests that cleavage of tau by MMP9 could contribute to neurofibrillary tangle formation.

***Vascular cognitive impairment and dementia*:** The gelatinases have also been shown to play a role in VCID, particularly during hemorrhagic transformation after stroke and intracerebral hemorrhage.

After a stroke occurs, the BBB around the ischemic area is weakened and bleeding into the brain can occur. Termed hemorrhagic transformation, this opening of the BBB occurs in 10% to 40% of patients with ischemic stroke (135, 136) and greatly increases the morbidity and mortality after stroke (137, 138). The only FDA approved therapy for stroke, tissue plasminogen activator (tPA), increases the occurrence of hemorrhagic transformation 10-fold when administered outside the narrow 3-hour window when it is effective (139, 140). While tPA works to restore blood flow to the ischemic area by breaking down fibrin based clots, it can activate and release MMP2, MMP9 and MMP3 (139, 141-143).

Hemorrhagic transformation after ischemic stroke can be separated into two phases: early phase (up to 18-24 hours after stroke onset) and late phase (24 hours after stroke onset) (144). During the early phase, leukocytes infiltrate the brain and are considered to be the main source of MMP9. Ischemic stroke quickly initiates an immune response causing leukocytes to bind to endothelial cells in the vasculature (145). In humans, MMP9 mRNA levels in peripheral leukocytes are increased as soon as 3-5 hours after stroke and activity of MMP9 peaks at 6-8 hours after stroke (145-147). Plasma levels of MMP9 have been shown to be predictive of hemorrhagic transformation and correlate with BBB injury (148-151). MMP9 and MMP2 are increased in plasma 3-8 hours after stroke in rats and mice as well (152, 153). The brain is also an important source of MMP2 in the early phase of hemorrhagic transformation. Primarily derived from astrocytes and endothelial cells, MMP2 is increased in the post-stroke brain

within 1-3 hours in rats and mice and remains elevated for several days (154-156). MMP14 is also increased after stroke, which could subsequently increase MMP2 activity (157, 158). This rise in MMP2 correlates with degradation of claudin-5 and occludin, two crucial tight junction proteins, leading to BBB breakdown in rodent models of stroke (105, 155, 159, 160).

In the late phase of hemorrhagic transformation, brain cells are the major source of MMPs. MMP9 can be expressed in astrocytes, neurons, microglia and endothelial cells and MMP9 is localized to these immunoreactive cells during the late phase of hemorrhagic transformation (112, 161). MMP3 was shown to be increased within 24 hours after stroke onset (162) and MMP3 knockout mice have a reduced rate of hemorrhagic transformation in a middle cerebral artery occlusion model with tPA treatment (163). This increase in MMP3 can increase the activity of MMP9 via cleavage of proMMP9, contributing to hemorrhagic transformation.

While the role of MMPs in hemorrhagic transformation after ischemic stroke has been studied in depth, their role in hemorrhagic stroke is less clear. Human studies have revealed elevated levels of MMP9 in peripheral blood after intracranial hemorrhage and were associated with worse neurological outcomes (164). Another study showed that while MMP2 levels remained stable after hemorrhagic stroke, MMP9 levels were increased and could possibly have contributed to cerebral edema after stroke (165). However, MMP9 is more commonly associated with CAA associated hemorrhage.

Mouse models

***Alzheimer's disease*:** Over the last 20 years, many mouse models of Aβ deposition have been created using the early onset familial mutations found in humans. One of the earliest mouse models was the PDAPP mouse first described by Dora Games in 1995 (166). The PDAPP mouse has a platelet derived growth factor-driven human APP gene with the Indiana mutation (V717F), which increases the $A\beta_{1-42}/A\beta_{1-40}$ ratio in humans. This mouse model shows cognitive decline around 4 months, plaque deposition and gliosis around 6 months and synaptic loss at 9 months. Another model using an APP mutation (Swedish mutation, KM670/671NL) is the Tg2576 mouse developed by Karen Hsiao in 1996 (167). This model shows synaptic loss at 4.5 months, cognitive decline around 6 months, gliosis at 10 months, and plaque deposition around 11 months. Mutations in PS1 have also been shown to cause early onset familial AD and have also been used to create mouse models of AD. In 1996, Karen Duff developed PS1 mouse models that increase the amount of $A\beta_{1-42}$ (168). One downside to single transgenic mice, like the Tg2576 mouse, is that they develop fewer plaques and plaque deposition occurs at a later age. To accelerate plaque deposition and to increase the plaque load, the double transgenic PS/APP mouse was developed in 1998 (169). Created by crossing the Tg2576 mouse and another mouse with a mutant PS1 gene (M146L), the PS/APP mouse shows plaque deposition starting at 6 months that increases with age, astrogliosis at 6 months, microglial activation at 12 months, and cognitive deficits around 15 months. Using this idea of double transgenic mouse models, Jankowsky

developed the APPSwe/PSEN1dE9 (APP/PS1) mouse (170, 171). The APP/PS1 mouse begins developing plaques around 6 months of age and has abundant levels by 9 months with no tangle formation. Astrogliosis also begins with plaque deposition at 6 months and increases with age (172). CAA has also been shown to appear as early as 6 months and increase with age, although progression was slower than the Tg2576 mouse, perhaps due to the higher $A\beta_{1-42}/A\beta_{1-40}$ ratio (173). Behavioral changes in these mice have been well characterized and show contextual memory deficits in fear conditioning tests starting at 6 months (174, 175). At 7 months, spatial learning is comparable to wildtype mice but is impaired by 12 months when tested on the Morris water maze (176, 177). While these models only represent one of the three characteristic pathologies of AD, they are sufficient for studying treatments that target $A\beta$ deposition.

***Vascular cognitive impairment and dementia*:** With many different causes of VCID, there have been several mouse models developed to study the disease. The bilateral common carotid artery stenosis model places micro-coils around the common carotid arteries to reduce blood flow to the brain and induces cognitive impairments and neuroinflammation (178). Both spontaneously hypertensive rats and cerebral autosomal dominant arteriopathy with subcortical infarcts and leukoencephalopathy (CADASIL) mice model cerebral small vessel disease, a common form of VCID. Spontaneously hypertensive rats develop high blood pressure with age and eventually develop ischemic lesions and memory impairments (179). The CADASIL mouse model, R90C, has white matter degeneration, age-associated vascular smooth muscle cell loss, and subcortical

infarcts (180, 181). Another set of mouse models that induce VCID involves the elevation of plasma homocysteine levels.

Homocysteine is a non-protein forming amino acid involved in the metabolism of cysteine and methionine (182). During normal metabolism, ATP activates methionine to form S-adenosylmethionine (SAM). SAM is a methyl donor to several different receptors and forms S-adenosylhomocysteine (SAH) as a by-product of this methyl reaction. SAH can then be hydrolyzed to form homocysteine. Homocysteine can also go through a re-methylation process to form methionine again. In this process, folate is reduced to tetrahydrofolate which is then converted to 5, 10-methylenetetrahydrofolate. Methylenetetrahydrofolate reductase (MTHFR) reduces 5, 10-methylenetetrahydrofate to 5-methyltetrahydrofolate. Finally, 5-methyltetrahydrofolate and vitamin B12 add a methyl group to homocysteine to form methionine again. Homocysteine can also go through a transsulfuration pathway to form cysteine. Serine can be enzymatically added to homocysteine by cystathionine β synthase (CBS) and vitamin B6 to form cystathionine (183). Cystathionine can then be cleaved by cystathionine gamma-lyase (CGL) to form cysteine. While cysteine can be converted back to cystathionine, cystathionine cannot be converted to homocysteine again. These homocysteine metabolic pathways are shown in Figure 1.2.

Elevated plasma homocysteine levels, termed hyperhomocysteinemia (HHcy), has been identified as a risk factor for cardiovascular disease, stroke, VCID, and AD (184-187). Normal levels of homocysteine range between 5-15

μmol/L. Levels between 15-30 μmol/L are considered mild, levels at 30-100 μmol/L are moderate and levels above 100 μmol/L are considered severe HHcy. In the periphery, homocysteine increases the formation of reactive oxygen species, which alters smooth muscle function and promotes proliferation of smooth muscles cells (188). Homocysteine also increases platelet aggregation which can contribute to brain infarcts (188). Serum homocysteine levels are inversely related to cognitive function in patients with dementia and elevated levels are more common among VCID patients than among AD patients (189, 190). While studies have shown an association between homocysteine levels and hippocampal atrophy, white matter lesions, and lacunar infarcts, the mechanism of HHcy-induced damage remains unknown (191, 192). It is unclear whether the increased risk of VCID is due to a direct effect of homocysteine or the lack of B vitamins which can cause HHcy.

To clarify this lack of clarity, several animal models have shown that high plasma levels of homocysteine are sufficient to cause cognitive deficits and vascular adverse events in the brain with and without B vitamin deficiency. Induction of HHcy in an animal model can be achieved via genetic manipulation or diet. Genetic manipulation of either CBS, which converts homocysteine to cystathionine, or MTHFR, which is the rate-limiting step in homocysteine conversion to methionine, can produce mouse models of HHcy. In humans, deficiencies in CBS result in elevated plasma levels of homocysteine and thrombosis, and are the most common cause of hereditary HHcy. $CBS^{+/-}$ heterozygote mice have a 50% lower CBS activity compared to wildtype mice

and develop mild HHcy (193). These mice show substantially decreased dilatory responses compared to controls (194) and it has also been shown that cerebral arteriolar walls are 25% thicker in $CBS^{+/-}$ heterozygote mice (195). In humans, there are several polymorphisms in MTHFR that produce HHcy and neurological conditions such as a progressive demyelinating neuropathy and cognitive impairment (196-198). Chen et al. deleted the MTHFR gene to create a mouse model of HHcy that exhibits motor and gait abnormalities within 5 weeks after birth (199). $MTHFR^{-/-}$ homozygotes also present with abnormal lipid deposition in the aorta and disruption of the laminar structure of the cerebellum with no obvious changes in the cortex or cerebrum.

Unlike MTHFR and CBS knockout mice, dietary induction of HHcy allows for age related HHcy to be studied. Dietary induction of HHcy in mice and rats can be achieved through a reduction in vitamins B6, B9 and B12, enrichment in methionine, or elevated levels of homocysteine. A combination of these diets can also be used to induce HHcy. Vitamins B6, B9 and B12 act as essential cofactors for the conversion of homocysteine to methionine or cysteine and enrichment in methionine causes an increase in conversion to homocysteine. In 2008, Treon et al. showed that feeding mice a B vitamin deficient diet resulted in cognitive impairment on the Morris water maze and decreased density of brain capillaries (200). Kim et al. fed 6-month-old Sprague-Dawley rats a folate deficient diet for 8 weeks and saw an increase in homocysteine levels, ultrastructural changes to cerebral capillaries, endothelial damage, swelling of pericytes, basement membrane thickening, and fibrosis (201). Rats fed a diet high in homocysteine for

5 or 15 months both showed cognitive impairments, decreased acetylcholine in the brain, and cortical microhemorrhages (202).

To develop a model of VCID, our research group took 3-month-old C57BL6 wildtype (WT) mice and placed them on a combination diet that was deficient in vitamins B6, B9 and B12 and enriched in methionine for 3 months (203). At the end of the 3 months, plasma homocysteine levels reached moderate levels in the mice on the homocysteine diet (82.93 ± 3.561 μmol/L compared to 5.89 ± 0.385 μmol/L in the control mice). When tested on the radial arm water maze, which tests spatial memory and requires hippocampal and cortical brain regions, these mice exhibited significant cognitive impairments (Figure 1.3A). Microhemorrhages were the main cerebrovascular pathology induced by the HHcy diet as shown by Prussian blue staining and MRI (Figure 1.3B). Neuroinflammation has been hypothesized to be a key mediator in VCID. In the HHcy mouse model, several pro-inflammatory cytokines were significantly increased compared to control mice while anti-inflammatory markers were not (Figure 1.3C). As mentioned earlier, MMP2 and MMP9 have been shown to degrade tight junctions and MMP9 can be activated by pro-inflammatory cytokines. qPCR showed a significant increase in MMP14, MMP2, MMP3 and MMP9 gene expression (Figure 1.3D) and gel zymography showed a significant increase in MMP2 and MMP9 activity (data not shown).

***Co-morbidity of AD and VCID*:** Using this mouse model of VCID via induction of HHcy, our research group then developed a co-morbidity mouse model to determine the effects of VCID on Aβ pathology (204). Six-month-old

APP/PS1 and wildtype mice were placed on either the control or HHcy diet for six months. Plasma homocysteine levels reached moderate levels again in both the APP/PS1 and wildtype mice and were significantly increased compared to controls (WT control: 6.85 ± 0.8 μmol/L, WT HHcy: 68.23 ± 12.1 μmol/L, APP/PS1 control: 7.65 ± 1.4 μmol/L, APP/PS1 HHcy: 64.21 ± 8.3 μmol/L). Using the two-day radial arm water maze to test cognitive changes, the APP/PS1 mice on the HHcy diet showed additive cognitive deficits (Figure 1.4A), suggesting an additive effect of the cerebrovascular pathology and Aβ deposition. The co-morbidity mice also showed a switch from an anti-inflammatory phenotype (M2a) to a pro-inflammatory phenotype (M1) (Figure 1.4B). Total levels of Aβ were not affected; however, there was a redistribution of amyloid. Congo red staining showed a decrease in parenchymal compact plaques and an increase in CAA in the APP/PS1 mice on the HHcy diet (Figure 1.4C). Analysis of microhemorrhages showed a significant increase in the APP/PS1 mice on the HHcy diet (Figure 1.4D) and gene expression analysis showed a significant increase in MMP14, MMP3 and MMP9 (Figure 1.4E). Overall, with the additive cognitive deficits and cerebrovascular pathology, this mouse model of HHcy in APP/PS1 mice can be used for studies of co-morbid dementia.

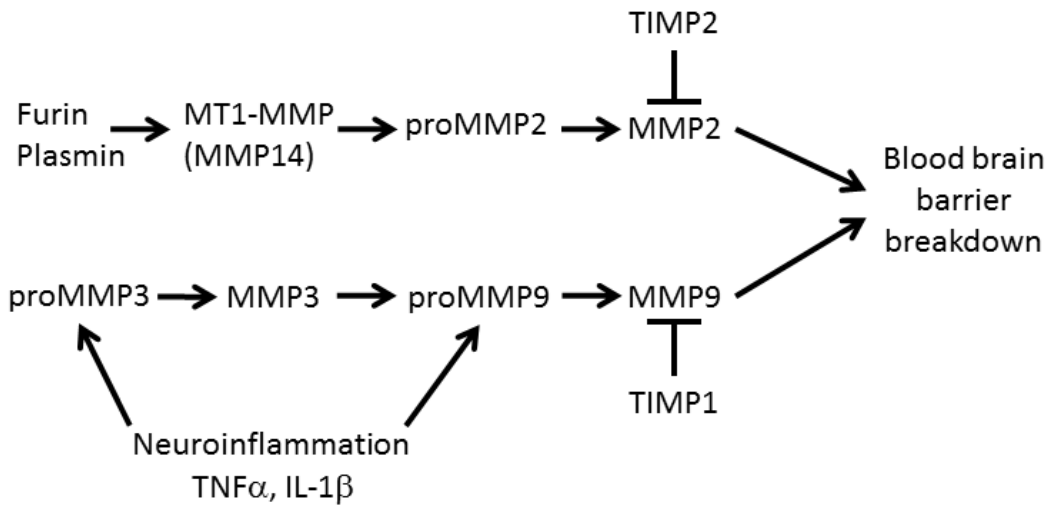

Figure 1.1 Summary of the MMP2 and MMP9 systems. Furin and plasmin increase MMP14 levels, which in turn forms a complex with proMMP2 and TIMP2 to activate MMP2. TIMP2 also inhibits MMP2 activity. Pro-inflammatory cytokines increase proMMP3 and proMMP9. MMP9 is activated by MMP3 and inhibited by TIMP1. Both MMP2 and MMP9 break down the blood brain barrier.

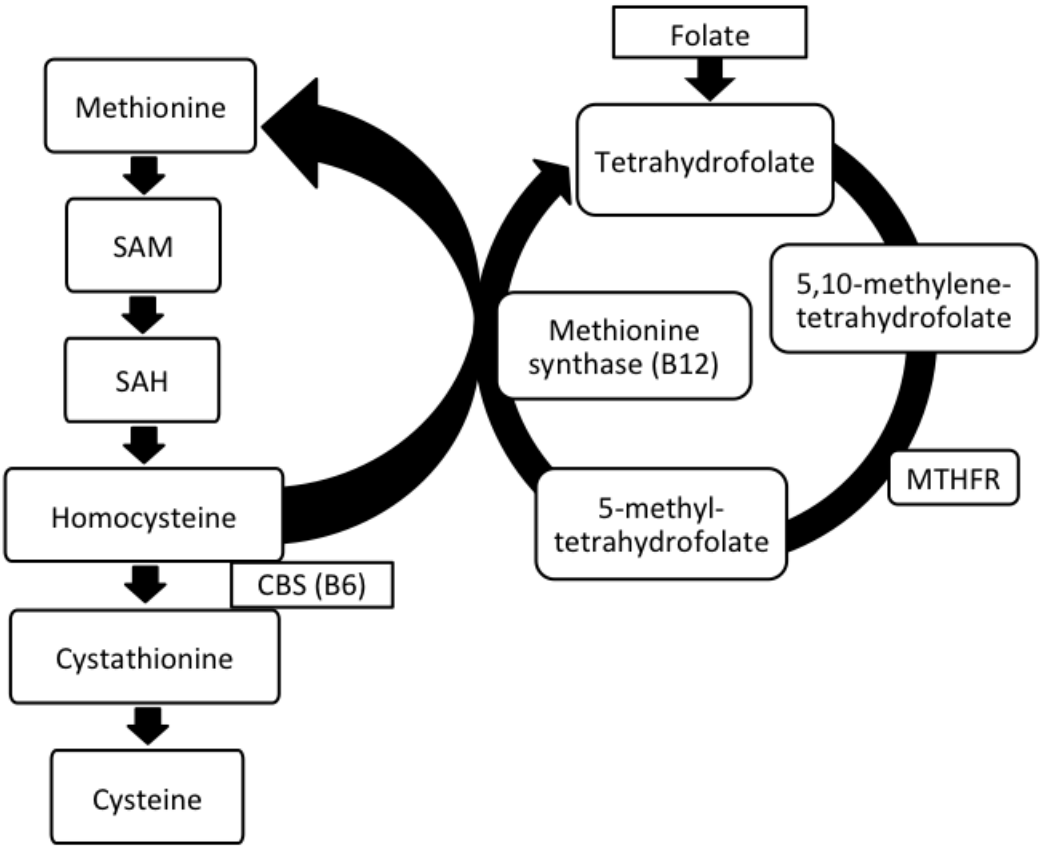

Figure 1.2 Biochemical pathways linking homocysteine and B vitamins.

Methionine is converted to homocysteine by methylation and subsequent hydrolysis. Homocysteine can be cycled back to methionine via the folate cycle, which is catalyzed by MTHFR and the essential cofactor vitamin B12. Alternatively, homocysteine can be further metabolized to cysteine via CBS and the essential cofactor vitamin B6. Homocysteine conversion to cysteine occurs primarily in the liver. All other reactions are ubiquitous.

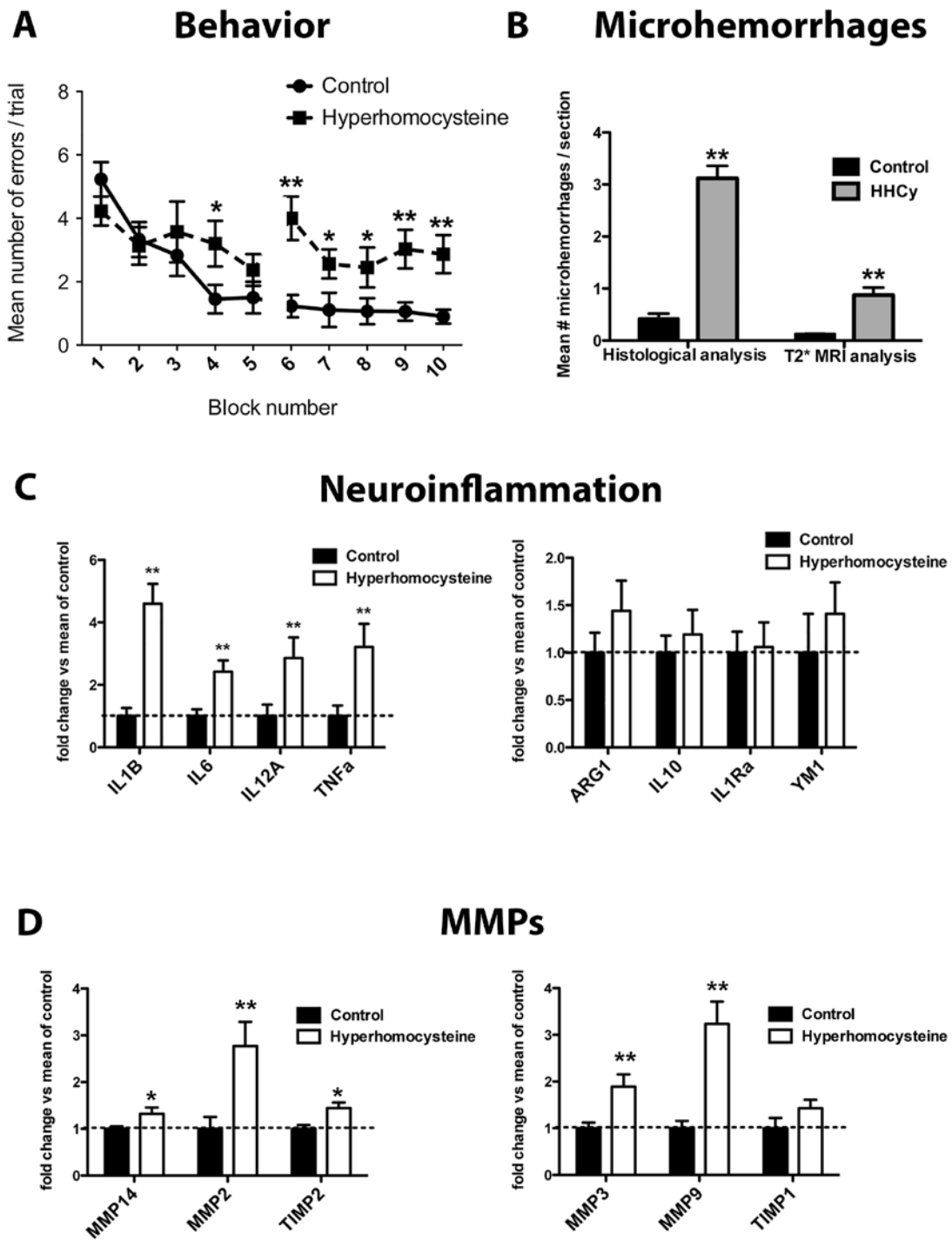

Figure 1.3 HHcy in wildtype mice models VCID. A) Two-day radial arm water maze data. Data are given as block numbers where each block is the average of 3 trials. * indicates P<0.05 and ** indicates P<0.01 by individual block t-test. B)

Prussian blue and MRI detected microhemorrhages. ** indicates P<0.01 by t-test. C) qPCR analysis for pro-inflammatory and anti-inflammatory markers (D) and MMP2 and MMP9 system markers. Data are shown as fold change from control. * indicates P<0.05 and ** indicates P<0.01 by t-test.

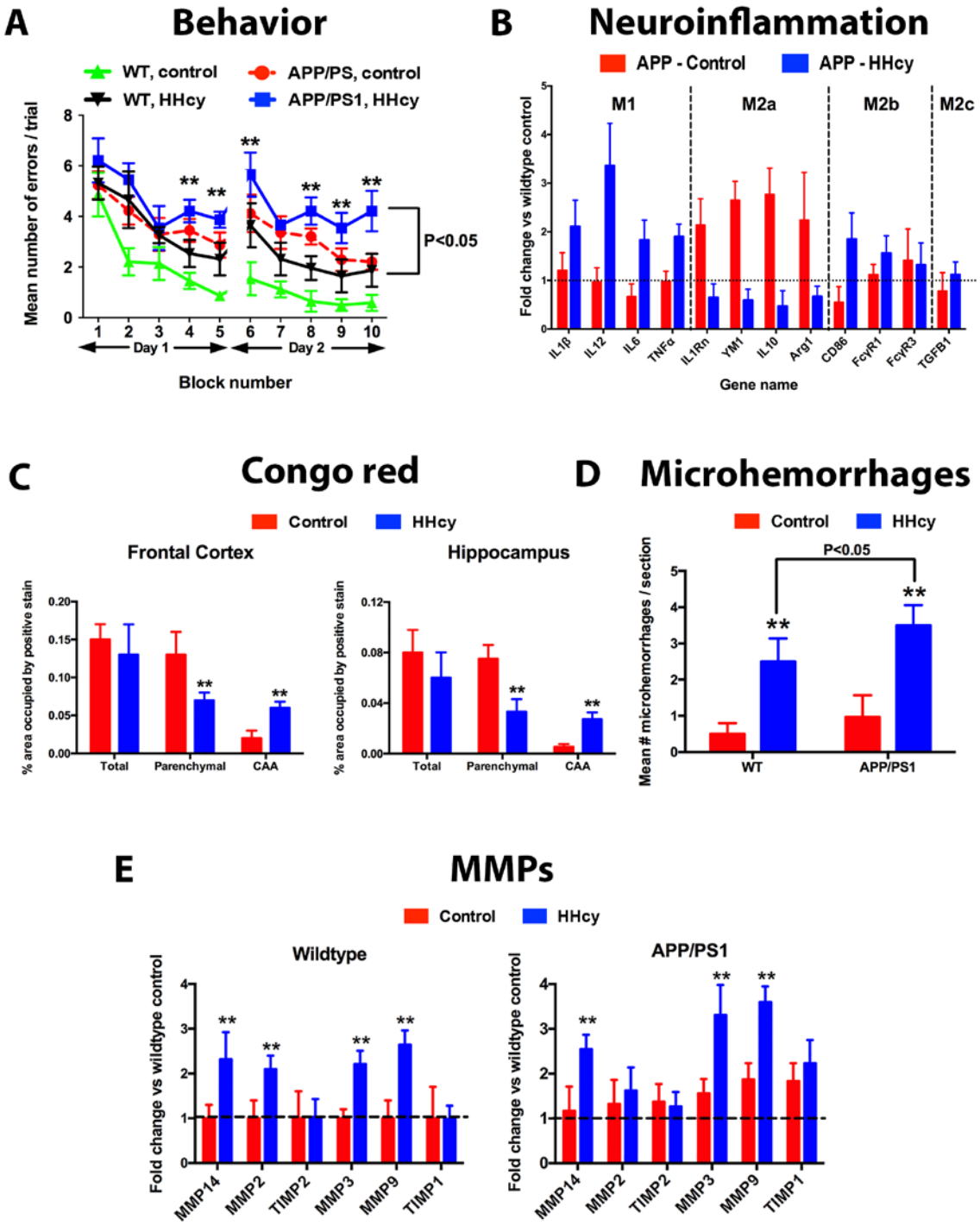

Figure 1.4 HHcy in APP/PS1 mice models co-morbid dementia. A) Two-day radial arm water maze data. Data are given as block numbers where each block is the average of 3 trials. ** indicates P<0.01 by individual block t-test. B) qPCR

analysis for pro-inflammatory and anti-inflammatory markers. Data are shown as fold change from control. C) Quantification of the percent area occupied by positive Congo red staining in the frontal cortex and hippocampus of APP/PS1 mice. ** indicates P<0.01 compared to APP/PS1 mice on control diet. D) Prussian blue detected microhemorrhages. ** indicates P<0.01 compared to the control group for the given genotype. E) qPCR analysis for MMP2 and MMP9 system markers. Data are shown as fold change from control. ** indicates P<0.01 compared to controls for each genotype.

Table 1.1 Specific markers for each inflammatory phenotype.

Pro-inflammatory (M1)	Wound healing and repair (M2a)	Immune complex mediated (M2b)	Acquired deactivation (M2c)
IL-1β	IL-10	CD86	TGF1β
TNFα	ARG1	FcγR1	SPHK1
IL-6	YM1	FcγR3	MRC1
IL-12a	Fizz	IL-10	IL-10
IL-12b	IL-1Ra	Low IL-12	Low IL-12
Marco	MRC1		
Low IL-10	Low IL-12		

Chapter 2

Transition from an M1 to a mixed neuroinflammatory phenotype increases amyloid deposition in APP/PS1 transgenic mice

Erica M. Weekman[1,2], Tiffany L. Sudduth[1,2], Erin L. Abner[1,3], Gabriel J. Popa[4], Michael D. Mendenhall[4], Holly M. Brothers[1], Kaitlyn Braun[1,2], Abigail Greenstein[1], and Donna M. Wilcock[1,2*]

University of Kentucky, [1]Sanders-Brown Center on Aging, [2]Department of Physiology, [3]Department of Epidemiology, [4]Department of Molecular and Cellular Biochemistry, Lexington KY 40536 USA

Abstract

The polarization to different neuroinflammatory phenotypes has been described in early Alzheimer's disease, yet the impact of these phenotypes on Aβ pathology remains unknown. Short term studies show that induction of an M1 neuroinflammatory phenotype reduces Aβ, but long term studies have not been performed that track the neuroinflammatory phenotype. Wildtype and APP/PS1 transgenic mice aged 3-4 months received a bilateral intracranial injection of adeno-associated viral (AAV) vectors expressing IFNγ or GFP in the frontal cortex and hippocampus. Mice were sacrificed 4 or 6 months post-injection. ELISA measurements were used for IFNγ protein levels and biochemical levels of Aβ. The neuroinflammatory phenotype was determined through qPCR. Microglia, astrocytes, and Aβ levels were assessed with immunohistochemistry. AAV expressing IFNγ induced an M1 neuroinflammatory phenotype at 4 months and a mixed phenotype along with an increase in Aβ at 6 months. Microglial staining

was increased at 6 months and astrocyte staining was decreased at 4 and 6 months in mice receiving AAV expressing IFNγ. Expression of IFNγ through AAV successfully induced an M1 phenotype at 4 months that transitioned to a mixed phenotype by 6 months. This transition also appeared with an increase in Aβ burden suggesting that a mixed phenotype, or enhanced expression of M2a and M2c markers, could contribute to increasing Aβ burden and disease progression.

Introduction

First described by Alois Alzheimer in 1907, Alzheimer's disease (AD) is a progressive, neurodegenerative disease characterized pathologically by the presence of amyloid plaques formed by amyloid-beta (Aβ) peptide aggregates and neurofibrillary tangles composed of hyperphosphorylated and aggregated tau protein (4). Alois Alzheimer also described inflammation in the form of microglia surrounding Aβ plaques. Numerous studies have shown that microglial activation results from a reaction to Aβ in AD (205-208). The overall role of neuroinflammation in AD remains relatively unknown.

Peripheral macrophages have been extensively characterized and shown to have distinct phenotypes dependent on their stimuli. The M1 phenotype, or classical activation, is associated with defense and attack and induces the release of pro-inflammatory cytokines such as interleukin 1-beta (IL-1β), tumor necrosis factor alpha (TNFα), interleukin 12 (IL-12) and interleukin 6 (IL-6) (79, 209). The M2 phenotypes are termed alternative activation and include the M2a, M2b and M2c states. The M2a phenotype is characterized by wound healing and high levels of arginase 1 (ARG1) and the chitinase-like protein YM1 (210). The

M2b phenotype is a combination of an M1 and M2a state and is associated with high levels of CD86 and the Fc gamma receptors 1 and 3 (FcγR1 and FcγR3) (210). Finally, the M2c phenotype is a deactivation state accompanied by high levels of transforming growth factor beta (TGFβ) and sphingosine kinase 1 (SPHK1) (79, 211). It has more recently been shown that microglia are also capable of expressing most, if not all, of these inflammatory mediators under the correct conditions.

The interferon family of cytokines is increased in human AD tissue and in the APP/PS1 mouse model and interferon gamma (IFNγ) is the main stimulant for microglia to produce an M1 phenotype by binding its receptor, increasing STAT1α, and increasing transcription of several M1 cytokine genes (212, 213). Some studies have used IFNγ to induce an M1 phenotype, with one study showing classical activation of microglia produces a decrease and another reporting an increase in Aβ burden (214, 215). Other studies have shown that inducing an M1 neuroinflammatory phenotype by introducing TNFα, IL-1β, or lipopolysaccharide (LPS) into the brain lowers Aβ burden (83, 88, 216, 217). However, these studies do not measure or track the different neuroinflammatory phenotypes along with the changes in Aβ burden over long periods of time. Additionally, engaging the immune system in the brain using anti-Aβ immunotherapy has been shown to be extremely efficacious in lowering Aβ load by increasing levels of pro-inflammatory cytokines (29, 38).

To better understand the long-term effects of an M1 neuroinflammatory phenotype, we bilaterally injected an adeno-associated viral (AAV) vector

expressing IFNγ into the frontal cortex and hippocampus of wildtype and APP/PS1 mice to induce an M1 phenotype and determine the effects on Aβ levels at 4 and 6 months after injection. We hypothesize that a long-term pro-inflammatory phenotype will lead to decreased levels of Aβ. We found that IFNγ induced an M1 phenotype at 4 months but transitioned to include an M2 phenotype by 6 months. The transition from an M1 to a mixed phenotype did not ameliorate Aβ levels at 6 months. Instead, Aβ levels were significantly higher, suggesting that a mixed phenotype could accelerate the disease process.

Methods

Animals: Female and male wildtype (WT) and APP/PS1 transgenic mice (C57BL6 mice carrying human APPSwe and PS1-dE9 mutations) (170) were bred in house and aged 3-4 months. Mice were randomly placed into one of eight groups based on adeno-associated virus serotype 8 (AAV-8) injection, genotype and survival: Fifteen wildtype mice were assigned to receive either AAV-8 expressing GFP (GFP-AAV) for 4 (N=2F, 1M) or 6 (N=3F, 3M) as a control, or AAV-8 expressing IFNγ (IFNγ-AAV) for 4 (N=2F, 1M) or 6 (N=2F, 1M) months. Twenty APP/PS1 mice were assigned to receive either GFP-AAV for 4 (N=2F, 2M) or 6 (N=4F, 4M) for a control, or IFNγ-AAV for 4 (N=2F, 1M) or 6 (N=2F, 3M) months. This study was approved by the University of Kentucky Institutional Animal Care and Use Committee and conformed to the National Institutes of Health Guide for the Care and Use of Animals in Research.

AAV preparation: The vector for preparing recombinant AAV was constructed by ligating the 1349 bp *Eco*RI/*Sal*I fragment carrying the IRES-GFP from

pSMPUW-IRES-GFP (Cell Biolabs, San Diego, CA) into *Eco*RI/*Sal*I-digested pZac2.1 (gift of Dr. Paul Murphy, University of Kentucky) to create ViCo1.28. The IFNγ insert was prepared by polymerase chain reaction amplification of cDNA clones obtained from Open Biosystems (GE Healthcare, Dharmacon RNAi and gene expression, Piscataway, NJ). The IFNγ PCR primer sequence used was CCCGCTAGCTCTGAGACAATGACCACCGCGGACCCCGAATCAGCAGCGA. The Open Biosystems Catalogue number for the sequence is MMM1013-99829104. The clone ID is 8733812 and the accession is BC119063. The primers introduced an *Nhe*I site at the 5'-end and a*Sac*II site at the 3'-end of the IFNγ gene to facilitate cloning into the corresponding sites in ViCo1.28. The fidelity of each clone was confirmed by DNA sequence analysis.

AAV8 coat protein-pseudotyped AAV2 viruses were prepared by co-transfecting 10 T225 culture flasks of 293LTV cells (Cell Biolabs, San Diego, CA) with 250μg pAAV2/8 (obtained from the University of Pennsylvania Viral Core), 500μg pAdΔF6 (gift of Dr. Paul Murphy, University of Kentucky) and, individually, 250μg of each cytokine clone using 5mg polyethyleneimine to enhance DNA uptake. After three days, the cells were harvested, washed, suspended in 13ml 150mM NaCl, 50mM Tris·Cl pH 8.4, 0.5% deoxycholate and 50U/ml of benzonase and incubated at 37°C for 30 min. An additional 2.8ml 5M NaCl was added and the incubation was continued for another 30 min. at 45°C. The cell suspension was then subjected to four freeze/thaw cycles (30 min at -80°C/30 min at 45°C). The lysate was then partially clarified by centrifugation at 18,500xg for 10 min at 20°. The supernatant was laid on top of an iodixanol step

gradient and centrifuged at 350,000xg for 1 hour at 18°C. The interface between the 40% and 54% iodixanol layers was withdrawn and spin-purified and concentrated using four washes with PBS in an Amicon Ultra-15 100,000 MWCO spin concentrator. The virus preparation was then titered using real-time PCR with primers directed against the CMV promoter region of the DNA encapsulated in the virions.

Bilateral intracranial injection: On the day of surgery, mice were anesthetized with isoflurane and placed into a stereotaxic apparatus (51733D digital dual manipulator mouse stereotaxic frame, Stoelting Co. Wood Dale, IL). A midsaggital incision was used to expose the skull. Using a dental drill mounted on the stereotaxic frame, a total of four burr holes were made. One hole for each frontal cortex and hippocampus. The following coordinates were used from bregma: frontal cortex, anteroposterior, +2.0mm, lateral +/- 2.0mm; hippocampus, anteroposterior -2.7mm, lateral +/- 2.5mm which have been previously established by the laboratory using dye injections to confirm appropriate placement. A 26 gauge needle attached to a 10μL Hamilton syringe (Hamilton, Reno, NV) containing the AAV at a concentration of 2×10^9 genomes / μl to be injected was lowered 3.0mm ventral to bregma, and a 2μL injection was made over a 4 minute period. The incision was cleaned and sutured. Sutures were removed two weeks after surgery. The virus was injected at the maximum titer possible based on the concentration supplied so as to achieve the greatest expression of IFNγ.

Tissue processing: After injection with a lethal dose of Beuthanasia-D, mice were perfused intracardially with 25mL of normal saline. Brains were removed rapidly and bisected in the midsaggital plane. The left side of the brain was immersion fixed in 4% paraformaldehyde. The right side was dissected with the frontal cortex and hippocampus being isolated and flash frozen in liquid nitrogen and then stored at -80˚C. The left hemibrain was passed through a series of 10, 20 and 30% sucrose solutions for cryprotection. Using a sliding microtome, 25μm frozen horizontal sections were collected and stored free floating in 1XDPBS containing sodium azide at 4˚C.

Immunohistochemistry: Six floating sections spaced 300μm apart spanning the injection site (1800μm-3600μm ventral to bregma) were immunostained by using commercially available antibodies against Aβ (Rabbit polyclonal $A\beta_{1\text{-}16}$, Life Technologies, Carlsbad, CA), CD11b (Rat monoclonal, AbD Serotec, Raleigh, NC), and GFAP (Rabbit polyclonal, Dako, Denmark). Immunohistochemistry was performed as previously described (218). Briefly, sections were quenched for endogenous peroxidase, blocked and permeabalized. They were then incubated overnight in primary antibody at 4ºC. (Aβ 1:3000, CD11b 1:3000, GFAP 1:10000). After washing, sections were incubated for two hours in the appropriate biotinylated secondary antibody (goat anti-rabbit IgG for Aβ and GFAP, goat anti-rat for CD11b, all 1:3000) (Vector Laboratories, Burlingame, CA). Sections were then washed and incubated for one hour in ABC. For CD11b and GFAP, color development was performed using the DAB substrate kit with Nickel (Vector

Laboratories, Burlingame, CA). For Aβ, color development was performed using powder DAB (Sigma, St. Louis, MO)

Stained sections were mounted, air dried overnight, dehydrated and coverslipped in DPX (Electron Microscopy Sciences, Hatfield, PA). Immunohistochemical analysis was performed by measuring percent area occupied by positive stain using the Nikon Elements BR image analysis system (Melville, NY) as described previously (94).

Quantitative RT-PCR: The Trizol plus RNA purification system (Life Technologies, Carlsbad, CA) was used to extract RNA from the frozen right hippocampus according to the manufacturer's instructions. RNA was quantified using the Biospec nano spectrophotometer (Shimaduz, Japan). cDNA was produced using the cDNA High Capacity kit (Life Technologies, Carlsbad, CA) according to the manufacturer's instructions. Real-time PCR was performed using the Fast TaqMan Gene Expression assay (Life Technologies, Carlsbad, CA). In each well of a 96 well plate, 0.5μL of cDNA (100ng, based on the RNA concentrations) was diluted with 6.5μL of RNase-free water. One microliter of the appropriate gene probe was added along with 10μL of the Fast TaqMan to each well. Target amplification was performed using ViiA7 (Applied Biosystems, Grand Island, NY). The thermal cycling conditions include a holding stage at 95˚C followed by 40 cycles of denaturation at 95˚C for 1 second and annealing/primer extension at 60˚C for 20 seconds. All genes were normalized to 18S rRNA. We determined the fold change for mice receiving IFNγ-AAV compared with mice

receiving GFP-AAV using the –ΔΔCt method (219). Table 2.1 shows the genes tested along with their PMID and Taqman ID.

ELISA measurement: Protein for Aβ and IFNγ analysis was extracted from the right frontal cortex in 1XDPBS with complete protease and phosphatase inhibitor (Pierce Biotechnology Inc., Rockford, IL). The samples were centrifuged at 10000xg at 4˚C for 15 minutes. The supernatant was removed and labeled the "soluble" extract. The pellet was homogenized in 250μL of 70% formic acid and centrifuged at 47000rpm at 4˚C for 1 hour. The supernatant was removed and neutralized 1:20 with 1M Tris-HCl and brought to a pH of 7 with HCl. This was labeled the "insoluble" extract. Protein concentrations for the soluble and insoluble extracts were determined using the BCA protein assay kit (Pierce Biotechnology Inc., Rockford, IL) according to the manufacturer's instructions. The Meso-Scale Discovery multiplex ELISA system was used to measure $A\beta_{1-38}$, $A\beta_{1-40}$, and $A\beta_{1-42}$ levels in the soluble and insoluble extracts (MSD, Gaithersburg, MD). The Meso-Scale Discovery Mouse Proinflammatory 7-Plex kit (MSD, Gaithersburg, MD) was used to measure IFNγ levels in the soluble extract. All steps were followed according to the manufacturer's directions except for the sample incubation time, which was left overnight.

Analysis: Data are presented as mean ± standard error (SEM). We used two-way analysis of variance (ANOVA) based on factors treatment (GFP-AAV or IFNγ–AAV injection) and survival time (4 or 6 months) to evaluate main effects and treatment-by-time interaction within genotype (WT and APP/PS1). No statistical comparisons were made across genotype. Because treatment effects

at each time point were of interest *a priori*, data are presented by treatment and time point whether or not the treatment-by-time interaction is significant.

Due to a high proportion of zero values, we used nonparametric two-way ANOVA on ranks to evaluate distributional differences in ELISA-determined IFNγ protein levels. Similarly, we used two-way ANOVA on ranks to evaluate differences in gene expression (measured by fold change from GFP) as these data did not meet parametric ANOVA assumptions. Ranks were assigned using the RANK procedure, and ANOVA was performed using the GLM procedure in SAS/STAT 9.3® (SAS, Cary, NC). Statistical significance was set at $P<0.05$.

Results

To determine that the IFNγ-AAV resulted in expression of IFNγ we performed ELISA measurement. Measurement of IFNγ in the protein extracted from the right frontal cortex showed a significant treatment effect such that mice injected with IFNγ-AAV had a 5000-fold increase in IFNγ levels at 4 and 6 months in both WT and APP/PS1 mice compared to mice receiving GFP-AAV (Figure 2.1). IFNγ levels within treatment groups were not different at 6 months compared to 4 months in WT or APP/PS1 mice.

To determine the neuroinflammatory phenotype, right hippocampal RNA was isolated and real time RT-PCR was performed for several genes specific to an M1, M2a, M2b, or M2c macrophage phenotype. Data are shown as fold change compared to GFP-AAV at each time point for each genotype. The GFP-AAV mice showed no significant change in neuroinflammation over time (data not shown). Overall, both WT and APP/PS1 mice responded to the IFNγ-AAV with a

robust M1 response. IL-12b was increased in IFNγ-AAV treated mice at 4 and 6 months in both genotypes, and IL-1β was increased at all time points except 4 months in APP/PS1 (Figure 2.2A-D). Additionally, IL-6 and IL-12a showed significant increases at the 6-month (but not 4 month) time points in both WT and APP/PS1 mice (Figure 2.2B and D). At the 6-month time point, but not at the 4-month time point, M2a gene YM1 was significantly increased in WT and APP/PS1 mice (Figure 2.2A-D). Also of note are increased M2b markers CD86, FcγR1 and FcγR3 and M2c markers TGFβ and SPHK1 at the 6-month time point (Figure 2.2B and D). Table 2.2 shows the fold change values for GFP-AAV and IFNγ-AAV treated mice. Interestingly, while it may appear that the APP/PS1 mice are less responsive to the IFNγ-AAV, it is actually due to the fact that APP/PS1 mice normally have an inflammatory response to the Aβ deposits in the brain and so the fold change achieved by the IFNγ-AAV is less than in WT.

Next, assessment of CD11b immunohistochemistry in the frontal cortex (images not shown) and the hippocampus (dentate gyrus shown, Figure 2.3A-H) was performed to determine the effect of IFNγ on microglia. In all four brain regions measured, for both WT and APP/PS1 mice receiving IFNγ-AAV, there were statistically significant increases in CD11b staining, as measured by percent area occupied by positive immunostain, at 6 months compared to 4 months that were not observed in mice receiving GFP-AAV (i.e., the treatment-by-time interaction is significant). In the frontal cortex, there was a statistically significant increase in microglial staining at 6 months but not 4 months in both WT and APP/PS1 mice injected with IFNγ-AAV compared to mice receiving GFP-

AAV (Figure 2.3I). At 6 months in WT mice, there were significant increases in staining in the CA1, CA3 and DG regions (Figure 2.3A-D, and I). APP/PS1 mice receiving IFNγ-AAV only showed modest, non-significant increases at 4 months (Figure 2.3E, F and I) but significant increases were observed in all hippocampal regions by 6 months (Figure 2.3G, H and I).

Evaluation of astrogliosis using GFAP immunohistochemistry was also performed on the frontal cortex (images not shown) and the hippocampus (dentate gyrus shown, Figure 2.4A-H). Distribution of GFAP staining in WT (Figure 2.4A and C) and APP/PS1 mice (Figure 2.4E and G) receiving GFP-AAV was typical for age and genotype (220). Curiously, IFNγ-AAV injection in both the WT and APP/PS1 mice resulted in decreased GFAP positive staining. We found significantly decreased GFAP staining 4 months after IFNγ-AAV injection in the CA1, CA3, and DG regions of WT mice (Figure 2.4A, B and I). There were no significant changes in GFAP staining in the CA1, CA3, or DG regions in the APP/PS1 mice at 4 months (Figure 2.4E, F and I). At 6 months, there was a significant decrease in astrocyte staining in the CA1, CA3 and DG regions in WT (Figure 2.4C, D and I) and in the DG in APP/PS1 mice (Figure 2.4G, H and I).

Finally, we examined the effect of IFNγ-AAV on Aβ levels in the APP/PS1 mice. Aβ levels were determined by immunohistochemistry and ELISA analysis. Aβ deposition in the GFP-AAV mice showed a typical distribution of APP/PS1 mice at this age both 4 and 6 months post injection (Figure 2.5A and C). Immunohistochemical analysis of the frontal cortex (images not shown) and the hippocampus (DG shown, Figure 2.5A-D) shows no significant change in Aβ

deposition 4 months post-injection (Figure 2.5A, B and E). But, at 6 months post injection, IFNγ-AAV resulted in increased Aβ deposition in the frontal cortex, CA1 and CA3 regions versus GFP-AAV treated mice. Aβ deposition was elevated significantly at 6 months compared to levels at 4 months in mice receiving IFNγ-AAV in all areas except the DG, where the effect was marginally significant (Figure 2.5B, D and E).

Biochemical detection of Aβ was performed on PBS soluble and insoluble (formic acid soluble) protein extracts from the left anterior cerebral cortex. $A\beta_{1-38}$, $A\beta_{1-40}$ and $A\beta_{1-42}$ were analyzed by multiplexed ELISA analysis (Table 2.3). IFNγ-AAV injection significantly increased soluble $A\beta_{1-40}$ and marginally increased $A\beta_{1-42}$ levels at 4 months relative to GFP-AAV injection in APP/PS1 mice (Table 2.3). Soluble $A\beta_{1-38}$, $A\beta 1_{-40}$ and $A\beta_{1-42}$ levels significantly increased from 4 to 6 months in both treatment groups at the same rate (i.e., the treatment-by-time interactions were not significant), but treatment group differences at 6 months were not significant due to higher variability in the IFNγ-AAV treated mice. Main effects for treatment were significant for soluble $A\beta_{1-38}$, $A\beta_{1-40}$ and $A\beta_{1-42}$. No significant changes due to treatment or time were observed for insoluble Aβ, with the exception of $A\beta_{1-38}$, where there was a main effect due to time ($p=0.024$).

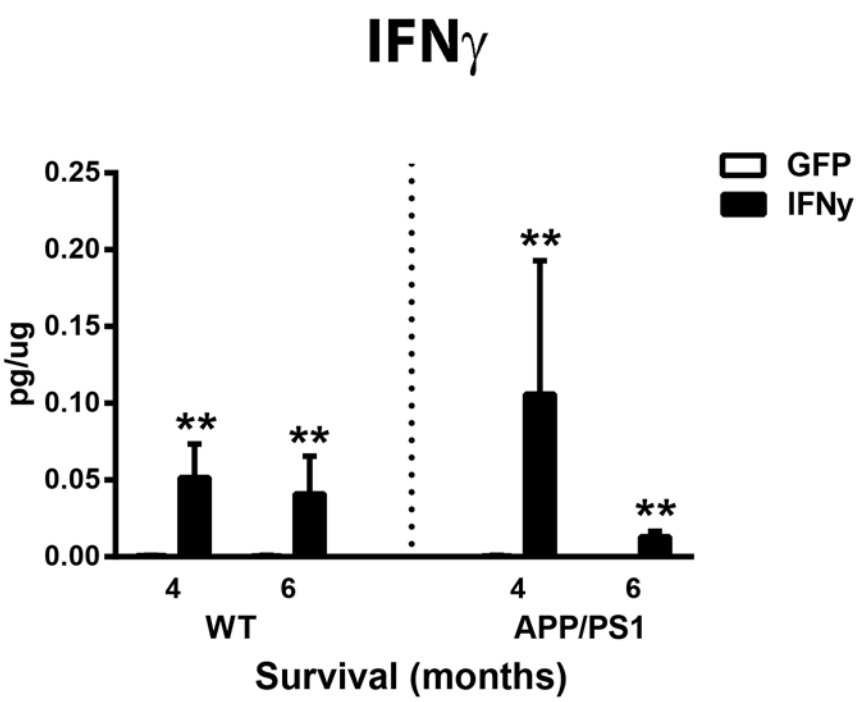

Figure 2.1 Protein analysis confirms IFNγ overexpression by AAV. IFNγ protein levels. ** indicates P<0.01 for IFNγ-AAV compared to GFP-AAV of that time point and genotype.

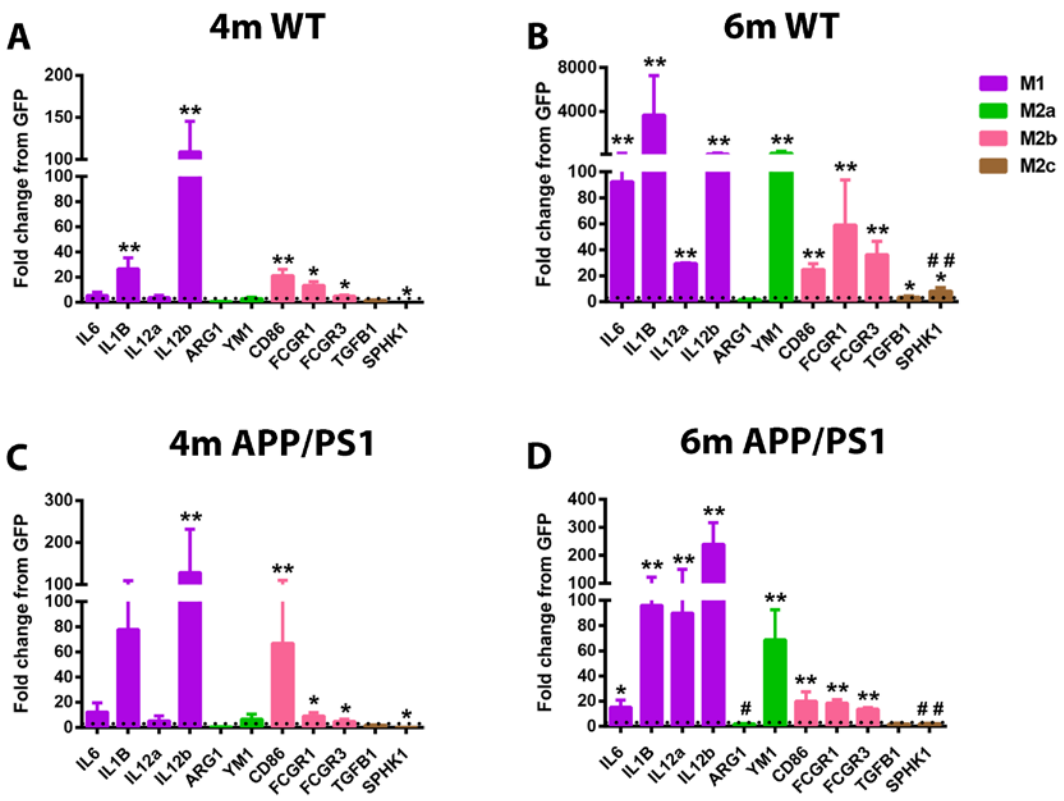

Figure 2.2 IFNγ induces an M1 neuroinflammatory phenotype. Relative gene expression for genes representative of the M1, M2a, M2b, and M2c phenotypes. Data are shown as fold change relative to mice receiving GFP-AAV at the given time point and genotype. A) Wildtype mice receiving IFNγ-AAV for 4 months. B) Wildtype mice receiving IFNγ-AAV for 6 months. C) APP/PS1 receiving IFNγ-AAV for 4 months. D) APP/PS1 receiving IFNγ-AAV for 6 months. * indicates P<0.05 for IFNγ-AAV compared to GFP-AAV of that time point and genotype. ** indicates P<0.01 for IFNγ-AAV compared to GFP-AAV of that time point and genotype. # indicates P<0.05 for 4 month IFNγ-AAV compared to 6 month IFNγ-AAV of that genotype. ## indicates P<0.01 for 4 month IFNγ-AAV compared to 6 month IFNγ-AAV of that genotype.

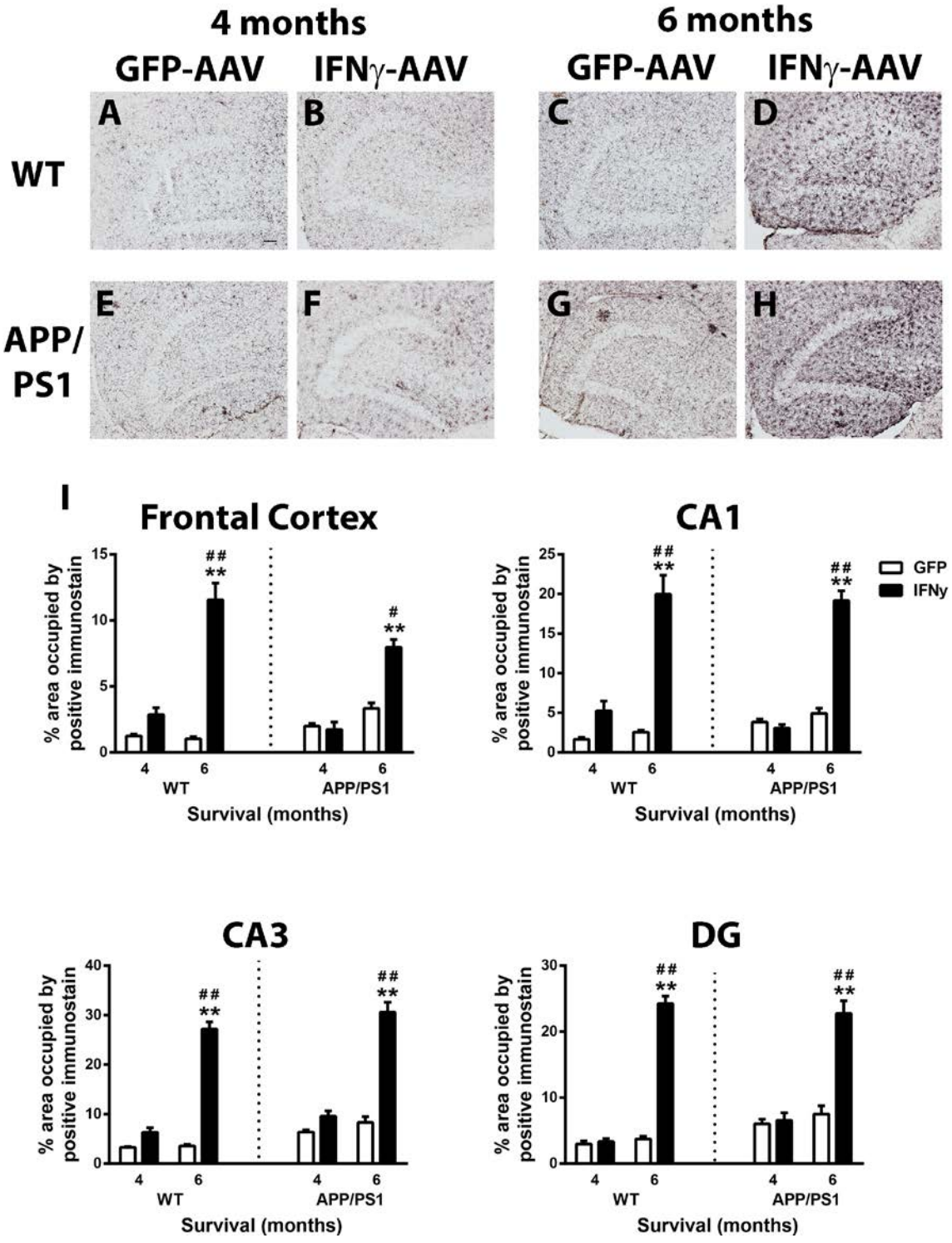

Figure 2.3 IFNγ causes an increase in CD11b staining. A-D) Dentate gyrus of wildtype mice receiving GFP-AAV or IFNγ-AAV. E-H) Dentate gyrus of APP/PS1 mice receiving GFP-AAV or IFNγ-AAV. I) Quantification of CD11b in the frontal

cortex, CA1, CA3, and DG. ** indicates P<0.01 for IFNγ-AAV compared to GFP-AAV of that time point and genotype. # indicates P<0.05 for 4 month IFNγ-AAV compared to 6 month IFNγ-AAV of that genotype. ## indicates P<0.01 for 4 month IFNγ-AAV compared to 6 month IFNγ-AAV of that genotype. Scale bar in A is for A-H and is equal to 50μm.

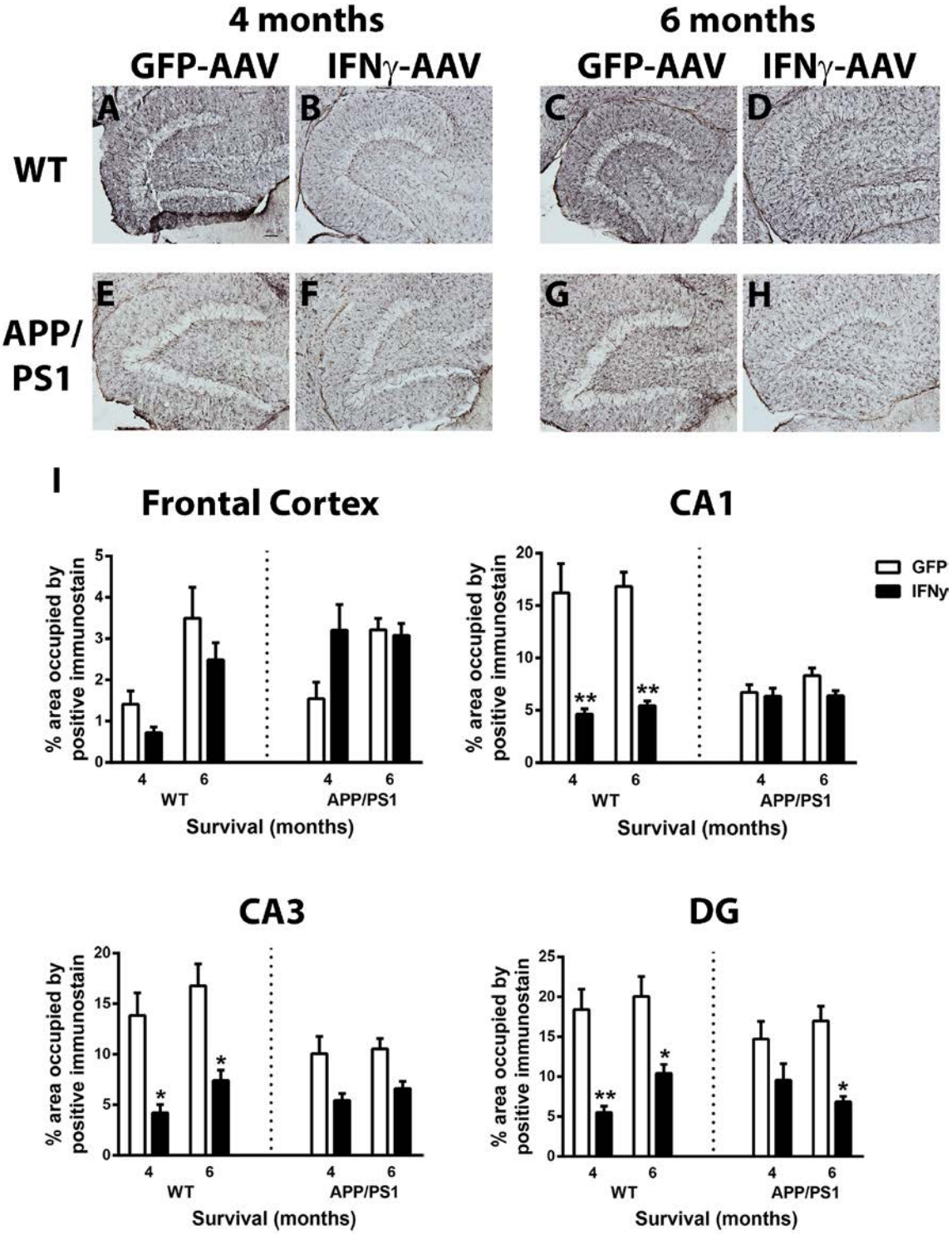

Figure 2.4. IFNγ causes a decrease in GFAP staining. A-D) Dentate gyrus of wildtype mice receiving GFP-AAV or IFNγ-AAV. E-H) Dentate gyrus of APP/PS1

mice receiving GFP-AAV or IFNγ-AAV. I) Quantification of GFAP in the frontal cortex, CA1, CA3, and DG. * indicates $P<0.05$ for IFNγ-AAV compared to GFP-AAV of that time point and genotype. ** indicates $P<0.01$ for IFNγ-AAV compared to GFP-AAV of that time point and genotype. Scale bar in A is for A-H and is equal to 50μm.

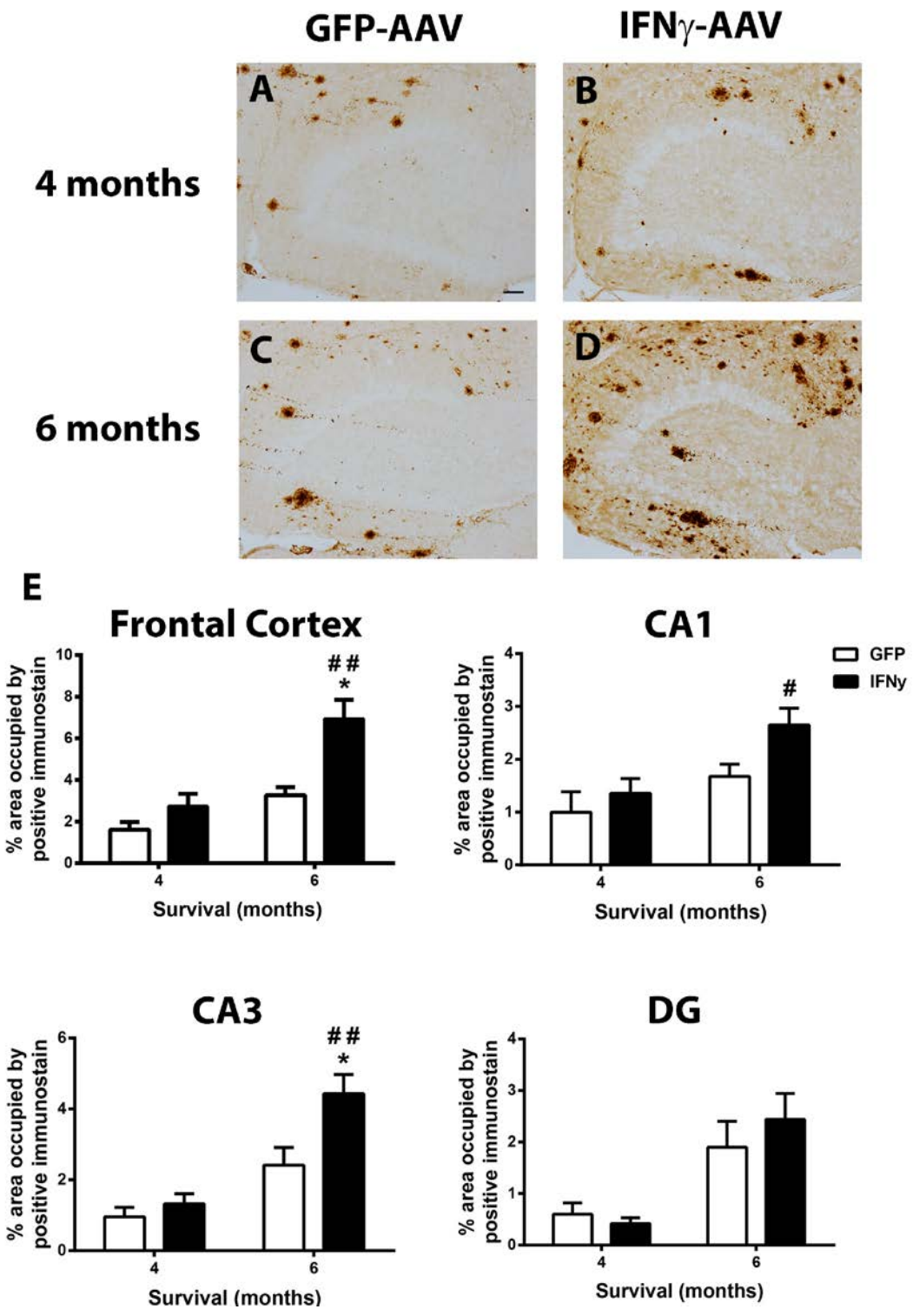

Figure 2.5 IFNγ increases Aβ deposition. A-D) Dentate gyrus of APP/PS1 mice receiving GFP-AAV or IFNγ-AAV. E) Quantification of Aβ in the frontal cortex,

CA1, CA3, and DG. * indicates P<0.05 for IFNγ-AAV compared to GFP-AAV of that time point and genotype. # indicates P<0.05 for 4 month IFNγ-AAV compared to 6 month IFNγ-AAV of that genotype. ## indicates P<0.01 for 4 month IFNγ-AAV compared to 6 month IFNγ-AAV of that genotype. Scale bar in A is for A-D and is equal to 50μm.

Table 2.1 Genes for RT-PCR.

Gene of interest	PMID	Taqman ID
IL-6	NM_031168.1	Mm.1019
IL-1β	NM_008361.3	Mm.222830
IL-12a	NM_008351.2	Mm.103783
IL-12b	NM_008352.2	Mm.239707
ARG1	NM_007482.3	Mm.154144
YM1 (Chil3)	NM_009892.2	Mm.387173
CD86	NM_019388.3	Mm.1452
FcγR1	NM_010186.5	Mm.150
FcγR3	NM_010188.5	Mm.22119
TGFβ1	NM_011577.1	Mm.248380
SPHK1	NM_011451.3	Mm.20944

Table 2.2 Fold change values for RT-PCR. Bolded font indicates P<0.05 compared to GFP-AAV of that time point and genotype.

	GFP-AAV				IFNγ-AAV			
	WT		APP/PS1		WT		APP/PS1	
Gene	4 mo	6 mo	4 mo	6 mo	4 mo	6 mo	4 mo	6 mo
IL-6	1.5 ± 0.51	1.4 ± 0.45	2.46 ± 1.36	1.16 ± 0.21	5.27 ± 2.8	**92.42 ± 81.72**	12.23 ± 7.43	**15.03 ± 5.81**
IL-1β	1.7 ± 0.72	1.2 ± 0.27	1.42 ± 0.57	1.15 ± 0.23	**26.55 ± 8.8**	**3673.4 ± 3599.1**	77.75 ± 31.53	**96.07 ± 25.74**
IL-12a	1.62 ± 0.68	1.25 ± 0.38	1.75 ± 0.79	1.4 ± 0.44	3.62 ± 1.9	**29.53 ± 0.43**	5.37 ± 3.92	**89.85 ± 60.30**
IL-12b	1.37 ± 0.94	1.29 ± 0.39	1.14 ± 0.43	1.68 ± 0.76	**108.96 ± 36.47**	**109.55 ± 79.82**	**128.58 ± 103.11**	**239.43 ± 77.25**
ARG1	1.95 ± 0.79	1.19 ± 0.34	1.41 ± 0.45	1.88 ± 0.75	0.55 ± 0.09	1.68 ± 0.30	0.49 ± 0.12	2.02 ± 0.36
YM1	1.87 ± 1.06	1.08 ± 0.19	1.31 ± 0.51	2.35 ± 1.17	2.91 ± 1.12	**184.47 ± 174.22**	6.48 ±4.07	**68.66 ± 23.88**
CD86	1.21 ± 0.3	1.56 ± 0.66	1.09 ± 0.22	1.3 ± 0.93	**21.2 ± 4.97**	**24.9 ± 4.51**	**66.85 ± 43.23**	**19.93 ± 7.52**
FcγR1	1.2 ± 0.28	1.10 ± 0.24	1.12 ± 0.26	1.36 ± 0.55	**13.45 ± 3.05**	**59 ± 34.83**	**9.11 ± 2.61**	**18.44 ± 2.65**
FcγR3	1.49 ± 0.46	1.05 ± 0.15	1.14 ± 0.31	1.27 ± 0.44	**4.9 ± 0.83**	**36.28 ± 10.41**	**4.89 ± 1.61**	**13.64 ± 1.17**
TGFβ1	1.45 ± 0.61	1.29 ± 0.40	1.07 ± 0.19	1.23 ± 0.26	1.58 ± 0.33	**3.53 ± 0.83**	1.95 ± 0.28	1.95 ± 0.74
SPHK1	2.01 ± 1.28	1.07 ± 0.18	1.46 ± 0.60	1.58 ± 0.77	**0.06 ± 0.02**	**8.23 ± 2.69**	**0.19 ± 0.03**	2.21 ± 0.28

Table 2.3 Soluble and insoluble Aβ levels measured by ELISA. Bolded font indicates $p<0.05$ compared to GFP-AAV of the same time point.

		Soluble (pg/μg protein)			Insoluble (pg/μg protein)		
AAV Injection	Survival (months)	$A\beta_{1-38}$	$A\beta_{1-40}$	$A\beta_{1-42}$	$A\beta_{1-38}$	$A\beta_{1-40}$	$A\beta_{1-42}$
GFP-AAV	4	1.67 ± 0.77	2.97 ± 0.28	12.90 ± 2.24	9.04 ± 1.99	98.70 ± 36.77	903.27 ± 56.1
GFP-AAV	6	3.16 ± 0.75	5.10 ± 0.44	25.37 ± 3.81	23.82 ± 2.83	335.53 ± 64.95	1634.87 ± 397.9
IFNγ-AAV	4	3.68 ± 0.23	**5.41 ± 0.91**	27.17 ± 4.94	20.56 ± 8.48	295.78 ± 87.63	2855.26 ± 1267.9
IFNγ-AAV	6	4.95 ± 0.51	6.57 ± 0.89	38.90 ± 7.35	27.10 ± 4.10	269.72 ± 55.2	2047.32 ± 436.0

Discussion

Alzheimer's disease, while characterized by Aβ plaques and neurofibrillary tangles, is associated with a robust neuroinflammatory response. Using the macrophage classification system of M1, M2a, M2b and M2c (79, 209) we recently showed that the neuroinflammatory state is highly variable in the early stages of Alzheimer's disease (95). This variability was apparent in a population that were clinically and pathologically indistinguishable suggesting that neuroinflammation may be a source of variability in the Alzheimer's population. Furthermore, we hypothesize the neuroinflammatory state will influence progression of the disease and also response to therapeutic interventions. To better determine the role these distinct neuroinflammatory phenotypes have on Aβ pathology, we developed AAV vectors to express IFNγ, the initiator of an M1 neuroinflammatory state (221, 222), with the goal of chronically polarizing the state of the brain to an M1 state. We then injected this into the brains of APP/PS1 mice and examined their pathological progression 4 and 6 months post-injection. Overall, our data suggest that while initially we did polarize the phenotype to M1, by 6 months the neuroinflammatory phenotype showed a combination of M1 and M2. Aβ deposition was unaffected by the M1 phenotype but increased when the combination of inflammatory markers were increased. Whether this increase in Aβ is due to the M2 phenotypes direct actions or indirect actions on the M1 microglia remains unclear.

Macrophage activation can be categorized as M1, M2a, M2b and M2c. M1 is characterized by high IL-12 and low IL-10 while the M2 phenotypes are

characterized by high IL-10 and low IL-12 (210). Additionally, M1 macrophages express high levels of IL-1β, TNFα and IL-6 (79). M2a macrophages are associated with wound healing and repair gene expression including YM1 and ARG1 (210). The M2b phenotype is very much like an M1 phenotype with the exception of the IL-10/IL-12 balance and high expression of CD86 (210). Finally, the M2c state is characterized by high TGFβ and SPHK1 (79, 211). IFNγ, with and without LPS or TNFα, is the typical M1 phenotype stimulus (221, 222). Using BV2 microglial cell cultures, we have previously shown that treatment of BV2 cells with IFNγ results in an M1 phenotype (80). We hypothesized that a continuous presence of IFNγ would chronically polarize the inflammatory state of the brain to an M1 state. We found that expression of IFNγ through intracranial injection of IFNγ-AAV successfully induced an M1 phenotype at 4 months post-injection, but over time this transitioned to a combined M1 and M2 phenotype by 6 months. Both the early M1 phenotype and the 6 month transition to a mixed phenotype were present in both wildtype and APP/PS1, indicating that the APP/PS1 mice and wildtype mice responded similarly to the IFNγ-AAV injection.

CD11b (CR3) has been used as one of a handful of microglial activation markers. In the mouse, CD11b labels all ramified, resting microglia while GFAP labels astrocytes and the intensity of the staining is generally increased with inflammatory stimuli (220, 223, 224). There is an assumption in the field that microglial activation and astrogliosis correspond to high levels of pro-inflammatory cytokines such as IL-1β and IL-6. In the current study, we find that CD11b immunostaining is not affected by the IFNγ-AAV injection at the 4 month

time point, when the neuroinflammatory state is primarily M1, but is only increased when M2 markers are also increased. We also find that GFAP staining decreases when M2 markers increase even though M1 genes are still high. These data suggest that more careful analysis of neuroinflammatory markers is necessary for appropriate interpretation of data. The CD11b data here would indicate that inflammation is only increased at the 6 month time point, yet, we see that at the 4 month time point IL-1β and IL-12 are significantly elevated.

The role of neuroinflammation on Aβ deposition remains controversial. Studies with LPS injection have shown both decreases and increases in Aβ with neuroinflammation (83, 217, 225). Additionally, microglial “activation” has been linked to both increased and decreased Aβ loads (223, 225). Our goal in this study was to determine the influence of an M1 neuroinflammatory phenotype on Aβ deposition. At the 4 month time-point, when M1 neuroinflammation predominates in the brains of mice injected with IFNγ-AAV, Aβ deposition appears unaffected with no significant difference between IFNγ-AAV and GFP-AAV injected mice. We do find increased Aβ deposition at the 6 month time point but this is in the presence of a mixed neuroinflammatory phenotype. At this time-point we see not only M1 markers including IL-12, IL-1β and IL-6, but also M2a marker YM1. This is not the first time that M1 markers have been associated with unchanging, or decreased Aβ deposition (215). Indeed, anti-Aβ immunotherapy initiates activation of M1 markers (89). Furthermore, we have previously shown that lithium treatment results in unchanging biochemical levels of Aβ but increased Aβ deposition accompanied by increased expression of M2a markers

YM1, ARG1 and IL-1 receptor antagonist (94). In this study we also see relatively unchanging biochemical levels of Aβ, increased Aβ deposition shown by an increase in Aβ staining and an increase in the expression of M2a markers at 6 months. This increase in Aβ staining at 6 months implies that a mixed neuroinflammatory phenotype increases Aβ burden. While the mechanism is unclear, it appears that an M2a phenotype promotes Aβ deposition in the absence of changing total Aβ levels. Future studies will attempt to elucidate the mechanism of this phenomenon.

Human data from Alzheimer's patients also shows a similar trend in neuroinflammatory switching. Our lab has previously shown that in early AD, patients are polarized towards either an M1 or an M2a phenotype (95). By end-stage AD, patients have a combined M1, M2a and M2c phenotype. Also, early AD patients polarized towards an M2a phenotype had an increased neuritic plaque load compared to those polarized towards an M1 phenotype. This suggests that the transition to a mixed phenotype is associated with disease progression and increased Aβ burden. Future studies on the effects of the neuroinflammatory phenotypes, especially an M2 phenotype, could provide possible therapeutic targets for AD progression and potential biomarkers to determine the stage of AD.

Conclusions

Expression of IFNγ through AAV successfully induced an M1 phenotype at 4 months that transitioned to a mixed phenotype by 6 months. This transition also appeared with an increase in Aβ burden suggesting that a mixed phenotype, or

enhanced expression of M2a and M2c markers, could contribute to increasing Aβ burden and disease progression.

Chapter 3

Hyperhomocysteinemia induced gene expression changes in astrocytes, microglia, endothelial cells and neurons

Erica M. Weekman[1,2], Abigail E. Woolums[1], Tiffany L. Sudduth[1], and Donna M. Wilcock[1,2]*

[1]Sanders-Brown Center on Aging, [2]Department of Physiology, University of Kentucky, Lexington, Kentucky, United States of America

Abstract

High levels of homocysteine, termed hyperhomocysteinemia, is a risk factor for vascular cognitive impairment, which is the second leading cause of dementia. While hyperhomocysteinemia induces microhemorrhages and cognitive decline in mice, the effects of hyperhomocysteinemia on each cell type remains unknown. Therefore, we determined the gene expression changes of separate cell cultures of astrocytes, microglia, endothelial cells and neurons after treatment with high levels of homocysteine for 24, 48, 72 and 96 hours. Astrocytes showed decreased levels of several potassium channels and aquaporin 4 up to 72 hours and an increase in matrix metalloproteinase 9 at 48 hours. Gene changes in microglia indicated an initial pro-inflammatory response at 48 hours, which transitioned to an anti-inflammatory response by 72 hours. Endothelial cells showed a disruption in several tight junction proteins at 72 hours and neurons had gene changes in kinases and phosphatases as well as changes in potassium channel gene expression. Overall, this data provides insight into the

specific effects of high levels of homocysteine and offers several possible therapeutic targets for vascular cognitive impairment.

Introduction

Homocysteine is a non-protein forming amino acid involved in the production of both methionine and cysteine. Mutations in the methylenetetrahydrofolate reductase or cystathionine beta synthase genes, or low levels of vitamins B6, B9 and B12 cause increased levels of plasma homocysteine (199, 226-229), termed hyperhomocysteinemia (HHcy). HHcy is a risk factor for both vascular cognitive impairment and dementia (VCID) and Alzheimer's disease (AD) (185, 186, 230); however, the mechanism of how HHcy leads to VCID or AD remains unknown.

Our lab has been working on HHcy induction in mice as a model of VCID. Alone, dietary HHcy induction through deficiency in vitamins B6, B9 and B12 and enrichment in methionine results in cognitive impairment, microhemorrhages, reduced cerebral blood flow and neuroinflammation (203). Induction of HHcy in APP/PS1 mice produces a co-morbidity mouse model producing aspects of both AD and VCID (204). The co-morbidity mouse model displayed additive cognitive deficits on the radial arm water maze. They also displayed significant increases in microglial staining and a switch from an anti-inflammatory phenotype to a pro-inflammatory phenotype. While there weren't significant changes in total Aβ levels, we did see a change in the location of Aβ, with more accumulating around the vasculature. We also saw a significant increase in microhemorrhages and matrix metalloproteinase 9 (MMP9) and MMP2 activity.

It has been unclear, from our in vivo studies, what the effects of homocysteine are on the individual cell types of the brain, which could help us elucidate possible therapeutic targets. To determine the cell specific effects of HHcy, we took separate cultures of C8-D1A astrocytes, BV2 microglia cells, N2a neurons and primary endothelial cells and treated them with 50μM of homocysteine for 24, 48, 72 and 96 hours. For each cell type, we analyzed the gene expression of several cell type specific markers, inflammatory markers and MMP9 system markers.

Methods

C8-D1A cell culture: C8-D1A cells were obtained directly from American Type Culture Collection (Catalogue No. CRL-2541, Manassas, VA). Cells were grown in 75 cm^2 flasks in DME media containing 10% fetal bovine serum and 1% penicillin-streptomycin (Life Technologies, Carlsbad, CA) until approximately 80% confluency was reached, usually after 7 days.

BV2 cell culture: BV2 cells, originally developed by Elisabetta Blasi (231), (courtesy of Dr. Linda Van Eldik) were grown in petri dishes in FX12 media containing 10% fetal bovine serum, 1% serum L-glutamate, and 1% penicillin-streptomycin (Life Technologies, Carlsbad, CA) until approximately 80% confluency was reached, usually after 3 days.

Primary endothelial cell culture: C57BL/6 mouse primary brain microvascular endothelial cells were obtained directly from Cell Biologics (Catalogue No. C57-6023, Chicago, IL). Cells were grown in 75 cm^2 flasks coated with a gelatin based coating solution (Cell Biologics, Chicago, IL). Endothelial cell media containing

vascular endothelial growth factor, endothelial cell growth supplement, heparin, epidermal growth factor, hydrocortisone, L-glutamine, an antibiotic-antimycotic solution and fetal bovine serum (Complete Mouse Endothelial Cell Medium w/ Kit, Cell Biologics, Chicago, IL) was used to grow the endothelial cells to approximately 80% confluency.

N2a cell culture: N2a cells (courtesy of Dr. John Gensel) (232) were grown in 75 cm^3 flasks in Optimem media containing 40% DME media, 10% fetal bovine serum, and 1% penicillin-streptomycin (Life Technologies, Carlsbad, CA) until approximately 80% confluency was reached, usually after 3 days.

HHcy treatment: Once the cells reached 80% confluency, the cells were trypsinized and re-suspended in 10mL of serum-free media. For the BV2 and N2a cells, 100μl of cells were placed in each well of a 6 well plate. For the C8-D1A cells, 500μL of cells were placed in each well of a 6 well plate. For the endothelial cells, 1mL of cells were placed in a $25cm^2$ flask coated with a gelatin based coating solution. For all cells, the volume in each well or flask was brought up to 2mL. No obvious cell death occurred while the cells were in serum free media. Once the cells reached 60-70% confluency, media was replaced with either serum-free media as the no-treatment control or 50μM homocysteine solution (Sigma, St. Louis, MO) in serum-free media, which is a moderate level of hyperhomocysteinemia. Cells were incubated at 5% CO_2 at 37° for 24, 48, 72, and 96 hours before removal. Media was aspirated and cells were rinsed in 1X DPBS (Life Technologies, Carlsbad, CA) and frozen at -20° until RNA isolation.

Cell treatments were run at least twice for each cell line in groups of two or three (N=4-6 per group).

Quantitative RT-PCR: Cell RNA was extracted from the frozen cells using cells scrapers in RLT buffer from the RNeasy Mini-kit (Qiagen, Valencia, CA). The subsequent steps of the extraction were done according to the manufacturer's instructions. The Biospec-Nano Spectrophotometer (Shimadzu, Kyoto, Japan) was used to quantify the nucleic acid concentration of each sample. cDNA was produced using the High Capacity kit (ThermoFisher, Walthan, MA) according to the manufacturer's instructions. The cDNA was produced using the Veriti™ 96-well Thermocycler (Applied Biosystems, Grand Island, NY) through heating and annealing cycles.

RT-PCR was performed using the Fast-TaqMan Gene Expression kit (Life Technologies, Carlsbad, CA) in 96-well plates. In each well, 1μL of the appropriate gene probe (Life Technologies, Carlsbad, CA) listed in Table 3.1 was added to 10μL of the Fast-TaqMan reagent along with 0.5μL of cDNA and 6.5μL of RNAse-free water for a final volume of 18μL. Real-time RT-PCR was performed using the ViiA™7 Real Time PCR system (Applied Biosystems, Grand Island, NY). All genes were normalized to the 18S rRNA gene. Fold change was determined using the $-\Delta\Delta Ct$ method and the homocysteine treated cells were compared to the control cells of the appropriate time point.

Analysis: Data are presented as mean ± SEM. Statistical analysis was performed using the JMP statistical analysis software program (SAS Institute,

Cary, NC). Student's t-test were performed and statistical significance was assigned when the P-value was <0.05.

Results

Astrocytes: Astrocytes treated with homocysteine show a trend for decreased aquaporin 4 (AQP4) levels up to 72 hours and then increase again at 96 hours; however this was not significant when compared to controls (Figure 3.1A). Glial fibrillary acidic protein (GFAP) levels increased up to 72 hours and then decreased at 96 hours, but again this was not significant when compared to controls. The ATP-sensitive inward rectifier potassium channel 10 (KCNJ10) had significantly increased gene expression levels at 24 hours when compared to controls. However by 48 and 72 hours levels were significantly decreased when compared to the 24 hour HHcy treated cells (Figure 3.1B). Levels of KCNJ10 were significantly increased at 96 hours when compared to 72 hour HHcy treated cells.

While there were no significant changes in the pro-inflammatory marker tumor necrosis factor alpha (TNFα) (Figure 3.1C), there was a significant decrease in the anti-inflammatory marker interleukin 1 receptor antagonist (IL1Ra) at 48 hours when compared to controls. There was also an overall trend for decreased IL1Ra up to 72 hours and then an increase at 96 hours. The other anti-inflammatory marker transforming growth factor beta 1 (TGFβ1) was increased at 48 hours but decreased at 72 hours.

There was a slight increase in MMP3 expression in astrocytes treated with homocysteine over the 96 hours, but this was not significant (Figure 3.1E).

However, MMP9 expression was significantly increased at 48 hours when compared to controls. Levels were significantly decreased again at 72 and 96 hours when compared to the 48 hour treated homocysteine cells (Figure 3.1F). Tissue inhibitor of matrix metalloproteinase 1 (TIMP1) gene expression levels increased over time with 96 hours significantly different from controls and 24 and 48 hour treated homocysteine cells.

Microglia: Microglia cells treated with homocysteine had an increase in the pro-inflammatory markers IL1β and TNFα and an increase in the anti-inflammatory marker TGFβ1 with peaks at 48 hours (Figure 3.2A). Levels decreased at 72 hours and again at 96 hours when compared to 48 hour homocysteine treated cells (Figure 3.2B). IL1Ra levels were significantly increased at 72 hours compared to controls and 48 hour homocysteine treated cells. Levels were significantly decreased by 96 hours when compared to 72 hour homocysteine treated cells. Cluster of differentiation 86 (CD86) had slight increases up to 72 hours and a decrease at 96 hours that was significantly different from the 72 hour homocysteine treated cells.

MMP9 levels were slightly increased at 24 hours but were significantly increased at 72 hours when compared to controls (Figure 3.2C) and 24, 48 and 96 hour homocysteine treated cells (Figure 3.2D). TIMP1 levels were significantly increased at 96 hours when compared to controls and 48 and 72 hour homocysteine treated cells.

Endothelial cells: Endothelial cells treated with homocysteine showed no changes in platelet endothelial cell adhesion molecule 1 (PECAM1) gene

expression levels over the 96 hours (Figure 3.3A). Claudin-5 (CLDN5) levels had increasing levels with a peak at 72 hours. Levels were significantly decreased at 96 hours when compared to 72 hour homocysteine treated cells (Figure 3.3B). Occludin (OCEL1) levels were significantly decreased at 48 hours when compared to controls but levels were significantly higher at 72 hours when compared to 48 and 96 hour homocysteine treated controls. Collagen type IV alpha 5 (COL4α5) had decreased levels with a peak at 72 hours. Levels were significantly increased at 96 hours when compared to all other homocysteine treated cells.

While there were no changes in TGFβ1, mannose receptor C type 1 (MRC1) had slightly increased levels 24 and 48 hours but decreases at 72 and 96 hours (Figure 3.3C, D).

Endothelial cells treated with homocysteine had significantly increased levels of MMP3 at 48 hours when compared to controls (Figure 3.3E). However, MMP9 levels, while slightly increased at 24 hours, were significantly decreased at 48 and 96 hours when compared to 24 hour homocysteine treated cells (Figure 3.3F). Levels were returned to normal at 72 hours. TIMP1 was only slightly increased at 48 hours with no significant changes.

Neurons: Neural cells treated with homocysteine had slight increases in amyloid precursor protein (APP) and granulin (GRN) at 48 hours but levels decreased at 72 hours and further decreased at 96 hours (Figure 3.4A). Both glycogen synthase kinase 3 beta (GSK3β), serine/threonine-protein phosphatase 2A (PPP2CA), and KCNMA1 increased up to 72 hours but decreased at 96 hours

when compared to 72 hour homocysteine treated cells (Figure 3.4B). KCNJ10 had significantly increased levels at 48 hours when compared to controls and levels were significantly decreased at 72 hours when compared to 48 hour homocysteine treated cells.

The pro-inflammatory marker TNFα had increased gene expression at 48 hours but returned to normal at 72 hours; however, this was not significant (Figure 3.4C). All the anti-inflammatory markers (IL1Ra, CD86 and TGFβ1) showed increased levels with a significant peak at 72 hours when compared to controls. It should be noted that while the fold changes for these inflammatory markers are dramatic, the cycle numbers were high, indicating the expression level was low in these neural cells. CD86 and TGFβ1 were significantly decreased at 96 hours when compared to 72 hour homocysteine treated cells (Figure 3.4D).

Both MMP9 and TIMP1 only had increases at 72 hours with levels returning to normal at 96 hours (Figure 3.4E, F).

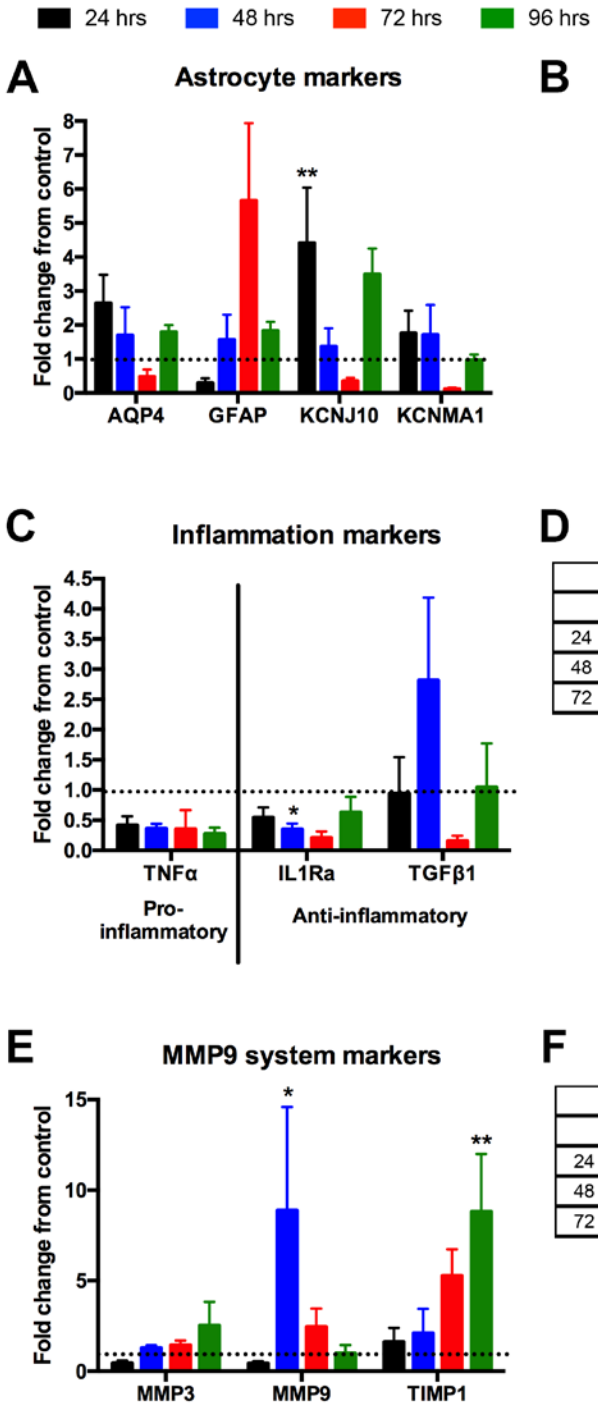

	AQP4			GFAP		
	48	72	96	48	72	96
24	0.39	0.07	0.51	0.7	0.1	0.63
48	X	0.32	0.94	X	0.2	0.93
72	X	X	0.35	X	X	0.21
	KCNJ10			KCNMA1		
	48	72	96	48	72	96
24	**0.02**	**0**	0.44	0.96	0.14	0.42
48	X	0.44	0.09	X	0.16	0.47
72	X	X	**0.02**	X	X	0.43

	TNFα			IL1Ra			TGF1β		
	48	72	96	48	72	96	48	72	96
24	0.95	0.94	0.87	0.82	0.69	0.92	0.23	0.61	0.95
48	X	0.99	0.93	X	0.87	0.74	X	0.11	0.26
72	X	X	0.93	X	X	0.61	X	X	0.57

	MMP3			MMP9			TIMP1		
	48	72	96	48	72	96	48	72	96
24	0.54	0.47	0.12	**0.01**	0.51	0.85	0.83	0.08	**0.001**
48	X	0.92	0.37	X	**0.04**	**0.01**	X	0.14	**0.003**
72	X	X	0.43	X	X	0.62	X	X	0.09

Figure 3.1 Astrocyte gene expression after HHcy treatment.

Relative gene expression of (A) astrocyte specific markers, (C) inflammatory markers, and (E) MMP9 system markers. Data are shown as a fold change from

the control cells at the appropriate time point. * indicates P<0.05, ** indicates P<0.01 compared to control cells at the appropriate time point. P values for homocysteine treated comparisons for (B) astrocyte specific markers, (D) inflammatory markers, and (F) MMP9 system markers. Significant differences are shown in bold.

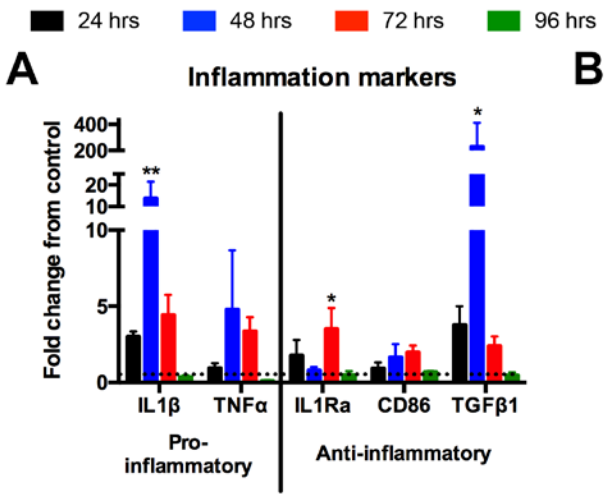

B

	IL1β			TNFα		
	48	72	96	48	72	96
24	**0.01**	0.73	0.53	0.06	0.21	0.68
48	X	**0.02**	**0**	X	0.48	**0.03**
72	X	X	0.31	X	X	0.11
	IL1Ra			CD86		
	48	72	96	48	72	96
24	0.34	0.09	0.21	0.24	0.1	0.73
48	X	**0.01**	0.76	X	0.61	0.13
72	X	X	**0**	X	X	**0.05**
	TGFβ1					
	48	72	96			
24	**0.02**	0.99	0.97			
48	X	**0.02**	**0.02**			
72	X	X	0.98			

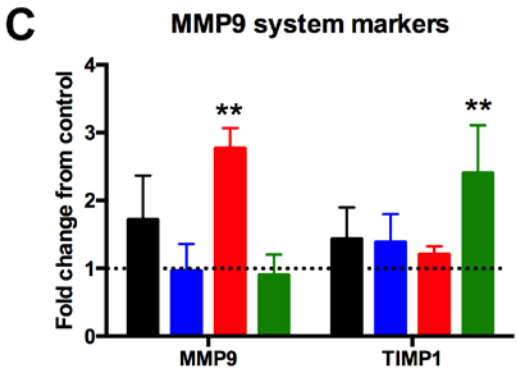

D

	MMP9			TIMP1		
	48	72	96	48	72	96
24	0.15	**0.045**	0.12	0.94	0.65	0.05
48	X	**0.001**	0.9	X	0.7	**0.045**
72	X	X	**0.0007**	X	X	**0.02**

Figure 3.2 Microglia gene expression after HHcy treatment.

Relative gene expression of (A) inflammatory markers and (C) MMP9 system markers. Data are shown as a fold change from the control cells at the appropriate time point. * indicates P<0.05, ** indicates P<0.01 compared to control cells at the appropriate time point. P values for homocysteine treated comparisons for (B) inflammatory markers and (D) MMP9 system markers. Significant differences are shown in bold.

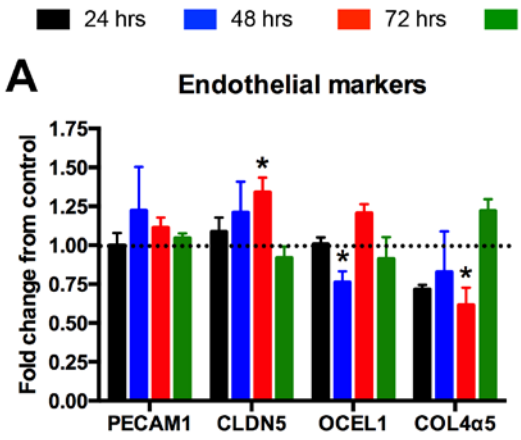

B

	PECAM1			CLDN5		
	48	72	96	48	72	96
24	0.23	0.54	0.8	0.41	0.1	0.27
48	X	0.55	0.33	X	0.39	0.06
72	X	X	0.71	X	X	**0.01**
	OCEL1			COL4α5		
	48	72	96	48	72	96
24	0.05	0.11	0.45	0.54	0.59	**0.01**
48	X	**0.001**	0.22	X	0.25	**0.04**
72	X	X	**0.02**	X	X	**0.003**

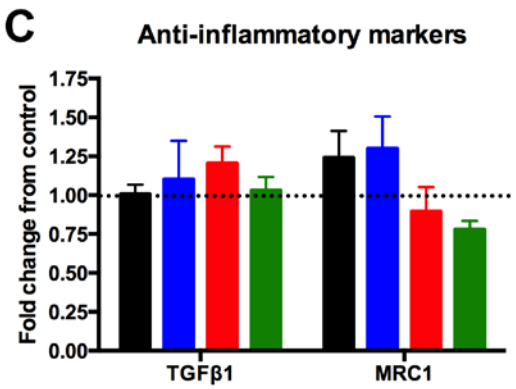

D

	TGFβ1			MRC1		
	48	72	96	48	72	96
24	0.6	0.28	0.9	0.79	0.14	0.05
48	X	0.57	0.69	X	0.09	**0.03**
72	X	X	0.33	X	X	0.62

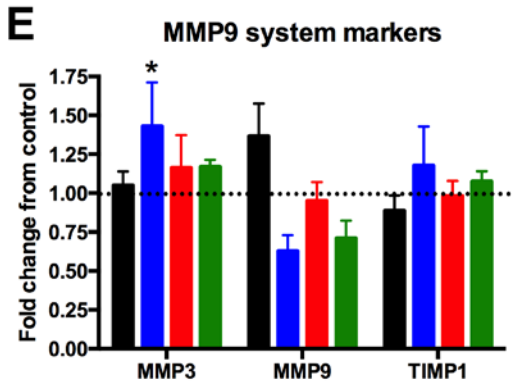

F

	MMP3			MMP9		
	48	72	96	48	72	96
24	0.07	0.58	0.55	**0.002**	0.06	**0.01**
48	X	0.19	0.21	X	0.14	0.7
72	X	X	0.97	X	X	0.27
	TIMP1					
	48	72	96			
24	0.1	0.58	0.28			
48	X	0.26	0.55			
72	X	X	0.59			

Figure 3.3 Endothelial cell gene expression after HHcy treatment.

Relative gene expression of (A) endothelial cell specific markers, (C) inflammatory markers, and (E) MMP9 system markers. Data are shown as a fold change from the control cells at the appropriate time point. * indicates $P<0.05$

compared to control cells at the appropriate time point. P values for homocysteine treated comparisons for (B) endothelial specific markers, (D) inflammatory markers, and (F) MMP9 system markers. Significant differences are shown in bold.

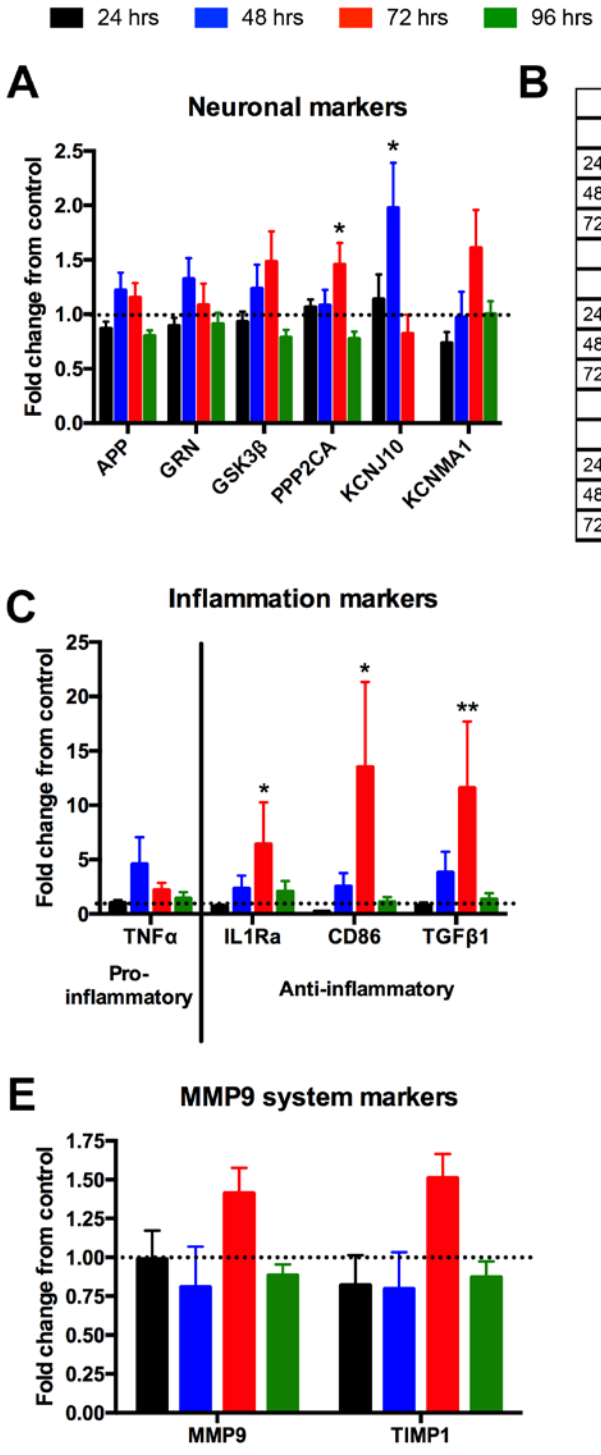

B

	APP			GRN		
	48	72	96	48	72	96
24	0.05	0.11	0.72	**0.046**	0.37	0.94
48	X	0.71	**0.02**	X	0.26	0.06
72	X	X	0.05	X	X	0.41
	GSK3β			PPP2CA		
	48	72	96	48	72	96
24	0.23	**0.03**	0.57	0.93	**0.03**	0.11
48	X	0.33	0.08	X	**0.04**	0.09
72	X	X	**0.01**	X	X	**0.0004**
	KCNJ10			KCNMA1		
	48	72	96	48	72	96
24	**0.046**	0.47	X	0.46	**0.01**	0.4
48	X	**0.02**	X	X	**0.049**	0.92
72	X	X	X	X	X	0.06

D

	TNFα			IL1Ra		
	48	72	96	48	72	96
24	**0.03**	0.45	0.79	0.49	**0.02**	0.55
48	X	0.14	0.05	X	0.1	0.9
72	X	X	0.62	X	X	0.07
	CD86			TGFβ1		
	48	72	96	48	72	96
24	0.64	**0.01**	0.86	0.4	**0.004**	0.87
48	X	**0.02**	0.74	X	**0.03**	0.47
72	X	X	**0.01**	X	X	**0.005**

F

	MMP9			TIMP1		
	48	72	96	48	72	96
24	0.52	0.14	0.71	0.93	**0.02**	0.85
48	X	**0.04**	0.79	X	**0.01**	0.79
72	X	X	0.07	X	X	**0.03**

Figure 3.4 Neural cell gene expression after HHcy treatment.

Relative gene expression of (A) neuron specific markers, (C) inflammatory markers, and (E) MMP9 system markers. Data are shown as a fold change from

the control cells at the appropriate time point. * indicates P<0.05, ** indicates P<0.01 compared to control cells at the appropriate time point. P values for homocysteine treated comparisons for (B) neuronal specific markers, (D) inflammatory markers, and (F) MMP9 system markers. Significant differences are shown in bold.

Table 3.1 Genes for RT-PCR.

Gene of interest	PMID	Taqman ID
IL1β	NM_008361.3	Mm.222830
TNFα	NM_013693.3	Mm.1293
IL1Ra	NM_031167.5	Mm.882
CD86	NM_019388.3	Mm.1452
TGF1β	NM_011577.1	Mm.248380
MRC1	NM_008625.2	Mm.2019
MMP3	NM_010809.1	Mm.4993
MMP9	NM_013599.3	Mm.4406
TIMP1	NM_001044384.1	Mm.8245
AQP4	NM_009700.2	Mm.250786
GFAP	NM_001131020.1	Mm.1239
KCNJ10	NM_001039484.1	Mm.254563
KCNMA1	NM_001253358.1	Mm.343607
PECAM1	AK037551.1	Mm.343951
CLDN5	NM_013805.4	Mm.22768
OCEL1	NM_008756.2	Mm.4807
COL4α5	NM_001163155.1	Mm.286892
APP	NM_001198823.1	Mm.277585
GRN	NM_008175.4	Mm.1568
GSK3β	NM_019827.6	Mm.394930
PPP2CA	NM_019411.4	Mm.00479816

Discussion

HHcy is a risk factor for both VCID and AD, the two most common forms of dementia. Our lab has developed a mouse model that induces HHcy to model VCID. In this mouse model, we see cognitive deficits, an increase in microglial staining, a pro-inflammatory phenotype and a significant increase in microhemorrhages (203). While we know the overall effect of HHcy on the brain, there is limited information on the cell specific effects of HHcy. We took cell cultures of astrocytes, microglia, endothelial cells and neural cells and treated them with homocysteine to determine gene expression changes. Astrocytes showed a decrease in several potassium channels and AQP4 with lows at 72 hours. Microglia cells showed an initial increase in pro-inflammatory markers at 48 hours but then an increase in anti-inflammatory markers at 72 hours. Endothelial cells showed an increase in claudin-5 up to 72 hours but a decrease in occludin. Neural cells treated with homocysteine showed an increase in several cell specific markers and anti-inflammatory markers with peaks at 72 hours.

Inflammation has been implicated as a possible mechanism for vascular damage in VCID (233) and induction of HHcy in mice to model VCID has shown a pro-inflammatory response (203), which can activate MMPs and lead to vascular breakdown and cognitive impairment. Inflammation has also been implicated in the disease process of AD and our co-morbidity mice show a switch from an anti-inflammatory phenotype to a pro-inflammatory phenotype. Both microglia and astrocytes are capable of secreting inflammatory cytokines and

proteases (234, 235) in response to a variety of different stimuli, thus controlling the inflammatory phenotype. When treated with HHcy in vitro, microglia show a transition from a pro-inflammatory response at 48 hours to an anti-inflammatory response at 72 hours. While our mouse models show a pro-inflammatory phenotype when on diet for 6 months, this cell data suggests that long-term exposure to HHcy would ultimately result in a switch to an anti-inflammatory phenotype. Astrocytes, neural cells and endothelial cells show a limited inflammatory response to HHcy with slight increases in anti-inflammatory markers around 48 and 72 hours. This shows that only microglia, rather than microglia and astrocytes, are the inflammatory phenotype mediators when HHcy is present.

One of the major proteases involved in tight junction breakdown is MMP9 (130, 144), which can be activated via inflammation, specifically the pro-inflammatory cytokines TNFα and IL1β (113, 114). Our VCID mouse model shows a significant increase in activation of MMP9 as well as increases in TNFα and IL1β, providing a possible mechanism for the increase in microhemorrhages (203, 204). At 48 hours, astrocytes and endothelial cells are the major source of MMP9 and MMP3, which is the activator of MMP9, respectively. However, at 72 hours, microglia are the main source of MMP9. Treatment of individual cell types with homocysteine has provided insight into the major source of MMP9 at different time points.

The response of cell specific genes to homocysteine can also generate therapeutic targets for treatment of VCID. In astrocytes, AQP4, KCNJ10 and

KCNMA1 were decreased, similarly peaking at 72 hours. These potassium channels and AQP4 channel are associated with homeostatic control of potassium buffering, water balance and are located at the astrocytic end-feet (236-238). The decreases seen in these astrocytic end-feet genes could lead to disruption of the neurovascular unit and blood flow to these damaged areas, contributing to the cognitive decline seen in our mouse model. Endothelial cells also play a major role in the neurovascular unit by maintaining the tight junctions that make up the blood brain barrier. Interruption of these tight junctions and consequently the blood brain barrier can lead to microhemorrhages that damage the surrounding brain tissue. Treatment of endothelial cells with homocysteine showed a significant disruption in tight junctions as shown by the decrease in gene expression of occludin, thus providing another mechanism via which HHcy causes microhemorrhages and cognitive decline. HHcy is also a risk factor for AD (230), which is characterized by Aβ plaques and tangles made of hyperphosphorylated tau (4). Neural cells, the source of hyperphosphorylated tau, show increases in the tau kinase GSK3β at 72 hours compared to 24 hours and a significant increase in the tau phosphatase PPP2CA at 72 hours. These homocysteine induced gene expression changes could lead to changes in tau phosphorylation, thus increasing the chance of developing a tauopathy from HHcy.

The responses of specific cell types to homocysteine provide a wide variety of targets for therapeutics. For example, targeting microglia to reduce the release of pro-inflammatory cytokines could help reduce MMP9 activation leading

to a decrease in tight junction breakdown. Astrocytic end-feet present another possible target to help reduce neurovascular damage and cognitive decline. GSK3β could also be targeted to help reduce the risk of developing tauopathies in HHcy patients. The gene changes seen here have the potential to be biomarkers for VCID and when compared to gene changes seen in AD, possible biomarkers for patients with VCID and AD. Other future studies would include protein expression and activity assays to confirm the gene expression changes. While HHcy may alter gene expression, this does not always translate to a change in protein levels or changes in activity of the proteins.

Chapter 4

Reduced efficacy of anti-Aβ immunotherapy in a mouse model of amyloid deposition and vascular cognitive impairment co-morbidity

Erica M. Weekman[1,2], Tiffany L. Sudduth[1,2], Carly N. Caverly[1,2], Timothy J. Kopper[2], Oliver W. Phillips, Dave K. Powell[3,4], and Donna M. Wilcock[1,2]*

University of Kentucky, [1]Sanders-Brown Center on Aging, [2]Department of Physiology, [3]Magnetic Resonance Imaging and Spectroscopy Center, [4]Department of Biomedical Engineering, Lexington, KY 40536 USA

Abstract

Vascular cognitive impairment and dementia (VCID) is the second most common form of dementia behind Alzheimer's disease (AD). It is estimated that 40% of AD patients also have some form of VCID. One promising therapeutic for AD is anti-Aβ immunotherapy, which uses antibodies against Aβ to clear it from the brain. While successful in clearing Aβ and improving cognition in mice, anti-Aβ immunotherapy failed to reach primary cognitive outcomes in several different clinical trials. We hypothesized that one potential reason the anti-Aβ immunotherapy clinical trials were unsuccessful was due to this high percent of VCID co-morbidity in the AD population. We used our unique model of VCID-amyloid co-morbidity to test this hypothesis. We placed 9 month old wildtype and APP/PS1 mice on either a control diet or a diet that induces hyperhomocysteinemia (HHcy). After being placed on the diet for 3 months, the mice then received intraperotineal injections of either IgG2a control or 3D6 for another 3 months. While we found that treatment of our co-morbidity model with

3D6 resulted in decreased total Aβ levels, there was no cognitive benefit of the anti-Aβ immunotherapy in our AD/VCID mice. Further, microhemorrhages were increased by 3D6 in the APP/PS1/control, but further increased in an additive fashion when 3D6 was administered to the APP/PS1/HHcy mice. This suggests that the use of anti-Aβ immunotherapy in patients with both AD and VCID would be ineffective on cognitive outcomes.

Introduction

Alzheimer's disease (AD) is the most common form of dementia and is characterized pathologically by amyloid plaques, composed of aggregated amyloid beta (Aβ) peptide, and neurofibrillary tangles, comprised of hyperphosphorylated tau (4, 239). Vascular cognitive impairment and dementia (VCID) is the second most common form of dementia and results from disruptions in blood flow to the brain such as stroke, hypoperfusion of the brain, microhemorrhages, and vasogenic edema (240). VCID and AD are not mutually exclusive though; it is estimated that 40% of AD patients also have some form of VCID (59-61, 241).

The most common hypothesis for the progression of AD is the amyloid cascade hypothesis, which states that Aβ aggregation leads to hyperphosphorylation of tau and tangle formation, which then leads to neurodegeneration (17, 18). As the leading hypothesis for the progression of AD, amyloid deposition and brain Aβ have become popular targets for many AD therapeutics. Immunotherapy targeting Aβ has been one of the most promising therapeutic interventions for AD since its initial report in 1999 (29). Anti-Aβ

immunotherapy uses antibodies targeting Aβ to reduce brain Aβ burden. Proposed mechanisms of action include microglial recruitment and Fcγ receptor mediated phagocytosis (36, 38), catalytic disaggregation and solublization (47), and the peripheral sink mechanism (37). The relative contribution of each mechanism on the overall efficacy of the antibody likely relies on the isotype and epitope of the specific antibody (36, 38, 48, 49, 242).

While preclinical mouse model studies have repeatedly demonstrated significant efficacy of anti-Aβ immunotherapy, both in reducing Aβ burden and improving cognition (29, 31, 43, 243), the clinical trials have remained underwhelming, failing to meet primary endpoints for efficacy in a number of trials to date (46, 244). While there has been discussion in the field that one reason for the lack of efficacy in clinical trials is that the disease is too advanced, we hypothesize that one reason for the lack of efficacy in clinical trials is the co-morbidity of other dementia-causing pathologies, such as VCID, as well as AD pathology.

To test our hypothesis, we are using our recently developed mouse model of Aβ deposition co-morbid with VCID (APP/PS1 + HHcy) (204), which develops additive cognitive deficits and redistribution of amyloid favoring the deposition of cerebral amyloid angiopathy (CAA). Using our co-morbidity model, we administered 3D6, an anti-Aβ antibody, or IgG2a, a control antibody to test passive immunotherapy efficacy in a mixed dementia mouse model. We found that there was no cognitive benefit of immunotherapy in our co-morbidity model

despite comparable reductions in total Aβ burden. This was accompanied by a reduced immune response to the immunotherapy.

Methods

Animals: Female and male wildtype (WT) and APP/PS1 mice (C57BL/6 mice carrying human APPSwe and PS1-dE9 mutations) (170) were bred in house and aged 9 months. Thirty-five WT mice and thirty-three APP/PS1 mice were placed on either a diet with low levels of folate, vitamins B6 and B12 and enriched with methionine (HHcy study group) or a control diet with normal levels of folate, vitamins B6 and B12 and methionine (control study group). The HHcy diet was Harlan Teklad TD97345 and the control diet was Harlan Teklad 5001 C (both from Harlan Laboratories, Madison, WI, USA). Once mice had received the diet for 3 months, they began weekly intraperitoneal (IP) injections of either 3D6 or IgG2a at 10mg/kg (Eli Lilly, Indianapolis, IN, USA) for 3 months. The anti-Aβ antibody 3D6**,** which is an IgG2b isotype, binds to both soluble and insoluble Aβ at the extreme amino terminus ($A\beta_{1-5}$) (41, 245). Although the control antibody and the anti-Aβ antibody are not similar isotypes, they both have similar immune functions with IgG2a actually having a higher affinity for FcγR1 (246). Control IgG2a antibodies have been shown to have no effect on Aβ burden (245). This study was approved by the University of Kentucky Institutional Animal Care and Use Committee and conformed to the National Institutes of Health Guide for the Care and Use of Animals in Research. Behavioral testing and magnetic resonance imaging was also performed and an experimental timeline with the number of animals per group is shown in Figure 4.1A and B.

Behavior testing: Radial arm water maze (RAWM) testing was performed at the University of Kentucky Rodent Behavior Core. The two-day RAWM was carried out as previously described (247). Briefly, a six-arm maze was submerged in a pool of water with a goal platform placed at the end of one arm. Each mouse was subjected to 15 trials each day with the mouse starting in a different arm for each trial and the goal platform remaining in the same arm. The number of errors (the number of incorrect arm entries) was counted over a 60 second period. Errors were averaged for 3 trials resulting in ten blocks over the two days. Blocks 1-5 comprise Day 1 trials while blocks 6-10 comprise Day 2 trials.

Magnetic resonance imaging: A subset of study mice were imaged by T2* magnetic resonance imaging (MRI). Three to four mice from each group were imaged 3 months after starting diet but before beginning IP antibody injections, again half way through IP antibody injections, and a third time immediately before tissue collection. Mice were imaged with a 7-T Bruker ClinScan MRI system (Bruker, Billerica, MA, USA) with an MRI CryoProbe, delivering 2.5 times the signal to noise of a standard room temperature radiofrequency coil, located at the Magnetic Resonance Imaging and Spectroscopy Center at the University of Kentucky. Fourteen coronal slices were acquired with a FLASH sequence with a TR 165ms, TE 15.3ms, 25 degree flip angle, 448 x 448 matrix, 0.4 mm thick, 20% gap, 0.033 mm x 0.033 mm resolution, 10 averages, and TA 24 minutes. Mice were anesthetized with 1.3% isoflorane using an MRI compatible vaporizer. They were then positioned prone and held in place on the scanning bed using tooth and ear bars. The animals were maintained at 37° with a water heated

scanning bed. Body temperature, heart, and respiration rates were monitored. T2* MRI images were analyzed by one blinded investigator who identified abnormalities that resembled hemorrhagic infarcts. These infarcts were counted and this number was normalized to the number of images counted to provide a per section count.

Tissue processing and histology: After a lethal injection of Beuthanasia-D, blood was collected for plasma and mice were perfused intracardially with 25mL normal saline. Brains were removed rapidly and bisected in the midsaggital plane with the left side being immersion fixed in 4% paraformaldehyde for 24 hours. The right side was dissected with the frontal cortex and hippocampus flash frozen in liquid nitrogen and then stored at -80°C. The left hemibrain was passed through a series of 10, 20 and 30% sucrose solutions for cryoprotection before sectioning. Using a sliding microtome, 25μm frozen horizontal sections were collected and stored free floating in 1xDPBS containing sodium azide at 4°C.

Eight sections spaced 600μm apart were selected for free floating immunohistochemistry for CD11b (rat monoclonal, AbD Serotec, Raleigh, NC, USA, 1:1000 dilution) and total Aβ (rabbit polyclonal $A\beta_{1\text{-}16}$, Life Technologies, Carlsbad, CA, USA, 1:3000 dilution). Immunohistochemistry was performed as previously described (248). Stained sections were mounted, air dried overnight, dehydrated and coverslipped in DPX (Electron Microscopy Sciences, Hatfield, PA, USA). Analysis was performed by measuring the percent area occupied by positive immunostain using the Nikon Elements AR image analysis system (Melville, NY, USA) as described previously (94).

Eight sections spaced 600μm apart were mounted on slides and stained for Congo red and Prussian blue as previously described (43, 249). Neutral red was used as a counterstain for Prussian blue. Congo red analysis was performed using the ZEISS Axio Scan.Z1 Slide Scanner (Carl Zeiss Microscopy, Germany) and the Nikon Elements AR image analysis system (Melville, NY, USA).

Plasma was analyzed for total homocysteine by the Clinical Laboratory of the University of Kentucky Hospital Laboratories.

Aβ ELISA: Biochemical analysis of Aβ levels was performed as previously described (250). Briefly soluble protein was extracted from the right frontal cortex using PBS with complete protease and phosphatase inhibitor (Pierce Biotechnology Inc., Rockford, Il, USA). After centrifugation, the supernatant was labeled the “soluble” extract and the pellet was homogenized in 70% formic acid. After centrifugation and neutralization with 1M Tris-HCl, the supernatant was labeled the “insoluble” extract. Protein concentrations were determined using the BCA protein assay kit (Pierce Biotechnology, Inc., Rockford, Il, USA). The Meso-Scale Discovery multiplex ELISA system was used to measure $A\beta_{1-38}$, $A\beta_{1-40}$, and $A\beta_{1-42}$ levels in the soluble and insoluble extracts (V-PLEX Aβ Peptide Panel 1 (6E10) Kit**;** MSD, Gaithersburg, MD, USA).

Quantitative real-time PCR: RNA was extracted from the right hippocampus using the E.Z.N.A. Total RNA kit (Omega Bio-Tek, Norcross, GA, USA) according to the manufacturer’s instructions. RNA was quantified using the Biospec nano spectrophotometer (Shimaduz, Japan). cDNA was produced using the cDNA High Capacity kit (ThermoFisher, Grand Island, NY, USA) according to

the manufacturer's instructions. Real-time PCR was performed using the Fast TaqMan Gene Expression assay (ThermoFisher, Grand Island, NY, USA). In each well of a 96-well plate, 0.5μL cDNA (100ng, based on the RNA concentrations) was diluted with 6.5μL RNase-free water. One microliter of the appropriate gene probe was added along with 10μL of Fast TaqMan to each well. Target amplification was performed using the ViiA7 (Applied Biosystems, Grand Island, NY, USA). All genes were normalized to 18S rRNA and the fold change was determined using the $-\Delta\Delta Ct$ method. Results from all APP/PS1 mice were compared to APP/PS1 mice on control diet with IgG2a treatment. Table 2.1 shows the genes tested along with their PMID and Taqman ID.

Analysis: Data are presented as mean ± SEM. Statistical analysis was performed using the JMP statistical analysis software program (SAS Institute, Cary, NC, USA). Radial arm water maze data were analyzed by repeated-measures analysis of variance (ANOVA). We also performed student's t-test on individual block data for the radial arm water maze analysis. For other data, one-way ANOVA and student's t-test were performed. Statistical significance was assigned when the P-value was <0.05.

Results

Administration of a diet deficient in folate, vitamins B6 and B12 and enriched in methionine to 9-month-old WT and APP/PS1 mice for 6 months resulted in elevated plasma homocysteine levels as shown in Figure 4.1C. In C57BL/6 mice, a level of homocysteine between 5 and 12μmol/L is considered normal. Elevated levels of homocysteine can be categorized as mild, with levels

between 12 and 30μmol/L, moderate, with levels between 30 and 100μmol/L and severe, with levels above 100μmol/L. The mice on control diet had plasma HHcy levels below the detection range of the clinical assay. Mice on our normal house chow also have levels below the detection range showing that mice on the control diet have a normal level of homocysteine. Plasma homocysteine levels in our mice on the HHcy diet reached moderate to severe levels ranging from 67-145μmol/L in all cases, thus inducing hyperhomocysteinemia. Due to the high variability, the only comparison showing significant differences was between the APP/PS1 mice on control diet receiving 3D6 and the APP/PS1 mice on the HHcy diet receiving the 3D6 treatment (Figure 4.1C).

We performed the two-day radial arm water maze to identify changes in spatial memory. Over the two days of testing, the WT mice on control diet with IgG2a treatment learned the task. They started the task making an average of three errors in the first block and ended with less than one error in the last block (Figure 4.2A). WT mice on the HHcy diet had similar cognitive deficits as previously reported (203), with no effect of 3D6 or IgG2a (Figure 4.2A)**.** APP/PS1 mice on control diet with IgG2a treatment did not learn the task over the two days and were significantly impaired compared to WT mice on control diet with IgG2a treatment by block 10, as expected from APP/PS1 mice of this age (Figure 4.2B). APP/PS1 mice on control diet with 3D6 treatment began the task with an average of about 4 errors in block 1 and were making less than one error by the last block, indicating that they did learn the task and they were indistinguishable from the WT mice on control diet with IgG2a treatment. APP/PS1 mice on the HHcy

diet with either IgG2a or 3D6 treatment did not learn the task, making a similar amount of errors in the first and last block. At the end of day 2, they made significantly more errors than the WT mice on control diet with IgG2a treatment or the APP/PS1 mice on control diet with 3D6 treatment as shown in the block 10 data in Figure 4.2D. The APP/PS1/HHcy mice did not show the additive effects we have previously reported in this mixed pathology APP/PS1/HHcy mouse (204), however, as can be seen from the learning curve of the APP/PS1 mice, there was essentially a “ceiling effect”, likely due to the older age of the mice in the current study. Therefore, we were unable to detect any potential worsening resulting from the HHcy component.

Total Aβ immunohistochemistry was used to determine the efficacy of an anti-Aβ immunotherapy to reduce Aβ levels in our co-morbidity model. In the frontal cortex, total Aβ was significantly reduced in the APP/PS1 mice on control diet with 3D6 treatment compared to APP/PS1 mice on control diet with IgG2a treatment (Figure 4.3E). Levels were slightly reduced in the APP/PS1 mice on the HHcy diet with 3D6 treatment but did not reach significance. In the hippocampus, total Aβ was significantly reduced in both the APP/PS1 mice on control and HHcy diet with 3D6 treatment compared to APP/PS1 mice on control diet with IgG2a treatment (Figure 4.3A-E). When APP/PS1 mice on HHcy diet with control antibody were compared to APP/PS1 mice on HHcy diet with 3D6 antibody, there was no significant difference. Biochemical levels of Aβ were also measured and are shown in Figure 4.3F. No significant differences were found

among any of the groups, likely due to the high variation among the individual samples.

Congo red analysis showed that amyloid levels were reduced in the parenchyma following 3D6 treatment in APP/PS1 mice on both the control diet and the HHcy diet when they were compared to APP/PS1 mice on control diet with control antibody (Figure 4.4E). This effect was more pronounced in the hippocampus than the frontal cortex. In contrast to the total amyloid reductions, the APP/PS1 mice on the HHcy diet showed significant increases in CAA relative to the APP/PS1 mice on control diet. This effect was not influenced by 3D6 administration, replicating our previous report that HHcy leads to redistribution of amyloid to the vasculature (204). 3D6 administration in the APP/PS1 mice on control diet caused a modest increase in CAA relative to control antibody.

We used T2* MRI imaging to detect microhemorrhages as described previously (203). At the first imaging session, 3 months into the diet but immediately prior to the initiation of anti-Aβ immunotherapy, we found modest, non-significant increases in microhemorrhages resulting from the administration of the HHcy inducing diet, consistent with our previous reports (Figure 4.5B). Six weeks into immunotherapy treatment, we found that there were significant increases in microhemorrhages resulting from the HHcy inducing diet; however, the control IgG2a and 3D6 groups were still comparable. In contrast, 12 weeks into immunotherapy treatment, immediately prior to cognitive testing and tissue harvest, we found that microhemorrhage numbers were significantly greater in

the APP/PS1 mice on the HHcy or control diet receiving 3D6 antibody than either the APP/PS1 mice on control diet or the HHcy diet receiving IgG2a treatment.

Prussian blue histological analysis of microhemorrhages showed a significant increase in the number of microhemorrhages in each of the groups compared to APP/PS1 mice on control diet with IgG2a treatment (Figure 4.6B). The APP/PS1 mice on the HHcy diet with IgG2a treatment also had significantly more microhemorrhages when compared to the 3D6 treated APP/PS1 mice on control diet. Also, the APP/PS1 mice on the HHcy diet with 3D6 treatment had a significant increase in microhemorrhages compared to all the other groups. The majority of microhemorrhages were located in the parietal and occipital cortex with no differences in location between any of the groups. Images of a positive Prussian microhemorrhage are shown in Figure 4.6A.

One of the proposed mechanisms for anti-Aβ immunotherapy's reduction of Aβ involves activation of microglia leading to phagocytosis of Aβ. We performed immunohistochemistry for CD11b, which labels both activated and resting microglia, in order to determine if there was an increase in total microglia. In both the frontal cortex and the hippocampus, CD11b was slightly increased in the APP/PS1 mice on control diet with 3D6 treatment compared to the APP/PS1 mice on control diet with IgG2a treatment (Figure 4.7E**),** but this was not significant. CD11b staining was significantly reduced in the frontal cortex in the APP/PS1 mice on the HHcy diet with 3D6 treatment compared to the APP/PS1 mice on control diet with 3D6 treatment. In the hippocampus, the APP/PS1 mice on the HHcy diet with IgG2a or 3D6 treatment had significantly reduced levels of

CD11b staining compared to the APP/PS1 mice on control diet with 3D6 treatment (Figure 4.7A-E). The amount of CD11b staining was also slightly reduced in the APP/PS1 mice on the HHcy diet with IgG2a or 3D6 treatment compared to APP/PS1 mice on control diet with IgG2a treatment.

Using several genetic markers specific to a pro-inflammatory, wound healing/repair or immune complex mediated macrophage phenotype (251, 252), we characterized the neuroinflammatory response. The data in Figure 4.8 is shown as a fold change from the APP/PS1 mice on control diet with IgG2a treatment. The APP/PS1 mice on control diet with 3D6 treatment showed a significant increase in several pro-inflammatory markers (specifically IL1β and TNFα) and increases in several immune complex mediated genes (FcγR1 and FcγR3) (Figure 4.8A and C). The APP/PS1 mice on the HHcy diet with IgG2a treatment showed elevations in several wound healing/repair genes (ARG1) (Figure 4.8B). The APP/PS1 mice on the HHcy diet with 3D6 treatment only showed significant changes in some immune complex mediated genes (FcγR1 and FcγR3) (Figure 4.8C). There were also several significant increases in the expression of the MMP2 and MMP9 system markers as shown in Figure 4.8D. The APP/PS1 mice on control diet with 3D6 treatment showed a significant increase in MMP2, MMP3 and MMP9. The APP/PS1 mice on the HHcy diet showed an increase in MMP9 expression as well.

A

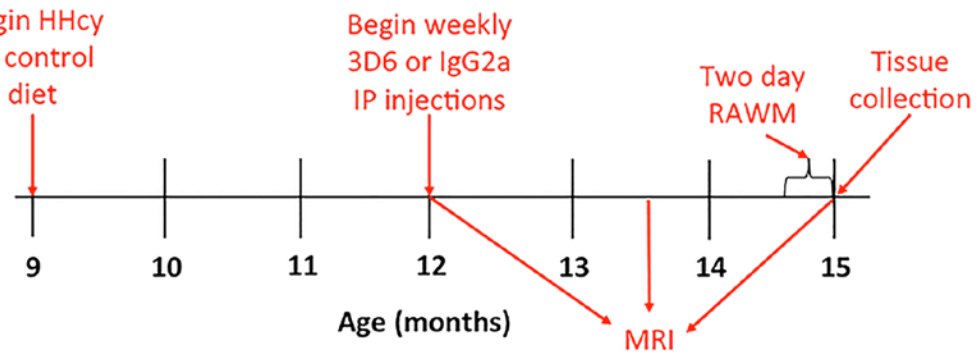

B

Genotype	Diet	Treatment
WT	Control	IgG2a (N=10; 3 females, 7 males)
		3D6 (N=11; 4 females, 7 males)
	HHcy	IgG2a (N=7; 2 females, 5 males)
		3D6 (N=7; 2 females, 5 males)
APP/PS1	Control	IgG2a (N=8; 3 females, 5 males)
		3D6 (N=8; 5 females, 3 males)
	HHcy	IgG2a (N=8; 4 females, 4 males)
		3D6 (N=9; 6 females, 3 males)

C

	Control Diet		HHcy Diet	
	IgG2a	3D6	IgG2a	3D6
APP/PS1	Below detection range	Below detection range	70.286 ± 26.385	145.433 ± 72.879
WT	Below detection range	Below detection range	67.400 ± 29.142	82.680 ± 21.408

Figure 4.1 Experimental setup. A) Mice were 9 months old when they began either the control or HHcy diet. After being on diet for 3 months, mice began a 3-month treatment of weekly IP injections of 3D6 or IgG2a at 10mg/kg. MRI was performed 3 months after starting the diet but before IP injection treatment, half way through treatment and immediately before tissue collection. The two-day radial arm water maze was also performed before tissue collection. B) Number of animals per experimental group. C) Quantification of plasma total homocysteine levels.

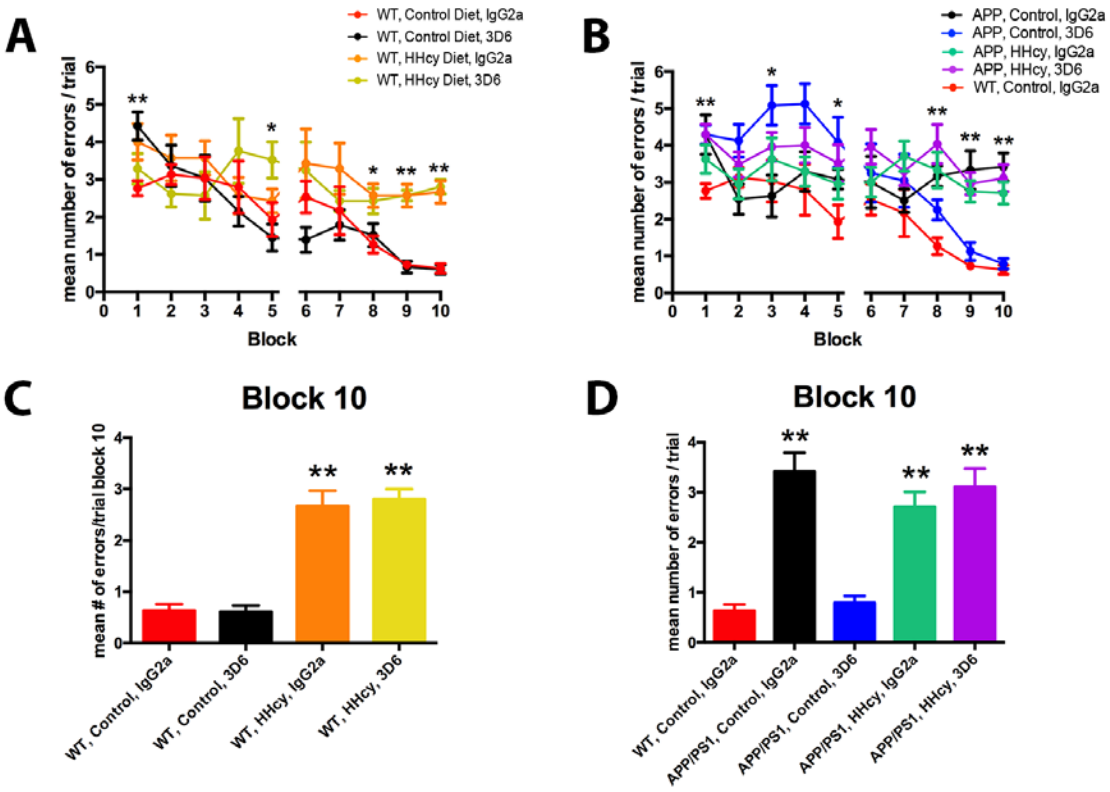

Figure 4.2 3D6 treatment does not improve cognition in APP/PS1 mice on the HHcy diet. Two-day radial arm water maze data is shown for WT mice (A) and APP/PS1 mice (B). The mean number of errors per trial was calculated for each block (each block is the average of three trials). * indicates P<0.05 and ** indicates P<0.01 by one-way ANOVA with all groups on each graph. Block 10 data is graphed for the WT mice (C) and the APP/PS1 mice (D). ** indicates P<0.01 compared to WT, control, IgG2a and WT, control, 3D6 for C and P<0.01 compared to WT, control, IgG2a and APP/PS1, control, 3D6 for D.

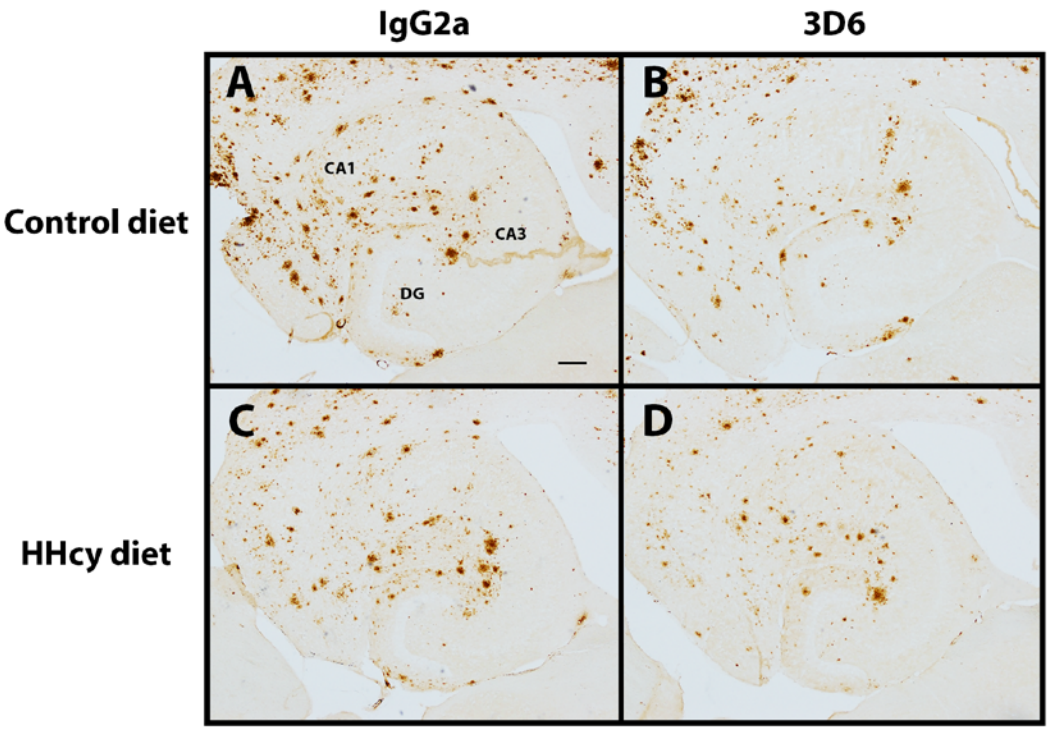

E

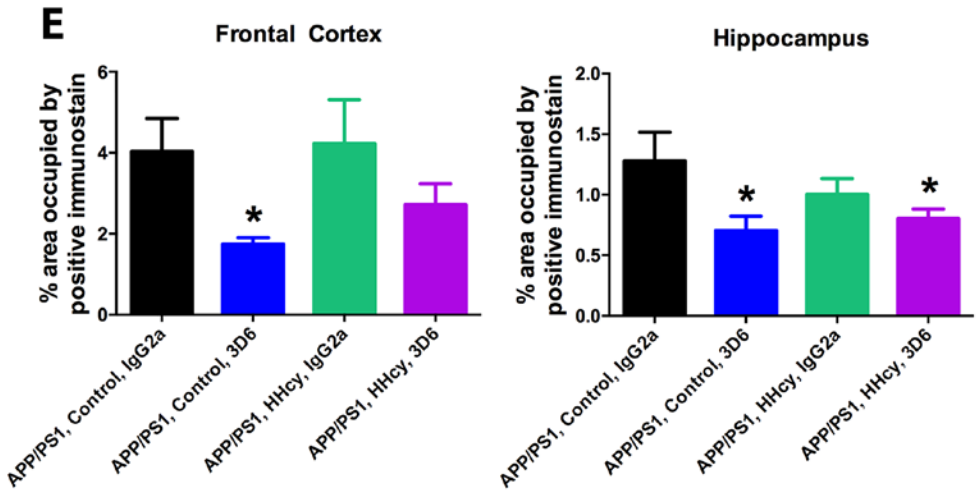

F

	Soluble (pg/μg)			Insoluble (pg/μg)		
	Aβ1-38	Aβ1-40	Aβ1-42	Aβ1-38	Aβ1-40	Aβ1-42
APP/PS1, Control, IgG2a	0.038 ± 0.009	0.875 ± 0.101	0.85 ± 0.174	9.537 ± 2.08	297.009 ± 20.812	508.564 ± 29.492
APP/PS1, Control, 3D6	0.032 ± 0.016	0.743 ± 0.064	0.771 ± 0.083	12.752 ± 2.149	409.106 ± 49.093	618.159 ± 60.094
APP/PS1, HHcy, IgG2a	0.029 ± 0.013	0.925 ± 0.093	0.788 ± 0.093	13.738 ± 3.102	429.409 ± 74.685	641.449 ± 80.04
APP/PS1, HHcy, 3D6	0.023 ± 0.007	0.859 ± 0.087	0.782 ± 0.113	12.373 ± 1.682	351.926 ± 39.171	589.695 ± 56.138

Figure 4.3 Total Aβ is reduced by 3D6 treatment. Representative images of Aβ staining in the hippocampus of APP/PS1, control, IgG2a (A), APP/PS1, control, 3D6 (B), APP/PS1, HHcy, IgG2a (C), and APP/PS1, HHcy, 3D6 (D) are shown. The cornu ammonis (CA) 1, CA3 and dentate gyrus (DG) are labeled in A for orientation. Scale bar in A = 120μm. E) Quantification of percent positive stain in the frontal cortex and hippocampus. * indicates $P<0.05$ compared to APP/PS1, control, IgG2a. F) Biochemical quantification of soluble and insoluble $A\beta_{1-38}$, $A\beta_{1-40}$ and $A\beta_{1-42}$ ± SEM.

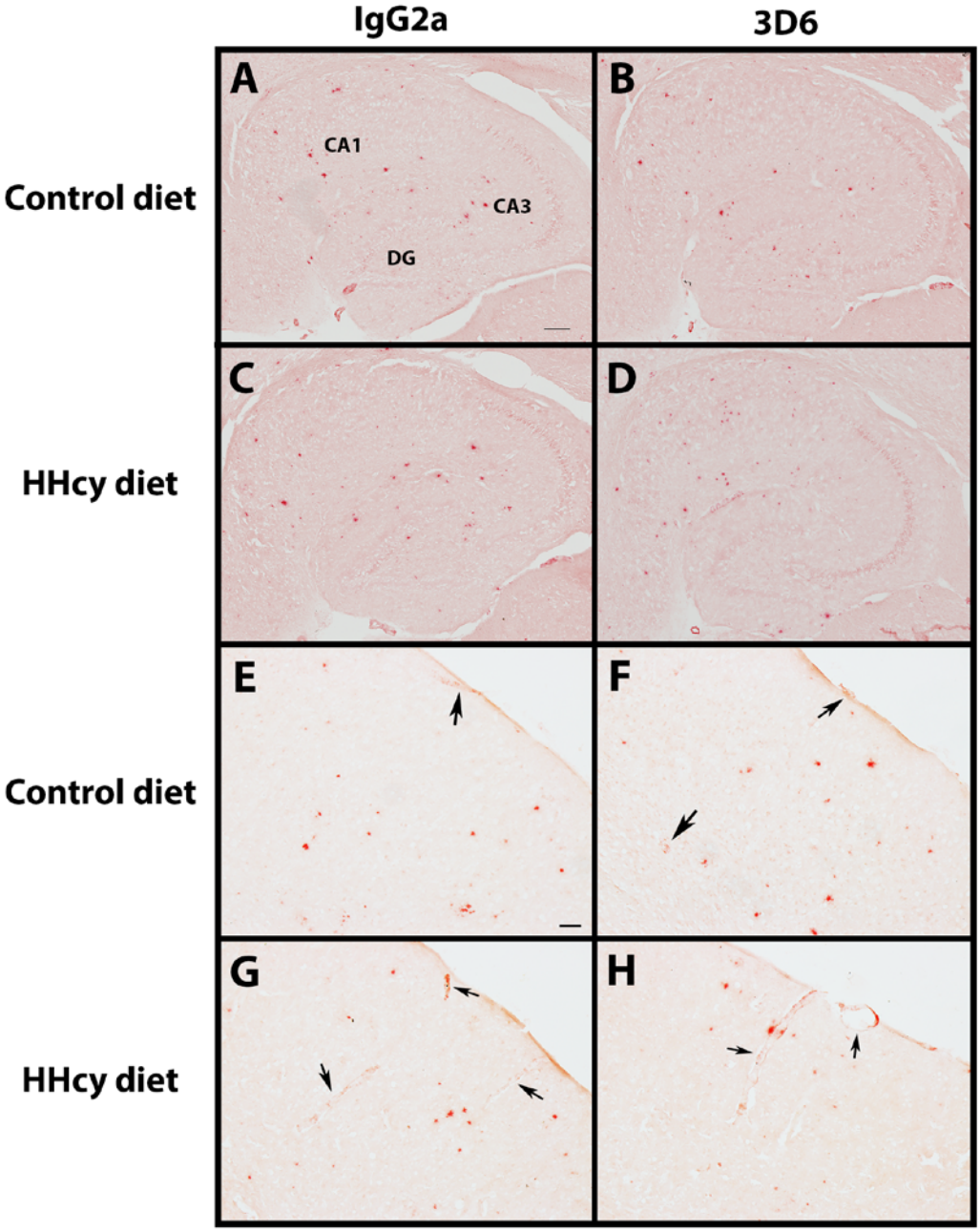
IgG2a
3D6
A
B
CA1
CA3
DG
Control diet
C
D
HHcy diet
E
F
Control diet
G
H
HHcy diet

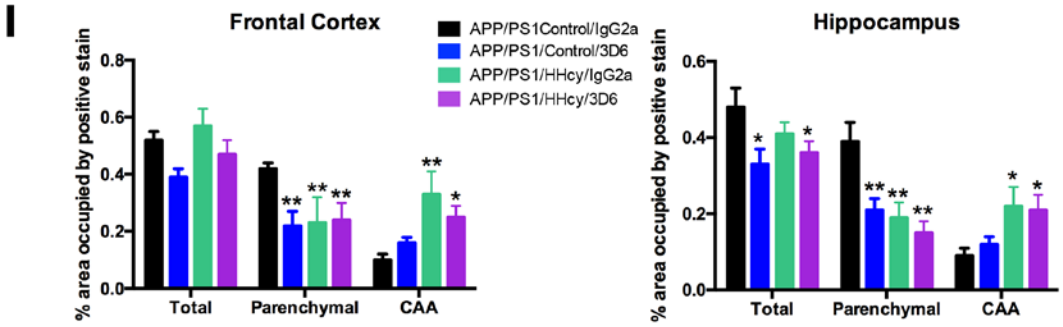
I
Frontal Cortex
APP/PS1Control/IgG2a
APP/PS1/Control/3D6
APP/PS1/HHcy/IgG2a
APP/PS1/HHcy/3D6
% area occupied by positive stain
0.0
0.2
0.4
0.6
0.8
Total
Parenchymal
CAA
Hippocampus
% area occupied by positive stain
0.0
0.2
0.4
0.6
Total
Parenchymal
CAA

Figure 4.4 HHcy redistributes amyloid to the vasculature. Representative images of Congo red staining in the hippocampus of APP/PS1, control, IgG2a (A), APP/PS1, control, 3D6 (B), APP/PS1, HHcy, IgG2a (C), and APP/PS1, HHcy, 3D6 (D) are shown. The CA1, CA3 and DG are labeled in A for orientation. Scale bar in A = 200μm. Representative images of Congo red staining in the cortex of APP/PS1, control, IgG2a (E), APP/PS1, control, 3D6 (F), APP/PS1, HHcy, IgG2a (G), and APP/PS1, HHcy, 3D6 (H) are shown. Scale bar in E = 50μm. Black arrows indicate Congo staining around a vessel (CAA). I) Quantification of percent positive stain in the frontal cortex and hippocampus. * indicates $P<0.05$, ** indicates $P<0.01$ compared to APP/PS1, control, IgG2a.

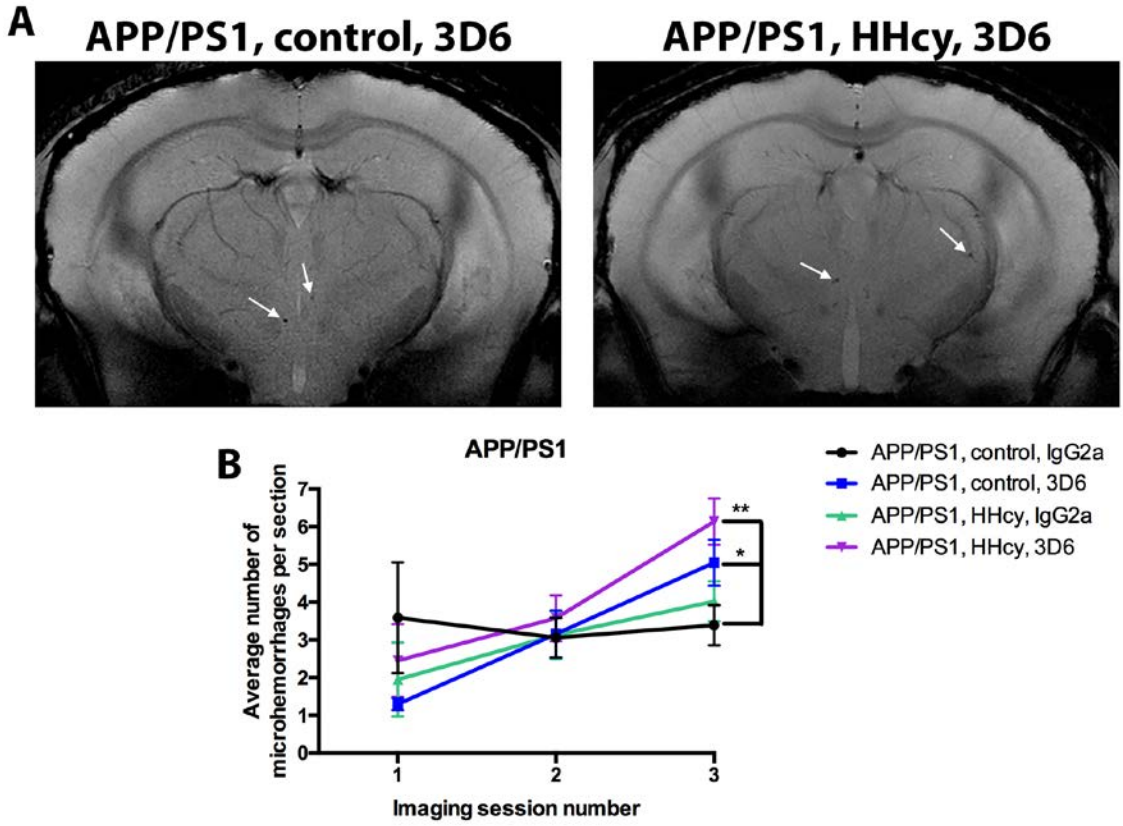

Figure 4.5 3D6 increases MRI detected microhemorrhages. A) Representative T2* images of 3D6 treated mice. Arrows indicate a microhemorrhage. B) Quantification of the number of microhemorrhages per section over the 3 imaging sessions. * indicates P<0.05, ** indicates P<0.01 compared to APP/PS1, control, IgG2a.

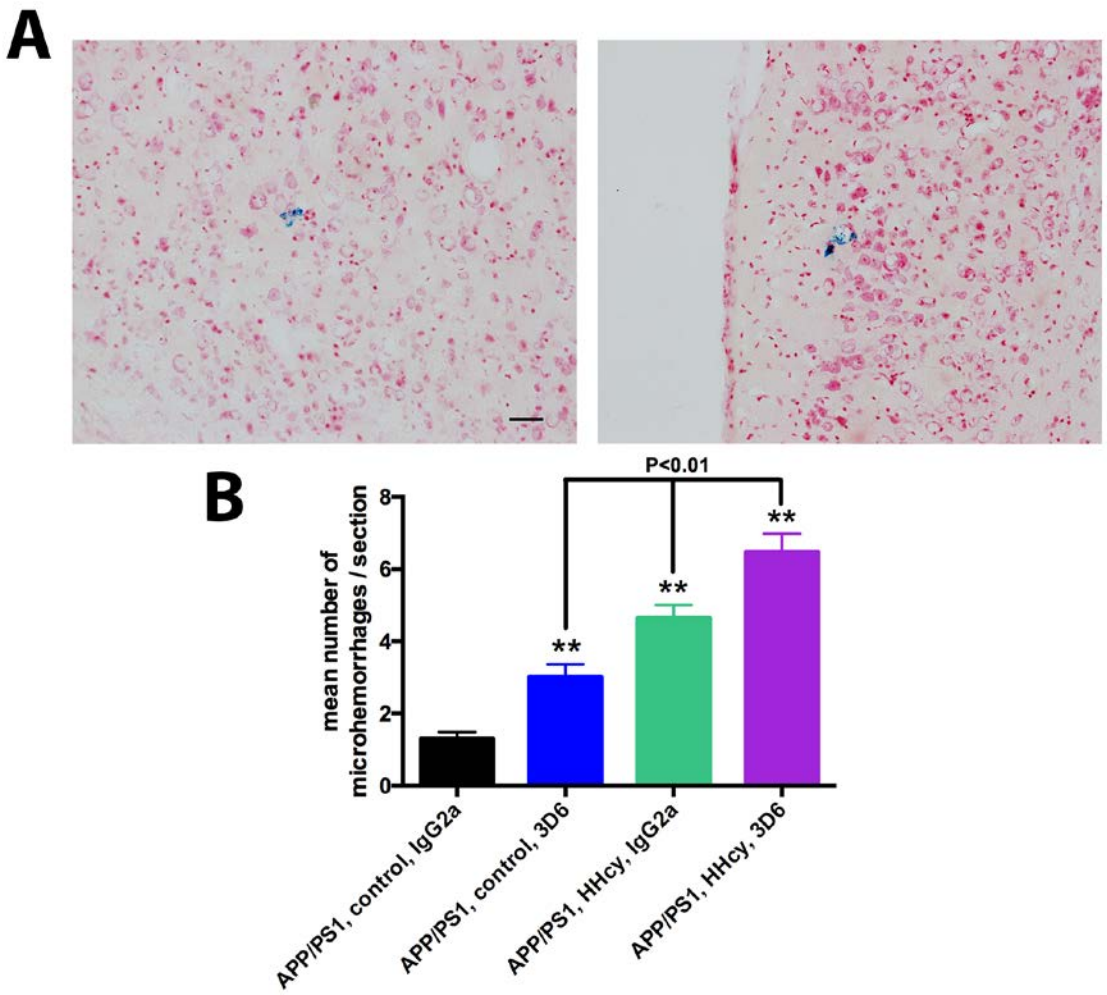

Figure 4.6 3D6 and HHcy increase Prussian blue detected microhemorrhages. A) Representative images of Prussian blue positive microhemorrhages in the frontal cortex. Scale bar = 120μm. B) Quantification of the mean number of microhemorrhages per section. ** indicates P<0.01 compared to APP/PS1, control, IgG2a**.** Black bars represent significant differences between connecting groups.

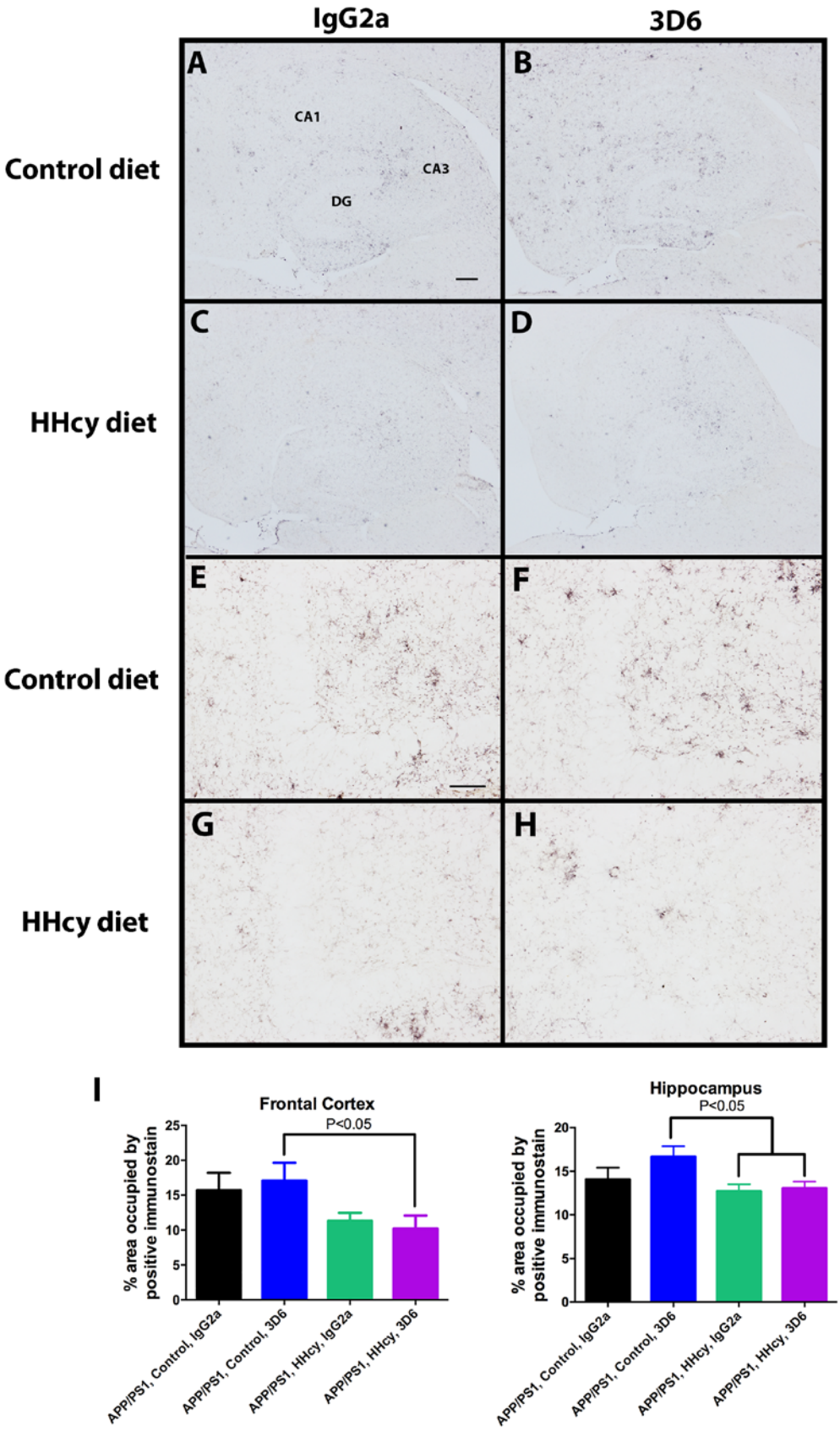
IgG2a
3D6
A
B
CA1
CA3
DG
Control diet
C
D
HHcy diet
E
F
Control diet
G
H
HHcy diet
I
Frontal Cortex
P<0.05
% area occupied by positive immunostain
25
20
15
10
5
0
APP/PS1, Control, IgG2a
APP/PS1, Control, 3D6
APP/PS1, HHcy, IgG2a
APP/PS1, HHcy, 3D6
Hippocampus
P<0.05
% area occupied by positive immunostain
20
15
10
5
0
APP/PS1, Control, IgG2a
APP/PS1, Control, 3D6
APP/PS1, HHcy, IgG2a
APP/PS1, HHcy, 3D6

Figure 4.7 CD11b staining is decreased in the HHcy groups. Representative images of CD11b staining in the hippocampus of APP/PS1, control, IgG2a (A), APP/PS1, control, 3D6 (B), APP/PS1, HHcy, IgG2a (C), and APP/PS1, HHcy, 3D6 (D) are shown. The CA1, CA3 and DG are labeled in A for orientation. Scale bar in A = 120μm. Higher magnification images of CD11b staining in the dentate gyrus of APP/PS1, control, IgG2a (E), APP/PS1, control, 3D6 (F), APP/PS1, HHcy, IgG2a (G), and APP/PS1, HHcy, 3D6 (H) are shown. Scale bar in E = 50μm. I) Quantification of percent positive stain in the frontal cortex and hippocampus.

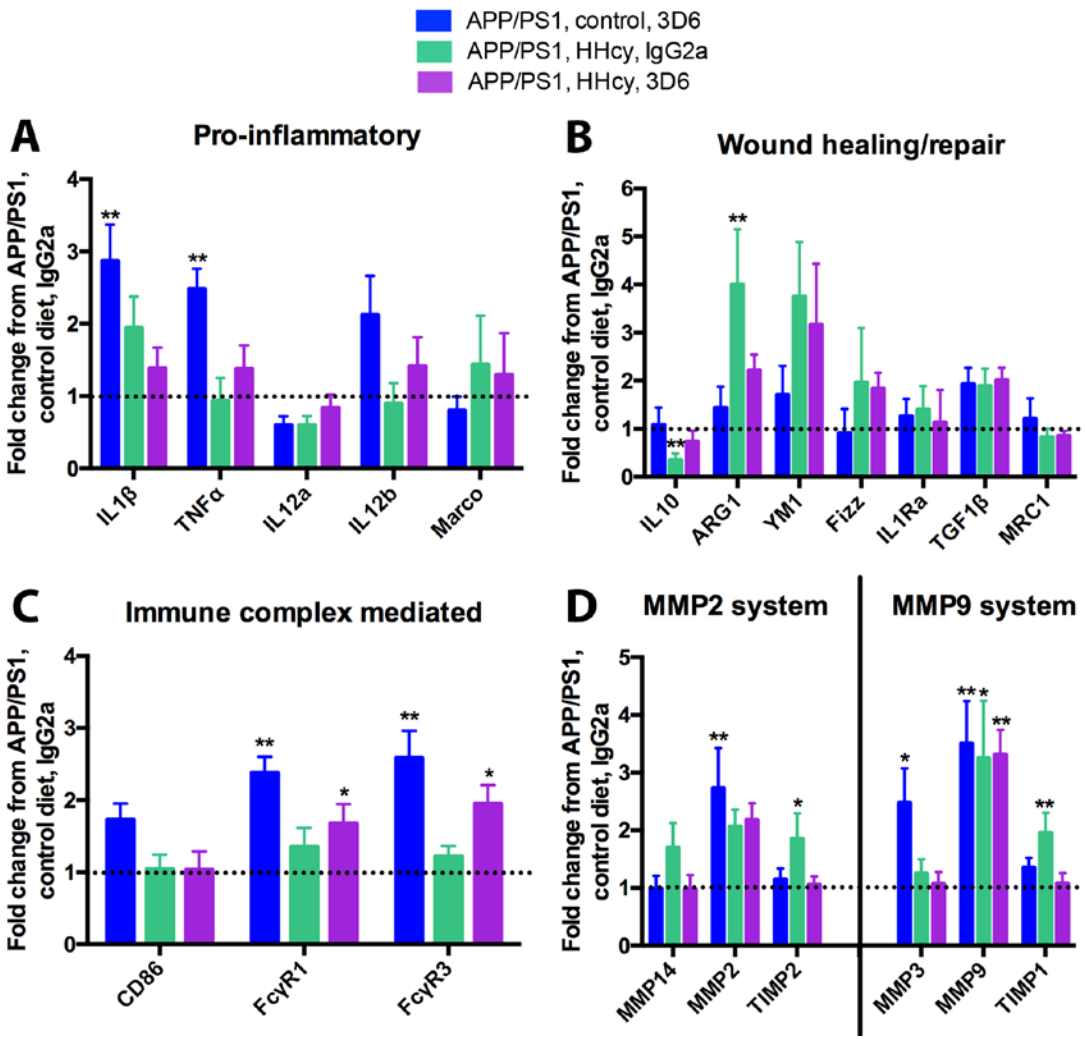

Figure 4.8 HHcy reduced inflammatory markers and increased the MMP system markers in both the IgG2a and 3D6 groups. Data are shown as a fold change from APP/PS1, control, IgG2a. Relative gene expression for pro-inflammatory markers (A), would healing/repair markers (B) immune complex mediated markers (C) and MMP2 and MMP9 system markers (D). * indicates $P<0.05$, ** indicates $P<0.01$ compared to APP/PS1, control, IgG2a.

Table 4.1: Genes for RT-PCR.

Gene of interest	PMID	Taqman ID
IL1β	NM_008361.3	Mm.222830
TNFα	NM_013693.3	Mm.1293
IL12a	NM_008351.2	Mm.103783
IL12b	NM_008352.2	Mm.239707
Marco	NM_010766.2	Mm.1856
IL10	NM_010548.2	Mm.874
ARG1	NM_007482.3	Mm.154144
YM1	NM_009892.2	Mm.387173
Fizz	NM_020509.3	Mm.441868
IL1Ra	NM_031167.5	Mm.882
CD86	NM_019388.3	Mm.1452
FcγR1	NM_010186.5	Mm.150
FcγR3	NM_010188.5	Mm.22119
TGF1β	NM_011577.1	Mm.248380
MRC1	NM_008625.2	Mm.2019
MMP14	NM_008608.3	Mm.280175
MMP2	NM_008610.2	Mm.29564
TIMP2	NM_011594.3	Mm.206505
MMP3	NM_010809.1	Mm.4993
MMP9	NM_013599.3	Mm.4406
TIMP1	NM_001044384.1	Mm.8245

Discussion

While AD is the most common form of dementia, VCID is the second most common and it is estimated that 40% of AD patients also have some form of VCID (59-61, 241). One promising therapeutic for AD is anti-Aβ immunotherapy, which uses antibodies against Aβ to clear it from the brain. In mice, anti-Aβ immunotherapy significantly reduced Aβ levels and improved cognitive outcomes (29, 31, 43, 243); however, in clinical trials, anti-Aβ immunotherapy failed to reach primary cognitive outcomes in several different clinical trials (46, 244). In addition, anti-Aβ immunotherapy has been associated with adverse cerebrovascular events. In mice, these manifested as microhemorrhages (40, 41, 43), while in clinical trials, it presented as vasogenic edema, detected using MRI imaging techniques. These adverse events were termed amyloid related imaging abnormalities (ARIA). Under this term, they were called ARIA-H (hemorrhagic) and ARIA-E (vasogenic edema) (253). We hypothesized that one potential reason the anti-Aβ immunotherapy clinical trials were unsuccessful, both cognitively and with respect to the ARIA, was due to this high percent of VCID co-morbidity in the AD population. We used our unique model of VCID-amyloid co-morbidity to test this hypothesis.

We placed 9 month old WT and APP/PS1 mice on either a control diet or a diet that induces HHcy. Our lab has previously shown that a diet deficient in vitamins B6 and B12 and folate and enriched in methionine induces HHcy (204), which is a risk factor for VCID and cardiovascular disease (185, 186). After being placed on the diet for 3 months, the mice then received IP injections of either

IgG2a or 3D6 for another 3 months. While we found that treatment of our co-morbidity model with 3D6 resulted in decreased total Aβ levels, there was no cognitive benefit of the anti-Aβ immunotherapy in our AD/VCID mice. Further, microhemorrhages were increased by 3D6 in the APP/PS1 on control diet, but further increased in an additive fashion when 3D6 was administered to the APP/PS1/HHcy mice.

Total Aβ deposition, which is mostly diffuse deposition, was reduced in the 3D6 treated animals, both APP/PS1 and APP/PS1/HHcy compared to APP/PS1 controls. Total Aβ deposition in the APP/PS1 mice on HHcy diet with 3D6 were not significantly different compared to APP/PS1 mice on HHcy diet with IgG2a**,** although did show trends for reduction. We found that amyloid distribution was altered when we examined Congo red staining. When we looked at parenchymal versus vascular Congophilic amyloid deposition using our previously described method (249), we saw that the HHcy diet resulted in an apparent redistribution of the amyloid to the vasculature, as CAA, replicating our previous finding (204). We did not find that 3D6 altered this outcome. Interestingly, despite the comparable levels of CAA between the 3D6 treated and control antibody treated APP/PS1/HHcy mice, microhemorrhages were significantly increased in the 3D6 treated mice, indicating that the microhemorrhages do not occur simply due to the presence of CAA, but that the anti-Aβ antibody causes a local reaction at the vessel, resulting in leakage.

We have previously shown that MMP activation, in particular MMP9, is associated with tight junction breakdown and microhemorrhages, both in

response to immunotherapy (254) and in the HHcy model (203, 204). MMP9 has been implicated in cerebrovascular injury including hemorrhagic transformation after stroke and microhemorrhage occurrence in CAA (130, 144). In our study, both 3D6 and HHcy significantly increased gene expression of MMP9, similar to previous studies. MMP3, an activator of MMP9, was also increased in the 3D6 treated control APP/PS1 mice.

It is unclear what mechanism is responsible for the increased MMP9 and MMP3 in the current study. MMP9 and MMP3 can be activated by pro-inflammatory cytokines such as IL1β and TNFα (113, 114). As a result of this literature and our previous data (203, 204), we explored neuroinflammation in the current study. Our findings were intriguing, and suggest that the immunotherapy did not result in an overt inflammatory response by the microglia. TNFα and IL1β were only significantly increased in the 3D6 treated control APP/PS1 mice and not in either of the HHcy treated groups. In fact, both the HHcy treated groups had a slight reduction in CD11b staining and did not show any changes in the majority of markers for any of the neuroinflammatory states. In our previous study, we showed that the APP/PS1 mice on the HHcy diet had a neuroinflammatory shift from wound healing and repair to a pro-inflammatory state (204). Due to the older age of the mice in this study (15 months rather than 12 months), and the addition of a treatment arm, the mice could have progressed past this neuroinflammatory shift. Unfortunately, we are only able to assess the changes post-mortem, and thus cannot know what changes preceded those reported here. Based on our data, we hypothesize that either there is a decrease

in the numbers of microglial cells, or the microglia could be senescent. The constant activation from high Aβ levels, long-term HHcy, and weekly administration of antibodies could force the microglia into senescence, resulting in the decreased CD11b staining and lack of immune activation. It is also possible that the decreased CD11b staining, which also labels other myeloid cells like monocytes, could also result from HHcy suppression of infiltration of peripheral cells, although this seems unlikely since the HHcy diet results in a microhemorrhage induction. Therefore, while MMP9 may be responsible for the tight junction breakdown leading to microhemorrhages, pro-inflammatory cytokines do not seem to be the stimulating factor in the current study.

Previous anti-Aβ immunotherapy studies have shown that the use of anti-Aβ antibodies significantly improves cognitive outcomes in mice (29, 31, 43, 243). While we saw that 3D6 treatment significantly reduced the number of errors APP/PS1 mice on control diet made making then indistinguishable from the WT controls, the presence of HHcy impeded those benefits. The APP/PS1 mice on the HHcy diet with 3D6 treatment did not benefit cognitively from the anti-Aβ immunotherapy. In fact, they were not significantly different from the APP/PS1 mice on the HHcy diet with IgG2a treatment by the end of the second day. This lack of cognitive benefits could be due to the increase in the number of microhemorrhages seen in the 3D6 treated HHcy mice compared to the 3D6 or HHcy controls, or the increased levels of CAA. We cannot rule out that there may have been a benefit to the APP/PS1/HHcy that was undetected in our selected behavioral task due to wildtype HHcy mice also reaching a ceiling effect. Future

studies will try to develop more sensitive behavioral tasks that may discriminate these effects. Despite the Aβ reductions in the APP/PS1/HHcy mice, the increase in vascular damage and leakage appears to negate any cognitive benefits of clearing the Aβ. This suggests that anti-Aβ immunotherapy in patients with VCID co-morbid with AD may be ineffective with respect to function outcomes. Prescreening subjects for cerebrovascular pathologies prior to enrollment in anti-Aβ immunotherapy clinical trials may reduce the adverse cerebrovascular events seen during treatment and this could result in significantly improved cognitive outcomes. Although anti-Aβ immunotherapy trials are moving towards treatment of prodromal AD, VCID still remains a concern since the immunotherapy could hasten any vascular dysfunction that is present but asymptomatic.

Chapter 5

Discussion

The chapter 5 discussion has been separated into the main themes of the entire dissertation. First, it begins with a brief summary of chapters 2-4, and then moves into a discussion on neuroinflammation and the details tying together chapters 2-4. Then, the discussion moves on to how each chapter provides crucial information regarding the vascular contributions to dementia. Finally, the last two sections discuss the larger translational implications of the three studies as well as future directions for this research.

Summary

Using an adeno-associated viral vector for long-term expression of IFNγ in Aβ depositing mice, a pro-inflammatory response was induced at 4 months, which transitioned to a mixed inflammatory phenotype by 6 months. While there was no change in Aβ deposition at 4 months, there was a significant increase after the transition to a mixed phenotype at 6 months. This suggests that the wound healing and repair inflammatory phenotype increased Aβ deposition and, therefore, disease progression. There are several studies that have attempted to determine the effect of a pro-inflammatory versus an anti-inflammatory phenotype on Aβ deposition; however, these were all acute experiments, only lasting up to a month and a half while our study induced a chronic pro-inflammatory phenotype.

Hyperhomocysteinemia is a risk factor for vascular disease as well as VCID (184-187), but little is known about the effects of high levels of

homocysteine on the individual cell types of the brain, especially microglia. We showed that treatment of microglia with high levels of homocysteine resulted in a pro-inflammatory response at 48 hours, but this transitioned into an anti-inflammatory phenotype by 72 hours. HHcy's effects on other cell types included a reduction in several potassium channels in astrocytes, changes in tight junction proteins in endothelial cells, and increases in kinases and phosphatases in neurons. These gene changes can be used as possible biomarkers for VCID patients as well as therapeutic targets.

While there is still much to be learned about AD and VCID as individual dementias, it is also crucial to study the co-morbidity of these two dementias, especially in regard to therapeutics. Because a large percentage of AD patients have co-morbid cerebrovascular pathologies, this could interfere with the efficacy of therapeutics targeting AD pathologies. We have shown that when Aβ depositing mice are placed on a diet that induces HHcy and then treated with an anti-Aβ antibody, there is significant Aβ clearance but no cognitive benefits. Interestingly, these mice also have a significant decrease in microglial staining and a limited inflammatory response.

Neuroinflammation

It is well known that inflammation and microglia play a role in the brain and in AD; however, this role remains unclear in AD. Initially, the presence of activated microglia was termed inflammation. Later, it was realized that microglia can be "classically" or "alternatively" activated. Using peripheral macrophage phenotypic nomenclature, these activation states were then termed M1 and M2.

Today, the neuroinflammation field has switched to pro-inflammatory and anti-inflammatory to describe the inflammatory phenotypes of the brain. Several studies have shown that microglia are capable of surrounding Aβ plaques and can phagocytose Aβ (255, 256). Microglia can also be stimulated by a variety of substances to produce an inflammatory phenotype in the brain. We have shown that high levels of homocysteine induced an initial pro-inflammatory phenotype in vitro and this remained true in wildtype mice with HHcy (203). This inflammatory phenotype can then affect Aβ levels. For example, short-term induction of a pro-inflammatory phenotype via LPS or TNFα led to Aβ clearance (83, 216). On the other hand, short-term induction of an anti-inflammatory phenotype exacerbated Aβ deposition (257). A recent study inducing a long-term anti-inflammatory phenotype via IL-10 showed a significant increase in Aβ deposition and worsened cognitive behavior (258). We have shown that long-term expression of IFNγ initially induced a pro-inflammatory phenotype, which did not affect Aβ levels. However, when the inflammatory phenotype switched to a mixed inflammatory phenotype by including several anti-inflammatory markers, we saw a significant increase in Aβ deposition.

When HHcy is induced long-term in Aβ depositing mice, it induced a switch from a wound healing and repair phenotype to a pro-inflammatory phenotype, similar to what we have shown in vitro (204). Again, this long-term pro-inflammatory phenotype did not affect total levels of Aβ; however, there was a redistribution of the amyloid from the parenchyma to the vasculature (204). This is somewhat similar to what we saw when anti-Aβ antibodies were used to clear

Aβ from the brain. The antibodies induced a pro-inflammatory phenotype, which, while it did lead to amyloid clearance, also increased CAA levels (39, 43, 243). This data suggest that the presence of both HHcy and anti-Aβ antibodies in Aβ depositing mice would lead to a significant increase in the pro-inflammatory response as well as high levels of CAA. We have shown that APP/PS1 mice with HHcy and 3D6 treatment have significant decreases in parenchymal amyloid deposition as well as increases in CAA. Interestingly, these mice do not have a significant pro-inflammatory response like the APP/PS1 mice on control diet with 3D6 treatment. In fact, they had a very limited inflammatory response with only a small increase in the immune complex mediated markers. While the inflammatory phenotype was limited to a small increase in immune complex mediated markers by the end of the study, it cannot be ruled out that there was an initial pro-inflammatory response to the HHcy and 3D6 that contributed to the decrease in parenchymal amyloid and increase in CAA. These studies add evidence that an anti-inflammatory phenotype increases Aβ deposition while a pro-inflammatory phenotype can help clear Aβ, perhaps through vascular clearance methods due to the increase in CAA that seems to be associated with the pro-inflammatory phenotype.

Vascular contributions to dementia

Our research group has shown that when HHcy is induced in both wildtype and APP/PS1 mice, there was a significant increase in microhemorrhages (203, 204). There is evidence to show that MMP2 and MMP9 degrade tight junctions, which can lead to BBB breakdown and microhemorrhage

(100, 120). In our mouse models of HHcy, we saw that both MMP2 and MMP9 had significantly elevated levels of gene expression and activity, suggesting that they are responsible for the increased microhemorrhages we observed. The APP/PS1 mice on the HHcy diet also showed a redistribution of Aβ leading to an increase in CAA and one of the major complications of CAA is intracerebral hemorrhage. Both MMP2 and MMP9 have been widely associated with BBB disruption and microhemorrhages in CAA.

Hernandez-Guillamon et al. looked at MMP2 and MMP9 expression in CAA patients (259). While plasma MMP2 and MMP9 levels did not discriminate between CAA patients and controls, MMP9 and MMP2 levels were higher in the hemorrhagic areas of CAA brains. proMMP9 and proMMP2 were significantly higher in hemorrhagic areas of patients who died from a fatal hemorrhage. MMP9 was mainly found in brain vessels and in neurons around the hemorrhage and the contralateral side, while MMP2 was mainly located in medium sized brain vessels and capillaries and was more pronounced around the hemorrhagic area. MMP2 was also expressed in reactive astrocytes surrounding Aβ affected vessels and its expression was clearly associated with the Aβ load in the vessel in grade 1 and 2 CAA. Briefly, grade 1 CAA is given when some amyloid deposits are found in otherwise normal vessels, grade 2 CAA is used when the vessel media is replaced by amyloid, grade 3 CAA is occurs when cracking of the vessel wall results in “vessel-within-vessel” appearance and affects at least 50% of the circumference of the vessel and finally, grade 4 CAA is given when scarring of the wall is observed as well as fibrinoid necrosis and traces of intermingled

amyloid deposits (260). In grade 3 CAA lesions, Aβ reactivity was very frequent and was found to have MMP2 expression in astrocytes surrounding the lesions. Unlike MMP2, MMP9 was found in some isolated macrophages around the grade 3 CAA lesions. There was some Aβ reactivity in grade 4 CAA lesions and strong gliosis was prominent with reactive astrocytes positive for MMP2. MMP9 expression was similar to grade 3 CAA.

Recent evidence suggests that Aβ may contribute to the BBB leakage that is associated with CAA. Isolated rat brain microvessels that are exposed to increasing concentrations of $A\beta_{1\text{-}40}$ showed a significant decrease in the expression of the tight junction proteins claudin-1 and claudin-5 as well as increased MMP2 and MMP9 expression (261). Microvessels from 9-month-old transgenic APP mice (Tg2576 strain with the Swedish mutation KM670/671NL) also showed increased permeability, decreased claudin-1 and claudin-5 as well as increased MMP2 and MMP9. Cultured human brain endothelial cells treated with $A\beta_{1\text{-}40}$ caused zonula occludens-1 (ZO-1), another tight junction protein that forms the BBB, to retreat from the plasma membrane, which in turn decreased transendothelial electrical resistance (262). Carrano et al. found decreased occludin, claudin-5 and ZO-1 in brain microvessels of postmortem CAA patient brain slices (263). These studies have shown that Aβ can contribute to the BBB breakdown via increased MMP expression and altered tight junction protein localization.

The prevailing hypothesis for AD progression is the amyloid hypothesis, which, briefly, states that the deposition of Aβ leads to hyperphosphorylation of

tau, which in turn leads to neurodegeneration (17). Using this hypothesis to develop therapeutics, anti-Aβ immunotherapy became the most promising approach for AD. Unfortunately, in clinical trials, vascular adverse events like microhemorrhages and vasogenic edema were reported with anti-Aβ treatment (46). MMP2 and MMP9 have been implicated in the BBB breakdown that occurs after anti-Aβ immunotherapy. In APPSw/NOS2-/- mice that received an active Aβ vaccination for 4 months, there was a significant increase in gene expression of furin and MMP2 and decreased TIMP2 levels (254). ELISA measurements confirmed these qPCR findings. There was also an increase in gene expression of MMP3 and a decrease in TIMP1 levels in the actively vaccinated transgenics. Protein measurements showed increased MMP3 and MMP9 as well. Within this study, gelatin zymography analysis also showed a significant increase in MMP2 and MMP9 activity in the transgenic mice treated with the active Aβ immunotherapy. Robust expression of MMP9 was also found to be associated with the vasculature. Similar results were found in passively immunized APPSw mice. In vitro studies using BV2 microglial cells showed that $A\beta_{1-42}$ fibrils increased MMP2 and MMP14 gene and protein levels (254). An increase in MMP9 and MMP3 occurred when BV2 cells were treated with either an anti-Aβ IgG-Aβ or anti-tau IgG-tau immune complex, showing that MMP9 activation requires the Fcγ receptor (254).

Anti-Aβ antibody studies have not taken into account the high percent of co-morbidity patients and the possible consequences on the vasculature in these patients (59-61). We showed that mice with Aβ deposition and HHcy with anti-Aβ

antibody treatment had a significant increase in microhemorrhages over the course of their treatment. They had more microhemorrhages per section than both the APP/PS1 mice on control diet with 3D6 and the APP/PS1 mice on the HHcy diet with the control antibody by the end of treatment. The co-morbidity mice on the immunotherapy also had a significant increase in the amount of CAA and the gene expression of MMP9, which could contribute to the increase in microhemorrhages.

The microhemorrhages seen in these models may also be a direct or indirect response to the high levels of homocysteine. In fact, there have been no studies to date that have shown what the direct effect of homocysteine is on individual cell types. We have shown that HHcy induces significant increases in MMP9 gene expression at 48 and 72 hours; however, the source of the MMP9 was different at each time point, thus providing crucial information that could be used for in vivo studies. Coinciding with this increase in MMP9 was an increase in pro-inflammatory cytokines from microglia, which could ultimately lead to a further increase in MMP9 in vivo due the activation of MMP9 by IL-1β and TNFα. While the increase in these pro-inflammatory cytokines and MMP9 could be indirect methods of the HHcy induced microhemorrhages, we also showed that endothelial cells exposed to high levels of homocysteine have a decrease in occludin-1 and collagen type IV at 48 and 72 hours, respectively, showing that homocysteine can have a direct effect on the vasculature.

Overall, Aβ accumulation around the vasculature, anti-Aβ immunotherapy, and the presence of high levels of homocysteine separately increased

expression of MMP2 and MMP9 and/or altered tight junction expression and localization. When combined, they significantly increased the number of microhemorrhages compared to groups that did not have all three. This common pathway of microhemorrhage occurrence could provide a potential therapeutic target for patients with AD and VCID receiving an anti-Aβ immunotherapy.

Translational implications

Since vitamins B6, B12 and folate are essential cofactors in the metabolism of homocysteine, deficiencies in any of these vitamins can cause HHcy. Deficiencies in B vitamins increase with age and are common in the elderly population. The prevalence of low vitamin B12 levels can range from 6-16% in elderly people (264, 265). Due to this high prevalence, clinical trials for B vitamin supplementation have been performed. Unfortunately, meta-analyses of these clinical trials reveal several issues with data analysis, vitamin levels and duration of the studies. In one meta-analysis of B vitamin clinical trials, 7 of the 9 trials were 12 months or shorter with the shortest one being only one month (266). In the trial with the largest number of participants (910), the levels of folic acid (0.2 mg) and vitamin B12 (1 μg) were too low to alter plasma homocysteine levels. In the FACIT trial (n=818), people in the Netherlands with homocysteine levels between 13 and 26 μM but with adequate vitamin B12 levels were given 0.8 mg/day of folic acid for three years (267). By the end of the trial there was a 26% reduction in plasma homocysteine compared to the placebo group. The placebo group also showed a reduction in sensorimotor speed, information processing speed and complex speed but this decline was slowed by the folic

acid treatment. In the VITACOG trial, volunteers with mild cognitive impairment were placed on a daily combination of folic acid (0.8 mg), vitamin B12 (0.5 mg) and vitamin B6 (20 mg) for two years (268). MRI scans at the beginning and end of the trial showed a significant slowing of global brain atrophy in the treatment group. While the VITACOG trial was not powered to determine changes in cognition, one analysis showed cognitive decline in episodic memory, semantic memory and global cognition was prevented in people with baseline plasma homocysteine above the median (11.3 μM) (269). These clinical trials present conflicting data and further trials are needed to determine the benefits of lowering homocysteine with B vitamins.

Another possible therapeutic could be the combination of anti-Aβ antibodies with MMP2 and MMP9 inhibitors to reduce the adverse cerebrovascular consequences. The majority of MMP inhibition studies for the cerebrovasculature have been performed in stroke studies to help reduce the severity of hemorrhagic transformation. In one study, inhibition of MMP2 with BB-1101 resulted in a reduction in edema and BBB permeability at 24 hours after stroke (159). This effect did not continue 48 hours after stroke though. In MMP2 deficient mice, there was a reduced rate of hemorrhagic transformation, smaller hemorrhage size and improved neurological function after stroke (156). In vivo studies show that inhibition of MMPs after delayed tPA treatment, which is known to increase the risk of hemorrhagic transformation in humans, resulted in reduced hemorrhage volumes, a reduction in MMP9 activity and an increase in occludin and ZO-1 proteins compared to mice treated with tPA alone (270). In vitro studies

with GM6001 treatment after tPA treatment with hypoxia and reoxygenation resulted in reduced cell damage and an increase in transendothelial electrical resistance due to a reduction in degradation of occludin and ZO-1 (270). Similar results were shown by Chen et al. where GM6001 treatment significantly reduced BBB breakdown and ameliorated brain edema by preventing the decrease in occludin and ZO-1 (271). In a model of permanent focal cerebral ischemia, treatment with SB-3CT, a gelatinase inhibitor, decreased MMP9 activity, decreased basement membrane laminin degradation, prevented pericyte lumen from contraction, and protected pericytes and endothelial cells (272). Repeated SB-3CT treatment can counteract degradation of neuronal laminin, protect neurons from ischemic cell death and ameliorate neurobehavioral outcomes after embolic middle cerebral artery occlusion in mice (272). SB-3CT also abolishes oxygen glucose deprivation induced reduction of occludin as well as decreases Evans blue extravasation and apoptotic cell death after subarachnoid hemorrhage (155, 273, 274). A recent clinical trial indicated that minocycline, which acts as an anti-inflammatory, could lower plasma MMP9 levels, even at 72 hours post stroke, and improve neurological outcomes in acute ischemic stroke patients treated with tPA (275). However, it is important to note that MMPs have also been implicated in the repair functions after cerebral ischemia such as neuroblast migration and neuronal plasticity; therefore, MMP inhibition may only be beneficial during a short window (112, 276). The success of these MMP inhibitors in reducing hemorrhagic transformation after stroke provides evidence

that they could be useful in preventing the microhemorrhages seen after anti-Aβ antibody treatment in AD and co-morbidity patients.

While co-treatment with an MMP inhibitor may be a future combination therapy, additional studies have been aimed at determining other immune modulators to clear Aβ. Recent genome wide association studies have identified rare missense variants in triggering receptor expressed on myeloid cells-2 (TREM2) that were associated with an increased risk of developing AD (277, 278). TREM2 is a member of the Ig superfamily of receptors and is expressed on a number of cells including dendritic cells, osteoclasts, tissue macrophages and on microglia. Possible functions of TREM2 include phagocytosis, proliferation, cell survival and regulation of inflammatory cytokine production (279-284). Cell culture studies show that exogenous expression of TREM2 on CHO or HEK293 cells increased phagocytic activity (280, 285). In AD, TREM2 has been shown to be upregulated within the vicinity of Aβ plaques and TREM2 haplosufficient or deficient mice have a significant reduction in the size and number of plaque-associated microglia (286, 287). This decrease in plaque-associated microgliosis was also accompanied by a decrease in the pro-inflammatory cytokines IL-1β and TNFα (283, 288). The effect of TREM2 deficiency on Aβ is less clear than its effect on microglia. One study showed that TREM2 haploinsufficiency had no effect on Aβ in 3 or 7-month-old APP/PS1-21 mice while another showed that TREM2 deficient mice had an increase in hippocampal Aβ in 8-month-old 5xFAD mice (283, 287). Another study showed a decrease in Aβ deposition in TREM2 knockout mice (288). Even with these conflicting results, TREM2 could be a

promising therapeutic approach outside of anti-Aβ antibodies to help clear Aβ in AD patients and may limit the presence of adverse cerebrovascular events seen with the anti-Aβ antibodies. It may also prove to be a potential therapeutic for co-morbidity patients since inflammation plays a role in both AD and VCID.

Conclusions and future studies

It is clear that inflammation plays a crucial role in both AD and VCID as well as the co-morbidity of these two dementias. Polarizing the inflammatory phenotype to a pro-inflammatory state did not affect AD progression, although the natural progression of the inflammatory state to include anti-inflammatory markers increased Aβ deposition. High levels of homocysteine induced a pro-inflammatory phenotype in microglia both in vitro and in vivo and led to increased microhemorrhages in vivo. When both Aβ deposition and HHcy are present, an anti-Aβ antibody inhibits the inflammatory response and fails to improve cognition. Although these studies provide crucial information regarding the role of inflammation in AD and VCID, they also raise questions about combination therapies for co-morbidity patients. Would the use of a different Alzheimer's therapeutic that doesn't induce microhemorrhages, such as a β secretase inhibitor or possibly activation of TREM2, be sufficient to improve cognition in co-morbidity patients? Recent research into β secretase inhibitors for AD treatment has proven them effective at lowering Aβ levels without increasing microhemorrhage occurrence (289). A β secretase inhibitor could be an effective treatment in co-morbidity patients if the increase in microhemorrhages due to the anti-Aβ immunotherapy hindered any potential cognitive benefits in the co-

morbidity group. However, if treatment of the underlying VCID is required, a combination of an anti-Aβ antibody with B vitamin supplementation might improve cognitive decline in patients with AD and HHcy-induced VCID. This combination treatment doesn't take into account the increase in microhemorrhages induced by the immunotherapy though, so perhaps a triple combination therapy of an anti-Aβ antibody, B vitamin supplementation, and an MMP inhibitor may be the best possible approach to reduce microhemorrhage occurrence while also clearing Aβ and reducing HHcy. Or to simplify the number of treatments, and thus reduce possible off target effects, the most promising combination therapy may be a β secretase inhibitor with B vitamin supplementation. This would allow for Aβ clearance and reduction of homocysteine levels without increasing the number of microhemorrhages.

While combination therapies are always a possibility, it may be simpler to target a common pathology of AD and VCID. One major overlap, of course, is the presence of neuroinflammation, specifically pro-inflammatory markers. Unfortunately, several clinical trials using non-steroidal anti-inflammatory drugs (NSAID) have not shown any beneficial results (290-292). While an NSAID may not be beneficial, a more specific treatment targeting one or more of the pro-inflammatory signaling pathways may be a more effective treatment. Targeting of the TNFα or IL-1β pathway could reduce the pro-inflammatory response as well as MMP9 activation and, therefore, reduce microhemorrhage occurrence in both AD and VCID. Another possible common target for treatment of co-morbidity patients is astrocytic end feet. The astrocytic end foot wraps around arterioles

and capillaries in the brain to help maintain ionic and osmotic homeostasis. Our research group has recently shown that astrocytic end feet were disrupted in the HHcy mouse model, specifically, the anchoring protein Dp71 was decreased and there was dislocalization of the aquaporin 4 channel (293). These changes were preceded by a pro-inflammatory response and cognitive impairment is only present after astrocytic end foot damage occurs. This suggests that the astrocytic end foot damage could be caused by the pro-inflammatory response and in turn causes the cognitive decline seen in our mouse model of VCID. Astrocytic end foot disruption has also been shown in a CAA mouse model as well as in humans with CAA (294). Therefore, reducing the damage to astrocytic end feet could improve cognition in both AD and VCID patients as well as co-morbidity patients.

Overall, neuroinflammation has been shown to be a major player in several aspects of both AD and VCID as well as their co-morbidity. However, there is still much to be learned about the precise mechanisms and consequences of neuroinflammation and future studies should focus on combination therapies, as well as therapies that target common pathologies in order for successful treatment of co-morbidity patients.

References

1. Prince M, Wimo A, Guerchet M, Ali G, Wu Y, Prina M. The Global Impact of Dementia: An Analysis of Prevalence, Incidence, Cost and Trends. Alzheimer's Disease International. 2015.
2. Prince M, Bryce R, Albanese E, Wimo A, Ribeiro W, Ferri CP. The global prevalence of dementia: a systematic review and metaanalysis. Alzheimer's & dementia : the journal of the Alzheimer's Association. 2013;9(1):63-75 e2. doi: 10.1016/j.jalz.2012.11.007. PubMed PMID: 23305823.
3. Alzheimer's A. 2016 Alzheimer's disease facts and figures. Alzheimer's & dementia : the journal of the Alzheimer's Association. 2016;12(4):459-509. PubMed PMID: 27570871.
4. Braak H, Braak E. Staging of Alzheimer's disease-related neurofibrillary changes. Neurobiology of aging. 1995;16(3):271-8; discussion 8-84. PubMed PMID: 7566337.
5. Artiga MJ, Bullido MJ, Frank A, Sastre I, Recuero M, Garcia MA, Lendon CL, Han SW, Morris JC, Vazquez J, Goate A, Valdivieso F. Risk for Alzheimer's disease correlates with transcriptional activity of the APOE gene. Human molecular genetics. 1998;7(12):1887-92. PubMed PMID: 9811931.
6. Bekris LM, Millard SP, Galloway NM, Vuletic S, Albers JJ, Li G, Galasko DR, DeCarli C, Farlow MR, Clark CM, Quinn JF, Kaye JA, Schellenberg GD, Tsuang D, Peskind ER, Yu CE. Multiple SNPs within and surrounding the apolipoprotein E gene influence cerebrospinal fluid apolipoprotein E protein levels. Journal of Alzheimer's disease : JAD. 2008;13(3):255-66. PubMed PMID: 18430993; PMCID: PMC3192652.
7. Bullido MJ, Artiga MJ, Recuero M, Sastre I, Garcia MA, Aldudo J, Lendon C, Han SW, Morris JC, Frank A, Vazquez J, Goate A, Valdivieso F. A polymorphism in the regulatory region of APOE associated with risk for Alzheimer's dementia. Nat Genet. 1998;18(1):69-71. doi: 10.1038/ng0198-69. PubMed PMID: 9425904.
8. Laws SM, Hone E, Gandy S, Martins RN. Expanding the association between the APOE gene and the risk of Alzheimer's disease: possible roles for APOE promoter polymorphisms and alterations in APOE transcription. Journal of neurochemistry. 2003;84(6):1215-36. PubMed PMID: 12614323.
9. Huang Y. Roles of apolipoprotein E4 (ApoE4) in the pathogenesis of Alzheimer's disease: lessons from ApoE mouse models. Biochem Soc Trans. 2011;39(4):924-32. doi: 10.1042/BST0390924. PubMed PMID: 21787325.
10. Dodart JC, Marr RA, Koistinaho M, Gregersen BM, Malkani S, Verma IM, Paul SM. Gene delivery of human apolipoprotein E alters brain Abeta burden in a mouse model of Alzheimer's disease. Proceedings of the National Academy of Sciences of the United States of America. 2005;102(4):1211-6. doi: 10.1073/pnas.0409072102. PubMed PMID: 15657137; PMCID: PMC544620.
11. Holtzman DM, Bales KR, Tenkova T, Fagan AM, Parsadanian M, Sartorius LJ, Mackey B, Olney J, McKeel D, Wozniak D, Paul SM. Apolipoprotein E isoform-dependent amyloid deposition and neuritic degeneration in a mouse model of Alzheimer's disease. Proceedings of the National Academy of Sciences

of the United States of America. 2000;97(6):2892-7. doi: 10.1073/pnas.050004797. PubMed PMID: 10694577; PMCID: PMC16026.
12. Goate A, Chartier-Harlin MC, Mullan M, Brown J, Crawford F, Fidani L, Giuffra L, Haynes A, Irving N, James L, et al. Segregation of a missense mutation in the amyloid precursor protein gene with familial Alzheimer's disease. Nature. 1991;349(6311):704-6. doi: 10.1038/349704a0. PubMed PMID: 1671712.
13. Levy E, Carman MD, Fernandez-Madrid IJ, Power MD, Lieberburg I, van Duinen SG, Bots GT, Luyendijk W, Frangione B. Mutation of the Alzheimer's disease amyloid gene in hereditary cerebral hemorrhage, Dutch type. Science. 1990;248(4959):1124-6. PubMed PMID: 2111584.
14. Levy-Lahad E, Wasco W, Poorkaj P, Romano DM, Oshima J, Pettingell WH, Yu CE, Jondro PD, Schmidt SD, Wang K, et al. Candidate gene for the chromosome 1 familial Alzheimer's disease locus. Science. 1995;269(5226):973-7. PubMed PMID: 7638622.
15. Levy-Lahad E, Wijsman EM, Nemens E, Anderson L, Goddard KA, Weber JL, Bird TD, Schellenberg GD. A familial Alzheimer's disease locus on chromosome 1. Science. 1995;269(5226):970-3. PubMed PMID: 7638621.
16. Van Broeckhoven C, Haan J, Bakker E, Hardy JA, Van Hul W, Wehnert A, Vegter-Van der Vlis M, Roos RA. Amyloid beta protein precursor gene and hereditary cerebral hemorrhage with amyloidosis (Dutch). Science. 1990;248(4959):1120-2. PubMed PMID: 1971458.
17. Hardy J, Selkoe DJ. The amyloid hypothesis of Alzheimer's disease: progress and problems on the road to therapeutics. Science. 2002;297(5580):353-6. doi: 10.1126/science.1072994. PubMed PMID: 12130773.
18. Hardy JA, Higgins GA. Alzheimer's disease: the amyloid cascade hypothesis. Science. 1992;256(5054):184-5. PubMed PMID: 1566067.
19. Selkoe DJ, Hardy J. The amyloid hypothesis of Alzheimer's disease at 25 years. EMBO Mol Med. 2016;8(6):595-608. doi: 10.15252/emmm.201606210. PubMed PMID: 27025652; PMCID: PMC4888851.
20. Mann DM, Esiri MM. The pattern of acquisition of plaques and tangles in the brains of patients under 50 years of age with Down's syndrome. Journal of the neurological sciences. 1989;89(2-3):169-79. PubMed PMID: 2522541.
21. Wisniewski KE, Wisniewski HM, Wen GY. Occurrence of neuropathological changes and dementia of Alzheimer's disease in Down's syndrome. Annals of neurology. 1985;17(3):278-82. doi: 10.1002/ana.410170310. PubMed PMID: 3158266.
22. Mann DM, Jones D, Prinja D, Purkiss MS. The prevalence of amyloid (A4) protein deposits within the cerebral and cerebellar cortex in Down's syndrome and Alzheimer's disease. Acta Neuropathol. 1990;80(3):318-27. PubMed PMID: 1698007.
23. Prasher VP, Farrer MJ, Kessling AM, Fisher EM, West RJ, Barber PC, Butler AC. Molecular mapping of Alzheimer-type dementia in Down's syndrome. Annals of neurology. 1998;43(3):380-3. doi: 10.1002/ana.410430316. PubMed PMID: 9506555.

24. Rovelet-Lecrux A, Hannequin D, Raux G, Le Meur N, Laquerriere A, Vital A, Dumanchin C, Feuillette S, Brice A, Vercelletto M, Dubas F, Frebourg T, Campion D. APP locus duplication causes autosomal dominant early-onset Alzheimer disease with cerebral amyloid angiopathy. Nat Genet. 2006;38(1):24-6. doi: 10.1038/ng1718. PubMed PMID: 16369530.
25. Spillantini MG, Bird TD, Ghetti B. Frontotemporal dementia and Parkinsonism linked to chromosome 17: a new group of tauopathies. Brain pathology. 1998;8(2):387-402. PubMed PMID: 9546295.
26. Hardy J, Duff K, Hardy KG, Perez-Tur J, Hutton M. Genetic dissection of Alzheimer's disease and related dementias: amyloid and its relationship to tau. Nat Neurosci. 1998;1(5):355-8. doi: 10.1038/1565. PubMed PMID: 10196523.
27. Jin M, Shepardson N, Yang T, Chen G, Walsh D, Selkoe DJ. Soluble amyloid beta-protein dimers isolated from Alzheimer cortex directly induce Tau hyperphosphorylation and neuritic degeneration. Proceedings of the National Academy of Sciences of the United States of America. 2011;108(14):5819-24. doi: 10.1073/pnas.1017033108. PubMed PMID: 21421841; PMCID: PMC3078381.
28. Shankar GM, Li S, Mehta TH, Garcia-Munoz A, Shepardson NE, Smith I, Brett FM, Farrell MA, Rowan MJ, Lemere CA, Regan CM, Walsh DM, Sabatini BL, Selkoe DJ. Amyloid-beta protein dimers isolated directly from Alzheimer's brains impair synaptic plasticity and memory. Nature medicine. 2008;14(8):837-42. doi: 10.1038/nm1782. PubMed PMID: 18568035; PMCID: PMC2772133.
29. Schenk D, Barbour R, Dunn W, Gordon G, Grajeda H, Guido T, Hu K, Huang J, Johnson-Wood K, Khan K, Kholodenko D, Lee M, Liao Z, Lieberburg I, Motter R, Mutter L, Soriano F, Shopp G, Vasquez N, Vandevert C, Walker S, Wogulis M, Yednock T, Games D, Seubert P. Immunization with amyloid-beta attenuates Alzheimer-disease-like pathology in the PDAPP mouse. Nature. 1999;400(6740):173-7. doi: 10.1038/22124. PubMed PMID: 10408445.
30. Janus C, Pearson J, McLaurin J, Mathews PM, Jiang Y, Schmidt SD, Chishti MA, Horne P, Heslin D, French J, Mount HT, Nixon RA, Mercken M, Bergeron C, Fraser PE, St George-Hyslop P, Westaway D. A beta peptide immunization reduces behavioural impairment and plaques in a model of Alzheimer's disease. Nature. 2000;408(6815):979-82. doi: 10.1038/35050110. PubMed PMID: 11140685.
31. Morgan D, Diamond DM, Gottschall PE, Ugen KE, Dickey C, Hardy J, Duff K, Jantzen P, DiCarlo G, Wilcock D, Connor K, Hatcher J, Hope C, Gordon M, Arendash GW. A beta peptide vaccination prevents memory loss in an animal model of Alzheimer's disease. Nature. 2000;408(6815):982-5. doi: 10.1038/35050116. PubMed PMID: 11140686.
32. Head E, Pop V, Vasilevko V, Hill M, Saing T, Sarsoza F, Nistor M, Christie LA, Milton S, Glabe C, Barrett E, Cribbs D. A two-year study with fibrillar beta-amyloid (Abeta) immunization in aged canines: effects on cognitive function and brain Abeta. The Journal of neuroscience : the official journal of the Society for Neuroscience. 2008;28(14):3555-66. doi: 10.1523/JNEUROSCI.0208-08.2008. PubMed PMID: 18385314.

33. Lemere CA, Beierschmitt A, Iglesias M, Spooner ET, Bloom JK, Leverone JF, Zheng JB, Seabrook TJ, Louard D, Li D, Selkoe DJ, Palmour RM, Ervin FR. Alzheimer's disease abeta vaccine reduces central nervous system abeta levels in a non-human primate, the Caribbean vervet. Am J Pathol. 2004;165(1):283-97. PubMed PMID: 15215183; PMCID: PMC1618542.
34. Nicoll JA, Wilkinson D, Holmes C, Steart P, Markham H, Weller RO. Neuropathology of human Alzheimer disease after immunization with amyloid-beta peptide: a case report. Nature medicine. 2003;9(4):448-52. doi: 10.1038/nm840. PubMed PMID: 12640446.
35. Schenk D. Amyloid-beta immunotherapy for Alzheimer's disease: the end of the beginning. Nature reviews Neuroscience. 2002;3(10):824-8. doi: 10.1038/nrn938. PubMed PMID: 12360327.
36. Bard F, Cannon C, Barbour R, Burke RL, Games D, Grajeda H, Guido T, Hu K, Huang J, Johnson-Wood K, Khan K, Kholodenko D, Lee M, Lieberburg I, Motter R, Nguyen M, Soriano F, Vasquez N, Weiss K, Welch B, Seubert P, Schenk D, Yednock T. Peripherally administered antibodies against amyloid beta-peptide enter the central nervous system and reduce pathology in a mouse model of Alzheimer disease. Nature medicine. 2000;6(8):916-9. doi: 10.1038/78682. PubMed PMID: 10932230.
37. DeMattos RB, Bales KR, Cummins DJ, Dodart JC, Paul SM, Holtzman DM. Peripheral anti-A beta antibody alters CNS and plasma A beta clearance and decreases brain A beta burden in a mouse model of Alzheimer's disease. Proceedings of the National Academy of Sciences of the United States of America. 2001;98(15):8850-5. doi: 10.1073/pnas.151261398. PubMed PMID: 11438712; PMCID: 37524.
38. Wilcock DM, DiCarlo G, Henderson D, Jackson J, Clarke K, Ugen KE, Gordon MN, Morgan D. Intracranially administered anti-Abeta antibodies reduce beta-amyloid deposition by mechanisms both independent of and associated with microglial activation. The Journal of neuroscience : the official journal of the Society for Neuroscience. 2003;23(9):3745-51. PubMed PMID: 12736345.
39. Wilcock DM, Munireddy SK, Rosenthal A, Ugen KE, Gordon MN, Morgan D. Microglial activation facilitates Abeta plaque removal following intracranial anti-Abeta antibody administration. Neurobiology of disease. 2004;15(1):11-20. PubMed PMID: 14751766.
40. Pfeifer M, Boncristiano S, Bondolfi L, Stalder A, Deller T, Staufenbiel M, Mathews PM, Jucker M. Cerebral hemorrhage after passive anti-Abeta immunotherapy. Science. 2002;298(5597):1379. doi: 10.1126/science.1078259. PubMed PMID: 12434053.
41. Racke MM, Boone LI, Hepburn DL, Parsadainian M, Bryan MT, Ness DK, Piroozi KS, Jordan WH, Brown DD, Hoffman WP, Holtzman DM, Bales KR, Gitter BD, May PC, Paul SM, DeMattos RB. Exacerbation of cerebral amyloid angiopathy-associated microhemorrhage in amyloid precursor protein transgenic mice by immunotherapy is dependent on antibody recognition of deposited forms of amyloid beta. The Journal of neuroscience : the official journal of the Society for Neuroscience. 2005;25(3):629-36. doi: 10.1523/JNEUROSCI.4337-04.2005. PubMed PMID: 15659599.

42. Schroeter S, Khan K, Barbour R, Doan M, Chen M, Guido T, Gill D, Basi G, Schenk D, Seubert P, Games D. Immunotherapy reduces vascular amyloid-beta in PDAPP mice. The Journal of neuroscience : the official journal of the Society for Neuroscience. 2008;28(27):6787-93. doi: 10.1523/JNEUROSCI.2377-07.2008. PubMed PMID: 18596154.
43. Wilcock DM, Rojiani A, Rosenthal A, Subbarao S, Freeman MJ, Gordon MN, Morgan D. Passive immunotherapy against Abeta in aged APP-transgenic mice reverses cognitive deficits and depletes parenchymal amyloid deposits in spite of increased vascular amyloid and microhemorrhage. Journal of neuroinflammation. 2004;1(1):24. doi: 10.1186/1742-2094-1-24. PubMed PMID: 15588287; PMCID: PMC539292.
44. Black RS, Sperling RA, Safirstein B, Motter RN, Pallay A, Nichols A, Grundman M. A single ascending dose study of bapineuzumab in patients with Alzheimer disease. Alzheimer Dis Assoc Disord. 2010;24(2):198-203. doi: 10.1097/WAD.0b013e3181c53b00. PubMed PMID: 20505438; PMCID: PMC3715117.
45. Salloway S, Sperling R, Gilman S, Fox NC, Blennow K, Raskind M, Sabbagh M, Honig LS, Doody R, van Dyck CH, Mulnard R, Barakos J, Gregg KM, Liu E, Lieberburg I, Schenk D, Black R, Grundman M, Bapineuzumab 201 Clinical Trial I. A phase 2 multiple ascending dose trial of bapineuzumab in mild to moderate Alzheimer disease. Neurology. 2009;73(24):2061-70. doi: 10.1212/WNL.0b013e3181c67808. PubMed PMID: 19923550; PMCID: PMC2790221.
46. Salloway S, Sperling R, Fox NC, Blennow K, Klunk W, Raskind M, Sabbagh M, Honig LS, Porsteinsson AP, Ferris S, Reichert M, Ketter N, Nejadnik B, Guenzler V, Miloslavsky M, Wang D, Lu Y, Lull J, Tudor IC, Liu E, Grundman M, Yuen E, Black R, Brashear HR, Bapineuzumab, Clinical Trial I. Two phase 3 trials of bapineuzumab in mild-to-moderate Alzheimer's disease. The New England journal of medicine. 2014;370(4):322-33. doi: 10.1056/NEJMoa1304839. PubMed PMID: 24450891.
47. Solomon B, Koppel R, Frankel D, Hanan-Aharon E. Disaggregation of Alzheimer beta-amyloid by site-directed mAb. Proceedings of the National Academy of Sciences of the United States of America. 1997;94(8):4109-12. PubMed PMID: 9108113; PMCID: PMC20576.
48. Wilcock DM, Colton CA. Immunotherapy, vascular pathology, and microhemorrhages in transgenic mice. CNS & neurological disorders drug targets. 2009;8(1):50-64. PubMed PMID: 19275636; PMCID: 2659468.
49. Zago W, Buttini M, Comery TA, Nishioka C, Gardai SJ, Seubert P, Games D, Bard F, Schenk D, Kinney GG. Neutralization of soluble, synaptotoxic amyloid beta species by antibodies is epitope specific. The Journal of neuroscience : the official journal of the Society for Neuroscience. 2012;32(8):2696-702. doi: 10.1523/JNEUROSCI.1676-11.2012. PubMed PMID: 22357853.
50. Jellinger KA, Attems J. Is there pure vascular dementia in old age? Journal of the neurological sciences. 2010;299(1-2):150-4. doi: 10.1016/j.jns.2010.08.038. PubMed PMID: 20869729.

51. Jellinger KA. Alzheimer disease and cerebrovascular pathology: an update. J Neural Transm (Vienna). 2002;109(5-6):813-36. doi: 10.1007/s007020200068. PubMed PMID: 12111471.
52. Auriel E, Greenberg SM. The pathophysiology and clinical presentation of cerebral amyloid angiopathy. Curr Atheroscler Rep. 2012;14(4):343-50. doi: 10.1007/s11883-012-0254-z. PubMed PMID: 22565298.
53. Vinters HV. Cerebral amyloid angiopathy. A critical review. Stroke; a journal of cerebral circulation. 1987;18(2):311-24. PubMed PMID: 3551211.
54. Pendlebury ST, Rothwell PM. Prevalence, incidence, and factors associated with pre-stroke and post-stroke dementia: a systematic review and meta-analysis. The Lancet Neurology. 2009;8(11):1006-18. doi: 10.1016/S1474-4422(09)70236-4. PubMed PMID: 19782001.
55. Tatemichi TK, Desmond DW, Mayeux R, Paik M, Stern Y, Sano M, Remien RH, Williams JB, Mohr JP, Hauser WA, et al. Dementia after stroke: baseline frequency, risks, and clinical features in a hospitalized cohort. Neurology. 1992;42(6):1185-93. PubMed PMID: 1603346.
56. Prencipe M, Ferretti C, Casini AR, Santini M, Giubilei F, Culasso F. Stroke, disability, and dementia: results of a population survey. Stroke; a journal of cerebral circulation. 1997;28(3):531-6. PubMed PMID: 9056607.
57. Leys D, Henon H, Mackowiak-Cordoliani MA, Pasquier F. Poststroke dementia. The Lancet Neurology. 2005;4(11):752-9. doi: 10.1016/S1474-4422(05)70221-0. PubMed PMID: 16239182.
58. Yang J, Wong A, Wang Z, Liu W, Au L, Xiong Y, Chu WW, Leung EY, Chen S, Lau C, Chan AY, Lau AY, Fan F, Ip V, Soo Y, Leung T, Ho CL, Wong LK, Mok VC. Risk factors for incident dementia after stroke and transient ischemic attack. Alzheimer's & dementia : the journal of the Alzheimer's Association. 2015;11(1):16-23. doi: 10.1016/j.jalz.2014.01.003. PubMed PMID: 24603162.
59. Bowler JV, Munoz DG, Merskey H, Hachinski V. Fallacies in the pathological confirmation of the diagnosis of Alzheimer's disease. Journal of neurology, neurosurgery, and psychiatry. 1998;64(1):18-24. PubMed PMID: 9436722; PMCID: PMC2169908.
60. Langa KM, Foster NL, Larson EB. Mixed dementia: emerging concepts and therapeutic implications. JAMA. 2004;292(23):2901-8. doi: 10.1001/jama.292.23.2901. PubMed PMID: 15598922.
61. Zekry D, Hauw JJ, Gold G. Mixed dementia: epidemiology, diagnosis, and treatment. Journal of the American Geriatrics Society. 2002;50(8):1431-8. PubMed PMID: 12165002.
62. James BD, Bennett DA, Boyle PA, Leurgans S, Schneider JA. Dementia from Alzheimer disease and mixed pathologies in the oldest old. JAMA. 2012;307(17):1798-800. doi: 10.1001/jama.2012.3556. PubMed PMID: 22550192; PMCID: PMC3368581.
63. Schneider JA, Bennett DA. Where vascular meets neurodegenerative disease. Stroke; a journal of cerebral circulation. 2010;41(10 Suppl):S144-6. doi: 10.1161/STROKEAHA.110.598326. PubMed PMID: 20876491; PMCID: PMC2967303.

64. Vemuri P, Knopman DS. The role of cerebrovascular disease when there is concomitant Alzheimer disease. Biochim Biophys Acta. 2016;1862(5):952-6. doi: 10.1016/j.bbadis.2015.09.013. PubMed PMID: 26408957; PMCID: PMC4808514.
65. Launer LJ, Hughes TM, White LR. Microinfarcts, brain atrophy, and cognitive function: the Honolulu Asia Aging Study Autopsy Study. Annals of neurology. 2011;70(5):774-80. doi: 10.1002/ana.22520. PubMed PMID: 22162060; PMCID: PMC3241005.
66. Lo RY, Jagust WJ, Alzheimer's Disease Neuroimaging I. Vascular burden and Alzheimer disease pathologic progression. Neurology. 2012;79(13):1349-55. doi: 10.1212/WNL.0b013e31826c1b9d. PubMed PMID: 22972646; PMCID: PMC3448744.
67. Marchant NL, Reed BR, DeCarli CS, Madison CM, Weiner MW, Chui HC, Jagust WJ. Cerebrovascular disease, beta-amyloid, and cognition in aging. Neurobiology of aging. 2012;33(5):1006 e25-36. doi: 10.1016/j.neurobiolaging.2011.10.001. PubMed PMID: 22048124; PMCID: PMC3274647.
68. Rosano C, Aizenstein HJ, Wu M, Newman AB, Becker JT, Lopez OL, Kuller LH. Focal atrophy and cerebrovascular disease increase dementia risk among cognitively normal older adults. J Neuroimaging. 2007;17(2):148-55. doi: 10.1111/j.1552-6569.2007.00093.x. PubMed PMID: 17441836.
69. Canobbio I, Abubaker AA, Visconte C, Torti M, Pula G. Role of amyloid peptides in vascular dysfunction and platelet dysregulation in Alzheimer's disease. Front Cell Neurosci. 2015;9:65. doi: 10.3389/fncel.2015.00065. PubMed PMID: 25784858; PMCID: PMC4347625.
70. Janota C, Lemere CA, Brito MA. Dissecting the Contribution of Vascular Alterations and Aging to Alzheimer's Disease. Mol Neurobiol. 2016;53(6):3793-811. doi: 10.1007/s12035-015-9319-7. PubMed PMID: 26143259.
71. Streit WJ, Kincaid-Colton CA. The brain's immune system. Sci Am. 1995;273(5):54-5, 8-61. PubMed PMID: 8966536.
72. Chan WY, Kohsaka S, Rezaie P. The origin and cell lineage of microglia: new concepts. Brain Res Rev. 2007;53(2):344-54. doi: 10.1016/j.brainresrev.2006.11.002. PubMed PMID: 17188751.
73. Monier A, Adle-Biassette H, Delezoide AL, Evrard P, Gressens P, Verney C. Entry and distribution of microglial cells in human embryonic and fetal cerebral cortex. J Neuropathol Exp Neurol. 2007;66(5):372-82. doi: 10.1097/nen.0b013e3180517b46. PubMed PMID: 17483694.
74. Benoit M, Desnues B, Mege JL. Macrophage polarization in bacterial infections. Journal of immunology. 2008;181(6):3733-9. PubMed PMID: 18768823.
75. Brown GC. Mechanisms of inflammatory neurodegeneration: iNOS and NADPH oxidase. Biochem Soc Trans. 2007;35(Pt 5):1119-21. doi: 10.1042/BST0351119. PubMed PMID: 17956292.
76. Varnum MM, Ikezu T. The classification of microglial activation phenotypes on neurodegeneration and regeneration in Alzheimer's disease

brain. Arch Immunol Ther Exp (Warsz). 2012;60(4):251-66. doi: 10.1007/s00005-012-0181-2. PubMed PMID: 22710659; PMCID: PMC4429536.
77. Szekanecz Z, Koch AE. Macrophages and their products in rheumatoid arthritis. Curr Opin Rheumatol. 2007;19(3):289-95. doi: 10.1097/BOR.0b013e32805e87ae. PubMed PMID: 17414958.
78. Mosser DM. The many faces of macrophage activation. Journal of leukocyte biology. 2003;73(2):209-12. PubMed PMID: 12554797.
79. Mosser DM, Edwards JP. Exploring the full spectrum of macrophage activation. Nature reviews Immunology. 2008;8(12):958-69. doi: 10.1038/nri2448. PubMed PMID: 19029990; PMCID: 2724991.
80. Wilcock DM. A changing perspective on the role of neuroinflammation in Alzheimer's disease. International journal of Alzheimer's disease. 2012;2012:495243. doi: 10.1155/2012/495243. PubMed PMID: 22844636; PMCID: 3403314.
81. McGeer EG, McGeer PL. The importance of inflammatory mechanisms in Alzheimer disease. Exp Gerontol. 1998;33(5):371-8. PubMed PMID: 9762518.
82. Herber DL, Maloney JL, Roth LM, Freeman MJ, Morgan D, Gordon MN. Diverse microglial responses after intrahippocampal administration of lipopolysaccharide. Glia. 2006;53(4):382-91. doi: 10.1002/glia.20272. PubMed PMID: 16288481.
83. Herber DL, Roth LM, Wilson D, Wilson N, Mason JE, Morgan D, Gordon MN. Time-dependent reduction in Abeta levels after intracranial LPS administration in APP transgenic mice. Experimental neurology. 2004;190(1):245-53. doi: 10.1016/j.expneurol.2004.07.007. PubMed PMID: 15473997.
84. Lee DC, Rizer J, Selenica ML, Reid P, Kraft C, Johnson A, Blair L, Gordon MN, Dickey CA, Morgan D. LPS- induced inflammation exacerbates phospho-tau pathology in rTg4510 mice. Journal of neuroinflammation. 2010;7:56. doi: 10.1186/1742-2094-7-56. PubMed PMID: 20846376; PMCID: PMC2949628.
85. Kitazawa M, Oddo S, Yamasaki TR, Green KN, LaFerla FM. Lipopolysaccharide-induced inflammation exacerbates tau pathology by a cyclin-dependent kinase 5-mediated pathway in a transgenic model of Alzheimer's disease. The Journal of neuroscience : the official journal of the Society for Neuroscience. 2005;25(39):8843-53. doi: 10.1523/JNEUROSCI.2868-05.2005. PubMed PMID: 16192374.
86. Wyss-Coray T, Lin C, Yan F, Yu GQ, Rohde M, McConlogue L, Masliah E, Mucke L. TGF-beta1 promotes microglial amyloid-beta clearance and reduces plaque burden in transgenic mice. Nature medicine. 2001;7(5):612-8. doi: 10.1038/87945. PubMed PMID: 11329064.
87. Montgomery SL, Mastrangelo MA, Habib D, Narrow WC, Knowlden SA, Wright TW, Bowers WJ. Ablation of TNF-RI/RII expression in Alzheimer's disease mice leads to an unexpected enhancement of pathology: implications for chronic pan-TNF-alpha suppressive therapeutic strategies in the brain. Am J Pathol. 2011;179(4):2053-70. doi: 10.1016/j.ajpath.2011.07.001. PubMed PMID: 21835156; PMCID: PMC3181376.

88. Shaftel SS, Kyrkanides S, Olschowka JA, Miller JN, Johnson RE, O'Banion MK. Sustained hippocampal IL-1 beta overexpression mediates chronic neuroinflammation and ameliorates Alzheimer plaque pathology. The Journal of clinical investigation. 2007;117(6):1595-604. doi: 10.1172/JCI31450. PubMed PMID: 17549256; PMCID: PMC1878531.
89. Wilcock DM, Zhao Q, Morgan D, Gordon MN, Everhart A, Wilson JG, Lee JE, Colton CA. Diverse inflammatory responses in transgenic mouse models of Alzheimer's disease and the effect of immunotherapy on these responses. ASN neuro. 2011;3(5):249-58. doi: 10.1042/AN20110018. PubMed PMID: 21995345; PMCID: 3227004.
90. Li Y, Liu L, Barger SW, Griffin WS. Interleukin-1 mediates pathological effects of microglia on tau phosphorylation and on synaptophysin synthesis in cortical neurons through a p38-MAPK pathway. The Journal of neuroscience : the official journal of the Society for Neuroscience. 2003;23(5):1605-11. PubMed PMID: 12629164; PMCID: PMC3833596.
91. Sheng JG, Mrak RE, Jones RA, Brewer MM, Zhou XQ, McGinness J, Woodward S, Bales K, Paul SM, Cordell B, Griffin WS. Neuronal DNA damage correlates with overexpression of interleukin-1beta converting enzyme in APPV717F mice. Neurobiology of aging. 2001;22(6):895-902. PubMed PMID: 11754996.
92. Li H, Li Q, Du X, Sun Y, Wang X, Kroemer G, Blomgren K, Zhu C. Lithium-mediated long-term neuroprotection in neonatal rat hypoxia-ischemia is associated with antiinflammatory effects and enhanced proliferation and survival of neural stem/progenitor cells. Journal of cerebral blood flow and metabolism : official journal of the International Society of Cerebral Blood Flow and Metabolism. 2011;31(10):2106-15. doi: 10.1038/jcbfm.2011.75. PubMed PMID: 21587270; PMCID: PMC3208156.
93. Rapaport MH, Manji HK. The effects of lithium on ex vivo cytokine production. Biol Psychiatry. 2001;50(3):217-24. PubMed PMID: 11513821.
94. Sudduth TL, Wilson JG, Everhart A, Colton CA, Wilcock DM. Lithium treatment of APPSwDI/NOS2-/- mice leads to reduced hyperphosphorylated tau, increased amyloid deposition and altered inflammatory phenotype. PloS one. 2012;7(2):e31993. doi: 10.1371/journal.pone.0031993. PubMed PMID: 22347510; PMCID: 3276493.
95. Sudduth TL, Schmitt FA, Nelson PT, Wilcock DM. Neuroinflammatory phenotype in early Alzheimer's disease. Neurobiology of aging. 2013;34(4):1051-9. doi: 10.1016/j.neurobiolaging.2012.09.012. PubMed PMID: 23062700; PMCID: 3579221.
96. Novak V, Hajjar I. The relationship between blood pressure and cognitive function. Nat Rev Cardiol. 2010;7(12):686-98. doi: 10.1038/nrcardio.2010.161. PubMed PMID: 20978471; PMCID: PMC3328310.
97. Marchesi C, Paradis P, Schiffrin EL. Role of the renin-angiotensin system in vascular inflammation. Trends Pharmacol Sci. 2008;29(7):367-74. doi: 10.1016/j.tips.2008.05.003. PubMed PMID: 18579222.

98. Faraci FM. Protecting against vascular disease in brain. Am J Physiol Heart Circ Physiol. 2011;300(5):H1566-82. doi: 10.1152/ajpheart.01310.2010. PubMed PMID: 21335467; PMCID: PMC3094081.
99. Sim FJ, Zhao C, Penderis J, Franklin RJ. The age-related decrease in CNS remyelination efficiency is attributable to an impairment of both oligodendrocyte progenitor recruitment and differentiation. The Journal of neuroscience : the official journal of the Society for Neuroscience. 2002;22(7):2451-9. doi: 20026217. PubMed PMID: 11923409.
100. Klein T, Bischoff R. Physiology and pathophysiology of matrix metalloproteases. Amino acids. 2011;41(2):271-90. doi: 10.1007/s00726-010-0689-x. PubMed PMID: 20640864; PMCID: 3102199.
101. Aziz F, Kuivaniemi H. Role of matrix metalloproteinase inhibitors in preventing abdominal aortic aneurysm. Ann Vasc Surg. 2007;21(3):392-401. doi: 10.1016/j.avsg.2006.11.001. PubMed PMID: 17484978; PMCID: PMC2128752.
102. Baruch RR, Melinscak H, Lo J, Liu Y, Yeung O, Hurta RA. Altered matrix metalloproteinase expression associated with oncogene-mediated cellular transformation and metastasis formation. Cell Biol Int. 2001;25(5):411-20. doi: 10.1006/cbir.2000.0647. PubMed PMID: 11401328.
103. Mirshafiey A, Asghari B, Ghalamfarsa G, Jadidi-Niaragh F, Azizi G. The significance of matrix metalloproteinases in the immunopathogenesis and treatment of multiple sclerosis. Sultan Qaboos Univ Med J. 2014;14(1):e13-25. PubMed PMID: 24516744; PMCID: PMC3916267.
104. Ram M, Sherer Y, Shoenfeld Y. Matrix metalloproteinase-9 and autoimmune diseases. J Clin Immunol. 2006;26(4):299-307. doi: 10.1007/s10875-006-9022-6. PubMed PMID: 16652230.
105. Yang Y, Estrada EY, Thompson JF, Liu W, Rosenberg GA. Matrix metalloproteinase-mediated disruption of tight junction proteins in cerebral vessels is reversed by synthetic matrix metalloproteinase inhibitor in focal ischemia in rat. Journal of cerebral blood flow and metabolism : official journal of the International Society of Cerebral Blood Flow and Metabolism. 2007;27(4):697-709. doi: 10.1038/sj.jcbfm.9600375. PubMed PMID: 16850029.
106. Hernandez-Guillamon M, Mawhirt S, Fossati S, Blais S, Pares M, Penalba A, Boada M, Couraud PO, Neubert TA, Montaner J, Ghiso J, Rostagno A. Matrix metalloproteinase 2 (MMP-2) degrades soluble vasculotropic amyloid-beta E22Q and L34V mutants, delaying their toxicity for human brain microvascular endothelial cells. The Journal of biological chemistry. 2010;285(35):27144-58. doi: 10.1074/jbc.M110.135228. PubMed PMID: 20576603; PMCID: 2930713.
107. Yan P, Hu X, Song H, Yin K, Bateman RJ, Cirrito JR, Xiao Q, Hsu FF, Turk JW, Xu J, Hsu CY, Holtzman DM, Lee JM. Matrix metalloproteinase-9 degrades amyloid-beta fibrils in vitro and compact plaques in situ. The Journal of biological chemistry. 2006;281(34):24566-74. doi: 10.1074/jbc.M602440200. PubMed PMID: 16787929.
108. Jin DK, Shido K, Kopp HG, Petit I, Shmelkov SV, Young LM, Hooper AT, Amano H, Avecilla ST, Heissig B, Hattori K, Zhang F, Hicklin DJ, Wu Y, Zhu Z, Dunn A, Salari H, Werb Z, Hackett NR, Crystal RG, Lyden D, Rafii S. Cytokine-mediated deployment of SDF-1 induces revascularization through recruitment of

CXCR4+ hemangiocytes. Nature medicine. 2006;12(5):557-67. doi: 10.1038/nm1400. PubMed PMID: 16648859; PMCID: 2754288.
109. Meighan SE, Meighan PC, Choudhury P, Davis CJ, Olson ML, Zornes PA, Wright JW, Harding JW. Effects of extracellular matrix-degrading proteases matrix metalloproteinases 3 and 9 on spatial learning and synaptic plasticity. Journal of neurochemistry. 2006;96(5):1227-41. doi: 10.1111/j.1471-4159.2005.03565.x. PubMed PMID: 16464240.
110. Nagy V, Bozdagi O, Matynia A, Balcerzyk M, Okulski P, Dzwonek J, Costa RM, Silva AJ, Kaczmarek L, Huntley GW. Matrix metalloproteinase-9 is required for hippocampal late-phase long-term potentiation and memory. The Journal of neuroscience : the official journal of the Society for Neuroscience. 2006;26(7):1923-34. doi: 10.1523/JNEUROSCI.4359-05.2006. PubMed PMID: 16481424; PMCID: 4428329.
111. Yong VW, Agrawal SM, Stirling DP. Targeting MMPs in acute and chronic neurological conditions. Neurotherapeutics : the journal of the American Society for Experimental NeuroTherapeutics. 2007;4(4):580-9. doi: 10.1016/j.nurt.2007.07.005. PubMed PMID: 17920539.
112. Zhao BQ, Wang S, Kim HY, Storrie H, Rosen BR, Mooney DJ, Wang X, Lo EH. Role of matrix metalloproteinases in delayed cortical responses after stroke. Nature medicine. 2006;12(4):441-5. doi: 10.1038/nm1387. PubMed PMID: 16565723.
113. Vecil GG, Larsen PH, Corley SM, Herx LM, Besson A, Goodyer CG, Yong VW. Interleukin-1 is a key regulator of matrix metalloproteinase-9 expression in human neurons in culture and following mouse brain trauma in vivo. Journal of neuroscience research. 2000;61(2):212-24. PubMed PMID: 10878594.
114. Galis ZS, Muszynski M, Sukhova GK, Simon-Morrissey E, Unemori EN, Lark MW, Amento E, Libby P. Cytokine-stimulated human vascular smooth muscle cells synthesize a complement of enzymes required for extracellular matrix digestion. Circulation research. 1994;75(1):181-9. PubMed PMID: 8013077.
115. Overall CM, Lopez-Otin C. Strategies for MMP inhibition in cancer: innovations for the post-trial era. Nature reviews Cancer. 2002;2(9):657-72. doi: 10.1038/nrc884. PubMed PMID: 12209155.
116. Sato H, Takino T, Okada Y, Cao J, Shinagawa A, Yamamoto E, Seiki M. A matrix metalloproteinase expressed on the surface of invasive tumour cells. Nature. 1994;370(6484):61-5. doi: 10.1038/370061a0. PubMed PMID: 8015608.
117. Seiki M. The cell surface: the stage for matrix metalloproteinase regulation of migration. Curr Opin Cell Biol. 2002;14(5):624-32. PubMed PMID: 12231359.
118. Strongin AY, Collier I, Bannikov G, Marmer BL, Grant GA, Goldberg GI. Mechanism of cell surface activation of 72-kDa type IV collagenase. Isolation of the activated form of the membrane metalloprotease. The Journal of biological chemistry. 1995;270(10):5331-8. PubMed PMID: 7890645.
119. Ridnour LA, Dhanapal S, Hoos M, Wilson J, Lee J, Cheng RY, Brueggemann EE, Hines HB, Wilcock DM, Vitek MP, Wink DA, Colton CA. Nitric oxide-mediated regulation of beta-amyloid clearance via alterations of MMP-

9/TIMP-1. Journal of neurochemistry. 2012;123(5):736-49. doi: 10.1111/jnc.12028. PubMed PMID: 23016931; PMCID: 3614913.
120. Candelario-Jalil E, Thompson J, Taheri S, Grossetete M, Adair JC, Edmonds E, Prestopnik J, Wills J, Rosenberg GA. Matrix metalloproteinases are associated with increased blood-brain barrier opening in vascular cognitive impairment. Stroke; a journal of cerebral circulation. 2011;42(5):1345-50. doi: 10.1161/STROKEAHA.110.600825. PubMed PMID: 21454822; PMCID: 3119779.
121. Jellinger KA. Alzheimer disease and cerebrovascular pathology: an update. Journal of neural transmission. 2002;109(5-6):813-36. doi: 10.1007/s007020200068. PubMed PMID: 12111471.
122. Maia LF, Vasconcelos C, Seixas S, Magalhaes R, Correia M. Lobar brain hemorrhages and white matter changes: Clinical, radiological and laboratorial profiles. Cerebrovascular diseases. 2006;22(2-3):155-61. doi: 10.1159/000093245. PubMed PMID: 16691025.
123. Goos JD, Kester MI, Barkhof F, Klein M, Blankenstein MA, Scheltens P, van der Flier WM. Patients with Alzheimer disease with multiple microbleeds: relation with cerebrospinal fluid biomarkers and cognition. Stroke; a journal of cerebral circulation. 2009;40(11):3455-60. doi: 10.1161/STROKEAHA.109.558197. PubMed PMID: 19762705.
124. Asahina M, Yoshiyama Y, Hattori T. Expression of matrix metalloproteinase-9 and urinary-type plasminogen activator in Alzheimer's disease brain. Clin Neuropathol. 2001;20(2):60-3. PubMed PMID: 11327298.
125. Bruno MA, Leon WC, Fragoso G, Mushynski WE, Almazan G, Cuello AC. Amyloid beta-induced nerve growth factor dysmetabolism in Alzheimer disease. J Neuropathol Exp Neurol. 2009;68(8):857-69. doi: 10.1097/NEN.0b013e3181aed9e6. PubMed PMID: 19606067.
126. Lorenzl S, Albers DS, Relkin N, Ngyuen T, Hilgenberg SL, Chirichigno J, Cudkowicz ME, Beal MF. Increased plasma levels of matrix metalloproteinase-9 in patients with Alzheimer's disease. Neurochem Int. 2003;43(3):191-6. PubMed PMID: 12689599.
127. Lorenzl S, Buerger K, Hampel H, Beal MF. Profiles of matrix metalloproteinases and their inhibitors in plasma of patients with dementia. Int Psychogeriatr. 2008;20(1):67-76. doi: 10.1017/S1041610207005790. PubMed PMID: 17697439.
128. Bruno MA, Mufson EJ, Wuu J, Cuello AC. Increased matrix metalloproteinase 9 activity in mild cognitive impairment. J Neuropathol Exp Neurol. 2009;68(12):1309-18. doi: 10.1097/NEN.0b013e3181c22569. PubMed PMID: 19915485; PMCID: PMC2810197.
129. Yin KJ, Cirrito JR, Yan P, Hu X, Xiao Q, Pan X, Bateman R, Song H, Hsu FF, Turk J, Xu J, Hsu CY, Mills JC, Holtzman DM, Lee JM. Matrix metalloproteinases expressed by astrocytes mediate extracellular amyloid-beta peptide catabolism. The Journal of neuroscience : the official journal of the Society for Neuroscience. 2006;26(43):10939-48. doi: 10.1523/JNEUROSCI.2085-06.2006. PubMed PMID: 17065436.

130. Lee JM, Yin KJ, Hsin I, Chen S, Fryer JD, Holtzman DM, Hsu CY, Xu J. Matrix metalloproteinase-9 and spontaneous hemorrhage in an animal model of cerebral amyloid angiopathy. Annals of neurology. 2003;54(3):379-82. doi: 10.1002/ana.10671. PubMed PMID: 12953271.
131. Ransohoff RM, Brown MA. Innate immunity in the central nervous system. The Journal of clinical investigation. 2012;122(4):1164-71. doi: 10.1172/JCI58644. PubMed PMID: 22466658; PMCID: PMC3314450.
132. Achilli C, Ciana A, Minetti G. Amyloid-beta (25-35) peptide induces the release of pro-matrix metalloprotease 9 (pro-MMP-9) from human neutrophils. Mol Cell Biochem. 2014;397(1-2):117-23. doi: 10.1007/s11010-014-2178-0. PubMed PMID: 25087121.
133. Nubling G, Levin J, Bader B, Israel L, Botzel K, Lorenzl S, Giese A. Limited cleavage of tau with matrix-metalloproteinase MMP-9, but not MMP-3, enhances tau oligomer formation. Experimental neurology. 2012;237(2):470-6. doi: 10.1016/j.expneurol.2012.07.018. PubMed PMID: 22890115.
134. Frost B, Jacks RL, Diamond MI. Propagation of tau misfolding from the outside to the inside of a cell. The Journal of biological chemistry. 2009;284(19):12845-52. doi: 10.1074/jbc.M808759200. PubMed PMID: 19282288; PMCID: PMC2676015.
135. Beslow LA, Smith SE, Vossough A, Licht DJ, Kasner SE, Favilla CG, Halperin AR, Gordon DM, Jones CI, Cucchiara AJ, Ichord RN. Hemorrhagic transformation of childhood arterial ischemic stroke. Stroke; a journal of cerebral circulation. 2011;42(4):941-6. doi: 10.1161/STROKEAHA.110.604199. PubMed PMID: 21350202; PMCID: 3066279.
136. Terruso V, D'Amelio M, Di Benedetto N, Lupo I, Saia V, Famoso G, Mazzola MA, Aridon P, Sarno C, Ragonese P, Savettieri G. Frequency and determinants for hemorrhagic transformation of cerebral infarction. Neuroepidemiology. 2009;33(3):261-5. doi: 10.1159/000229781. PubMed PMID: 19641332.
137. Berger C, Fiorelli M, Steiner T, Schabitz WR, Bozzao L, Bluhmki E, Hacke W, von Kummer R. Hemorrhagic transformation of ischemic brain tissue: asymptomatic or symptomatic? Stroke; a journal of cerebral circulation. 2001;32(6):1330-5. PubMed PMID: 11387495.
138. Fiorelli M, Bastianello S, von Kummer R, del Zoppo GJ, Larrue V, Lesaffre E, Ringleb AP, Lorenzano S, Manelfe C, Bozzao L. Hemorrhagic transformation within 36 hours of a cerebral infarct: relationships with early clinical deterioration and 3-month outcome in the European Cooperative Acute Stroke Study I (ECASS I) cohort. Stroke; a journal of cerebral circulation. 1999;30(11):2280-4. PubMed PMID: 10548658.
139. Tissue plasminogen activator for acute ischemic stroke. The National Institute of Neurological Disorders and Stroke rt-PA Stroke Study Group. The New England journal of medicine. 1995;333(24):1581-7. doi: 10.1056/NEJM199512143332401. PubMed PMID: 7477192.
140. Lees KR, Bluhmki E, von Kummer R, Brott TG, Toni D, Grotta JC, Albers GW, Kaste M, Marler JR, Hamilton SA, Tilley BC, Davis SM, Donnan GA, Hacke W, Ecass AN, Group Er-PS, Allen K, Mau J, Meier D, del Zoppo G, De Silva DA,

Butcher KS, Parsons MW, Barber PA, Levi C, Bladin C, Byrnes G. Time to treatment with intravenous alteplase and outcome in stroke: an updated pooled analysis of ECASS, ATLANTIS, NINDS, and EPITHET trials. Lancet. 2010;375(9727):1695-703. doi: 10.1016/S0140-6736(10)60491-6. PubMed PMID: 20472172.
141. Kelly MA, Shuaib A, Todd KG. Matrix metalloproteinase activation and blood-brain barrier breakdown following thrombolysis. Experimental neurology. 2006;200(1):38-49. doi: 10.1016/j.expneurol.2006.01.032. PubMed PMID: 16624294.
142. Suzuki Y, Nagai N, Umemura K. Novel situations of endothelial injury in stroke--mechanisms of stroke and strategy of drug development: intracranial bleeding associated with the treatment of ischemic stroke: thrombolytic treatment of ischemia-affected endothelial cells with tissue-type plasminogen activator. Journal of pharmacological sciences. 2011;116(1):25-9. PubMed PMID: 21498957.
143. Wang X, Lee SR, Arai K, Lee SR, Tsuji K, Rebeck GW, Lo EH. Lipoprotein receptor-mediated induction of matrix metalloproteinase by tissue plasminogen activator. Nature medicine. 2003;9(10):1313-7. doi: 10.1038/nm926. PubMed PMID: 12960961.
144. Jickling GC, Liu D, Stamova B, Ander BP, Zhan X, Lu A, Sharp FR. Hemorrhagic transformation after ischemic stroke in animals and humans. Journal of cerebral blood flow and metabolism : official journal of the International Society of Cerebral Blood Flow and Metabolism. 2014;34(2):185-99. doi: 10.1038/jcbfm.2013.203. PubMed PMID: 24281743; PMCID: 3915212.
145. Sandoval KE, Witt KA. Blood-brain barrier tight junction permeability and ischemic stroke. Neurobiology of disease. 2008;32(2):200-19. doi: 10.1016/j.nbd.2008.08.005. PubMed PMID: 18790057.
146. Stamova B, Xu H, Jickling G, Bushnell C, Tian Y, Ander BP, Zhan X, Liu D, Turner R, Adamczyk P, Khoury JC, Pancioli A, Jauch E, Broderick JP, Sharp FR. Gene expression profiling of blood for the prediction of ischemic stroke. Stroke; a journal of cerebral circulation. 2010;41(10):2171-7. doi: 10.1161/STROKEAHA.110.588335. PubMed PMID: 20798371; PMCID: 2987675.
147. Tang Y, Xu H, Du X, Lit L, Walker W, Lu A, Ran R, Gregg JP, Reilly M, Pancioli A, Khoury JC, Sauerbeck LR, Carrozzella JA, Spilker J, Clark J, Wagner KR, Jauch EC, Chang DJ, Verro P, Broderick JP, Sharp FR. Gene expression in blood changes rapidly in neutrophils and monocytes after ischemic stroke in humans: a microarray study. Journal of cerebral blood flow and metabolism : official journal of the International Society of Cerebral Blood Flow and Metabolism. 2006;26(8):1089-102. doi: 10.1038/sj.jcbfm.9600264. PubMed PMID: 16395289.
148. Castellanos M, Leira R, Serena J, Pumar JM, Lizasoain I, Castillo J, Davalos A. Plasma metalloproteinase-9 concentration predicts hemorrhagic transformation in acute ischemic stroke. Stroke; a journal of cerebral circulation. 2003;34(1):40-6. PubMed PMID: 12511748.

149. Castellanos M, Sobrino T, Millan M, Garcia M, Arenillas J, Nombela F, Brea D, Perez de la Ossa N, Serena J, Vivancos J, Castillo J, Davalos A. Serum cellular fibronectin and matrix metalloproteinase-9 as screening biomarkers for the prediction of parenchymal hematoma after thrombolytic therapy in acute ischemic stroke: a multicenter confirmatory study. Stroke; a journal of cerebral circulation. 2007;38(6):1855-9. doi: 10.1161/STROKEAHA.106.481556. PubMed PMID: 17478737.
150. Demir R, Ulvi H, Ozel L, Ozdemir G, Guzelcik M, Aygul R. Relationship between plasma metalloproteinase-9 levels and volume and severity of infarct in patients with acute ischemic stroke. Acta neurologica Belgica. 2012;112(4):351-6. doi: 10.1007/s13760-012-0067-4. PubMed PMID: 22581515.
151. Montaner J, Molina CA, Monasterio J, Abilleira S, Arenillas JF, Ribo M, Quintana M, Alvarez-Sabin J. Matrix metalloproteinase-9 pretreatment level predicts intracranial hemorrhagic complications after thrombolysis in human stroke. Circulation. 2003;107(4):598-603. PubMed PMID: 12566373.
152. Lu A, Clark JF, Broderick JP, Pyne-Geithman GJ, Wagner KR, Khatri P, Tomsick T, Sharp FR. Mechanical reperfusion is associated with post-ischemic hemorrhage in rat brain. Experimental neurology. 2009;216(2):407-12. doi: 10.1016/j.expneurol.2008.12.020. PubMed PMID: 19162014; PMCID: 2659349.
153. Lu A, Clark JF, Broderick JP, Pyne-Geithman GJ, Wagner KR, Ran R, Khatri P, Tomsick T, Sharp FR. Reperfusion activates metalloproteinases that contribute to neurovascular injury. Experimental neurology. 2008;210(2):549-59. doi: 10.1016/j.expneurol.2007.12.003. PubMed PMID: 18187134; PMCID: 2588410.
154. Heo JH, Lucero J, Abumiya T, Koziol JA, Copeland BR, del Zoppo GJ. Matrix metalloproteinases increase very early during experimental focal cerebral ischemia. Journal of cerebral blood flow and metabolism : official journal of the International Society of Cerebral Blood Flow and Metabolism. 1999;19(6):624-33. doi: 10.1097/00004647-199906000-00005. PubMed PMID: 10366192.
155. Liu J, Jin X, Liu KJ, Liu W. Matrix metalloproteinase-2-mediated occludin degradation and caveolin-1-mediated claudin-5 redistribution contribute to blood-brain barrier damage in early ischemic stroke stage. The Journal of neuroscience : the official journal of the Society for Neuroscience. 2012;32(9):3044-57. doi: 10.1523/JNEUROSCI.6409-11.2012. PubMed PMID: 22378877; PMCID: 3339570.
156. Suofu Y, Clark JF, Broderick JP, Kurosawa Y, Wagner KR, Lu A. Matrix metalloproteinase-2 or -9 deletions protect against hemorrhagic transformation during early stage of cerebral ischemia and reperfusion. Neuroscience. 2012;212:180-9. doi: 10.1016/j.neuroscience.2012.03.036. PubMed PMID: 22521821; PMCID: 3367043.
157. Liu W, Rosenberg GA, Shi H, Furuichi T, Timmins GS, Cunningham LA, Liu KJ. Xanthine oxidase activates pro-matrix metalloproteinase-2 in cultured rat vascular smooth muscle cells through non-free radical mechanisms. Archives of biochemistry and biophysics. 2004;426(1):11-7. doi: 10.1016/j.abb.2004.03.029. PubMed PMID: 15130778.

158. Yang Y, Rosenberg GA. Blood-brain barrier breakdown in acute and chronic cerebrovascular disease. Stroke; a journal of cerebral circulation. 2011;42(11):3323-8. doi: 10.1161/STROKEAHA.110.608257. PubMed PMID: 21940972; PMCID: 3584169.
159. Rosenberg GA, Estrada EY, Dencoff JE. Matrix metalloproteinases and TIMPs are associated with blood-brain barrier opening after reperfusion in rat brain. Stroke; a journal of cerebral circulation. 1998;29(10):2189-95. PubMed PMID: 9756602.
160. Rosenberg GA, Kornfeld M, Estrada E, Kelley RO, Liotta LA, Stetler-Stevenson WG. TIMP-2 reduces proteolytic opening of blood-brain barrier by type IV collagenase. Brain research. 1992;576(2):203-7. PubMed PMID: 1381261.
161. del Zoppo GJ, Frankowski H, Gu YH, Osada T, Kanazawa M, Milner R, Wang X, Hosomi N, Mabuchi T, Koziol JA. Microglial cell activation is a source of metalloproteinase generation during hemorrhagic transformation. Journal of cerebral blood flow and metabolism : official journal of the International Society of Cerebral Blood Flow and Metabolism. 2012;32(5):919-32. doi: 10.1038/jcbfm.2012.11. PubMed PMID: 22354151; PMCID: PMC3345906.
162. Suzuki Y, Nagai N, Umemura K, Collen D, Lijnen HR. Stromelysin-1 (MMP-3) is critical for intracranial bleeding after t-PA treatment of stroke in mice. Journal of thrombosis and haemostasis : JTH. 2007;5(8):1732-9. doi: 10.1111/j.1538-7836.2007.02628.x. PubMed PMID: 17596135.
163. Cuadrado E, Rosell A, Penalba A, Slevin M, Alvarez-Sabin J, Ortega-Aznar A, Montaner J. Vascular MMP-9/TIMP-2 and neuronal MMP-10 up-regulation in human brain after stroke: a combined laser microdissection and protein array study. Journal of proteome research. 2009;8(6):3191-7. doi: 10.1021/pr801012x. PubMed PMID: 19317417.
164. Abilleira S, Montaner J, Molina CA, Monasterio J, Castillo J, Alvarez-Sabin J. Matrix metalloproteinase-9 concentration after spontaneous intracerebral hemorrhage. Journal of neurosurgery. 2003;99(1):65-70. doi: 10.3171/jns.2003.99.1.0065. PubMed PMID: 12854746.
165. Rosell A, Ortega-Aznar A, Alvarez-Sabin J, Fernandez-Cadenas I, Ribo M, Molina CA, Lo EH, Montaner J. Increased brain expression of matrix metalloproteinase-9 after ischemic and hemorrhagic human stroke. Stroke; a journal of cerebral circulation. 2006;37(6):1399-406. doi: 10.1161/01.STR.0000223001.06264.af. PubMed PMID: 16690896.
166. Games D, Adams D, Alessandrini R, Barbour R, Berthelette P, Blackwell C, Carr T, Clemens J, Donaldson T, Gillespie F, et al. Alzheimer-type neuropathology in transgenic mice overexpressing V717F beta-amyloid precursor protein. Nature. 1995;373(6514):523-7. doi: 10.1038/373523a0. PubMed PMID: 7845465.
167. Hsiao K, Chapman P, Nilsen S, Eckman C, Harigaya Y, Younkin S, Yang F, Cole G. Correlative memory deficits, Abeta elevation, and amyloid plaques in transgenic mice. Science. 1996;274(5284):99-102. PubMed PMID: 8810256.
168. Duff K, Eckman C, Zehr C, Yu X, Prada CM, Perez-tur J, Hutton M, Buee L, Harigaya Y, Yager D, Morgan D, Gordon MN, Holcomb L, Refolo L, Zenk B,

Hardy J, Younkin S. Increased amyloid-beta42(43) in brains of mice expressing mutant presenilin 1. Nature. 1996;383(6602):710-3. doi: 10.1038/383710a0. PubMed PMID: 8878479.
169. Holcomb L, Gordon MN, McGowan E, Yu X, Benkovic S, Jantzen P, Wright K, Saad I, Mueller R, Morgan D, Sanders S, Zehr C, O'Campo K, Hardy J, Prada CM, Eckman C, Younkin S, Hsiao K, Duff K. Accelerated Alzheimer-type phenotype in transgenic mice carrying both mutant amyloid precursor protein and presenilin 1 transgenes. Nature medicine. 1998;4(1):97-100. PubMed PMID: 9427614.
170. Jankowsky JL, Fadale DJ, Anderson J, Xu GM, Gonzales V, Jenkins NA, Copeland NG, Lee MK, Younkin LH, Wagner SL, Younkin SG, Borchelt DR. Mutant presenilins specifically elevate the levels of the 42 residue beta-amyloid peptide in vivo: evidence for augmentation of a 42-specific gamma secretase. Human molecular genetics. 2004;13(2):159-70. doi: 10.1093/hmg/ddh019. PubMed PMID: 14645205.
171. Jankowsky JL, Slunt HH, Ratovitski T, Jenkins NA, Copeland NG, Borchelt DR. Co-expression of multiple transgenes in mouse CNS: a comparison of strategies. Biomol Eng. 2001;17(6):157-65. PubMed PMID: 11337275.
172. Kamphuis W, Mamber C, Moeton M, Kooijman L, Sluijs JA, Jansen AH, Verveer M, de Groot LR, Smith VD, Rangarajan S, Rodriguez JJ, Orre M, Hol EM. GFAP isoforms in adult mouse brain with a focus on neurogenic astrocytes and reactive astrogliosis in mouse models of Alzheimer disease. PloS one. 2012;7(8):e42823. doi: 10.1371/journal.pone.0042823. PubMed PMID: 22912745; PMCID: PMC3418292.
173. Garcia-Alloza M, Robbins EM, Zhang-Nunes SX, Purcell SM, Betensky RA, Raju S, Prada C, Greenberg SM, Bacskai BJ, Frosch MP. Characterization of amyloid deposition in the APPswe/PS1dE9 mouse model of Alzheimer disease. Neurobiology of disease. 2006;24(3):516-24. doi: 10.1016/j.nbd.2006.08.017. PubMed PMID: 17029828.
174. Janus C, Flores AY, Xu G, Borchelt DR. Behavioral abnormalities in APPSwe/PS1dE9 mouse model of AD-like pathology: comparative analysis across multiple behavioral domains. Neurobiology of aging. 2015;36(9):2519-32. doi: 10.1016/j.neurobiolaging.2015.05.010. PubMed PMID: 26089165.
175. Kilgore M, Miller CA, Fass DM, Hennig KM, Haggarty SJ, Sweatt JD, Rumbaugh G. Inhibitors of class 1 histone deacetylases reverse contextual memory deficits in a mouse model of Alzheimer's disease. Neuropsychopharmacology. 2010;35(4):870-80. doi: 10.1038/npp.2009.197. PubMed PMID: 20010553; PMCID: PMC3055373.
176. Lalonde R, Kim HD, Maxwell JA, Fukuchi K. Exploratory activity and spatial learning in 12-month-old APP(695)SWE/co+PS1/DeltaE9 mice with amyloid plaques. Neurosci Lett. 2005;390(2):87-92. doi: 10.1016/j.neulet.2005.08.028. PubMed PMID: 16169151.
177. Volianskis A, Kostner R, Molgaard M, Hass S, Jensen MS. Episodic memory deficits are not related to altered glutamatergic synaptic transmission and plasticity in the CA1 hippocampus of the APPswe/PS1deltaE9-deleted transgenic mice model of ss-amyloidosis. Neurobiology of aging.

2010;31(7):1173-87. doi: 10.1016/j.neurobiolaging.2008.08.005. PubMed PMID: 18790549.
178. Shibata M, Ohtani R, Ihara M, Tomimoto H. White matter lesions and glial activation in a novel mouse model of chronic cerebral hypoperfusion. Stroke; a journal of cerebral circulation. 2004;35(11):2598-603. doi: 10.1161/01.STR.0000143725.19053.60. PubMed PMID: 15472111.
179. Yamori Y, Horie R, Handa H, Sato M, Fukase M. Pathogenetic similarity of strokes in stroke-prone spontaneously hypertensive rats and humans. Stroke; a journal of cerebral circulation. 1976;7(1):46-53. PubMed PMID: 1258104.
180. Ruchoux MM, Domenga V, Brulin P, Maciazek J, Limol S, Tournier-Lasserve E, Joutel A. Transgenic mice expressing mutant Notch3 develop vascular alterations characteristic of cerebral autosomal dominant arteriopathy with subcortical infarcts and leukoencephalopathy. Am J Pathol. 2003;162(1):329-42. doi: 10.1016/S0002-9440(10)63824-2. PubMed PMID: 12507916; PMCID: PMC1851116.
181. Utku U, Celik Y, Uyguner O, Yuksel-Apak M, Wollnik B. CADASIL syndrome in a large Turkish kindred caused by the R90C mutation in the Notch3 receptor. Eur J Neurol. 2002;9(1):23-8. PubMed PMID: 11784372.
182. Selhub J. Homocysteine metabolism. Annu Rev Nutr. 1999;19:217-46. doi: 10.1146/annurev.nutr.19.1.217. PubMed PMID: 10448523.
183. Locasale JW. Serine, glycine and one-carbon units: cancer metabolism in full circle. Nature reviews Cancer. 2013;13(8):572-83. doi: 10.1038/nrc3557. PubMed PMID: 23822983; PMCID: PMC3806315.
184. Beydoun MA, Beydoun HA, Gamaldo AA, Teel A, Zonderman AB, Wang Y. Epidemiologic studies of modifiable factors associated with cognition and dementia: systematic review and meta-analysis. BMC Public Health. 2014;14:643. doi: 10.1186/1471-2458-14-643. PubMed PMID: 24962204; PMCID: PMC4099157.
185. Bostom AG, Rosenberg IH, Silbershatz H, Jacques PF, Selhub J, D'Agostino RB, Wilson PW, Wolf PA. Nonfasting plasma total homocysteine levels and stroke incidence in elderly persons: the Framingham Study. Annals of internal medicine. 1999;131(5):352-5. PubMed PMID: 10475888.
186. Eikelboom JW, Lonn E, Genest J, Jr., Hankey G, Yusuf S. Homocyst(e)ine and cardiovascular disease: a critical review of the epidemiologic evidence. Annals of internal medicine. 1999;131(5):363-75. PubMed PMID: 10475890.
187. Graham IM, Daly LE, Refsum HM, Robinson K, Brattstrom LE, Ueland PM, Palma-Reis RJ, Boers GH, Sheahan RG, Israelsson B, Uiterwaal CS, Meleady R, McMaster D, Verhoef P, Witteman J, Rubba P, Bellet H, Wautrecht JC, de Valk HW, Sales Luis AC, Parrot-Rouland FM, Tan KS, Higgins I, Garcon D, Andria G, et al. Plasma homocysteine as a risk factor for vascular disease. The European Concerted Action Project. JAMA. 1997;277(22):1775-81. PubMed PMID: 9178790.
188. Welch GN, Loscalzo J. Homocysteine and atherothrombosis. The New England journal of medicine. 1998;338(15):1042-50. doi: 10.1056/NEJM199804093381507. PubMed PMID: 9535670.

189. Clarke R, Harrison G, Richards S, Vital Trial Collaborative G. Effect of vitamins and aspirin on markers of platelet activation, oxidative stress and homocysteine in people at high risk of dementia. J Intern Med. 2003;254(1):67-75. PubMed PMID: 12823643.
190. Miller JW, Green R, Mungas DM, Reed BR, Jagust WJ. Homocysteine, vitamin B6, and vascular disease in AD patients. Neurology. 2002;58(10):1471-5. PubMed PMID: 12034781.
191. Firbank MJ, Narayan SK, Saxby BK, Ford GA, O'Brien JT. Homocysteine is associated with hippocampal and white matter atrophy in older subjects with mild hypertension. Int Psychogeriatr. 2010;22(5):804-11. doi: 10.1017/S1041610210000499. PubMed PMID: 20374668.
192. Vermeer SE, van Dijk EJ, Koudstaal PJ, Oudkerk M, Hofman A, Clarke R, Breteler MM. Homocysteine, silent brain infarcts, and white matter lesions: The Rotterdam Scan Study. Annals of neurology. 2002;51(3):285-9. PubMed PMID: 11891822.
193. Watanabe M, Osada J, Aratani Y, Kluckman K, Reddick R, Malinow MR, Maeda N. Mice deficient in cystathionine beta-synthase: animal models for mild and severe homocyst(e)inemia. Proceedings of the National Academy of Sciences of the United States of America. 1995;92(5):1585-9. PubMed PMID: 7878023; PMCID: PMC42564.
194. Weiss N, Heydrick SJ, Postea O, Keller C, Keaney JF, Jr., Loscalzo J. Influence of hyperhomocysteinemia on the cellular redox state--impact on homocysteine-induced endothelial dysfunction. Clin Chem Lab Med. 2003;41(11):1455-61. doi: 10.1515/CCLM.2003.223. PubMed PMID: 14656025.
195. Baumbach GL, Sigmund CD, Bottiglieri T, Lentz SR. Structure of cerebral arterioles in cystathionine beta-synthase-deficient mice. Circulation research. 2002;91(10):931-7. PubMed PMID: 12433838.
196. Clayton PT, Smith I, Harding B, Hyland K, Leonard JV, Leeming RJ. Subacute combined degeneration of the cord, dementia and parkinsonism due to an inborn error of folate metabolism. Journal of neurology, neurosurgery, and psychiatry. 1986;49(8):920-7. PubMed PMID: 3755752; PMCID: PMC1028954.
197. Hyland K, Smith I, Bottiglieri T, Perry J, Wendel U, Clayton PT, Leonard JV. Demyelination and decreased S-adenosylmethionine in 5,10-methylenetetrahydrofolate reductase deficiency. Neurology. 1988;38(3):459-62. PubMed PMID: 3347350.
198. Surtees R, Leonard J, Austin S. Association of demyelination with deficiency of cerebrospinal-fluid S-adenosylmethionine in inborn errors of methyl-transfer pathway. Lancet. 1991;338(8782-8783):1550-4. PubMed PMID: 1683972.
199. Chen Z, Karaplis AC, Ackerman SL, Pogribny IP, Melnyk S, Lussier-Cacan S, Chen MF, Pai A, John SW, Smith RS, Bottiglieri T, Bagley P, Selhub J, Rudnicki MA, James SJ, Rozen R. Mice deficient in methylenetetrahydrofolate reductase exhibit hyperhomocysteinemia and decreased methylation capacity, with neuropathology and aortic lipid deposition. Human molecular genetics. 2001;10(5):433-43. PubMed PMID: 11181567.

200. Troen AM, Shea-Budgell M, Shukitt-Hale B, Smith DE, Selhub J, Rosenberg IH. B-vitamin deficiency causes hyperhomocysteinemia and vascular cognitive impairment in mice. Proceedings of the National Academy of Sciences of the United States of America. 2008;105(34):12474-9. doi: 10.1073/pnas.0805350105. PubMed PMID: 18711131; PMCID: 2517600.
201. Kim JM, Lee H, Chang N. Hyperhomocysteinemia due to short-term folate deprivation is related to electron microscopic changes in the rat brain. J Nutr. 2002;132(11):3418-21. PubMed PMID: 12421861.
202. Pirchl M, Ullrich C, Humpel C. Differential effects of short- and long-term hyperhomocysteinaemia on cholinergic neurons, spatial memory and microbleedings in vivo in rats. Eur J Neurosci. 2010;32(9):1516-27. doi: 10.1111/j.1460-9568.2010.07434.x. PubMed PMID: 21044172.
203. Sudduth TL, Powell DK, Smith CD, Greenstein A, Wilcock DM. Induction of hyperhomocysteinemia models vascular dementia by induction of cerebral microhemorrhages and neuroinflammation. Journal of cerebral blood flow and metabolism : official journal of the International Society of Cerebral Blood Flow and Metabolism. 2013;33(5):708-15. doi: 10.1038/jcbfm.2013.1. PubMed PMID: 23361394; PMCID: 3652696.
204. Sudduth TL, Weekman EM, Brothers HM, Braun K, Wilcock DM. beta-amyloid deposition is shifted to the vasculature and memory impairment is exacerbated when hyperhomocysteinemia is induced in APP/PS1 transgenic mice. Alzheimer's research & therapy. 2014;6(3):32. doi: 10.1186/alzrt262. PubMed PMID: 24991237; PMCID: 4078260.
205. Gallagher JJ, Finnegan ME, Grehan B, Dobson J, Collingwood JF, Lynch MA. Modest amyloid deposition is associated with iron dysregulation, microglial activation, and oxidative stress. Journal of Alzheimer's disease : JAD. 2012;28(1):147-61. doi: 10.3233/JAD-2011-110614. PubMed PMID: 21971404.
206. Maezawa I, Zimin PI, Wulff H, Jin LW. Amyloid-beta protein oligomer at low nanomolar concentrations activates microglia and induces microglial neurotoxicity. The Journal of biological chemistry. 2011;286(5):3693-706. doi: 10.1074/jbc.M110.135244. PubMed PMID: 20971854; PMCID: 3030372.
207. Paranjape GS, Terrill SE, Gouwens LK, Ruck BM, Nichols MR. Amyloid-beta(1-42) protofibrils formed in modified artificial cerebrospinal fluid bind and activate microglia. Journal of neuroimmune pharmacology : the official journal of the Society on NeuroImmune Pharmacology. 2013;8(1):312-22. doi: 10.1007/s11481-012-9424-6. PubMed PMID: 23242692; PMCID: 3587657.
208. Akiyama H, Barger S, Barnum S, Bradt B, Bauer J, Cole GM, Cooper NR, Eikelenboom P, Emmerling M, Fiebich BL, Finch CE, Frautschy S, Griffin WS, Hampel H, Hull M, Landreth G, Lue L, Mrak R, Mackenzie IR, McGeer PL, O'Banion MK, Pachter J, Pasinetti G, Plata-Salaman C, Rogers J, Rydel R, Shen Y, Streit W, Strohmeyer R, Tooyoma I, Van Muiswinkel FL, Veerhuis R, Walker D, Webster S, Wegrzyniak B, Wenk G, Wyss-Coray T. Inflammation and Alzheimer's disease. Neurobiology of aging. 2000;21(3):383-421. PubMed PMID: 10858586; PMCID: 3887148.
209. Mantovani A, Sica A, Sozzani S, Allavena P, Vecchi A, Locati M. The chemokine system in diverse forms of macrophage activation and polarization.

Trends in immunology. 2004;25(12):677-86. doi: 10.1016/j.it.2004.09.015. PubMed PMID: 15530839.
210. Edwards JP, Zhang X, Frauwirth KA, Mosser DM. Biochemical and functional characterization of three activated macrophage populations. Journal of leukocyte biology. 2006;80(6):1298-307. doi: 10.1189/jlb.0406249. PubMed PMID: 16905575; PMCID: 2642590.
211. Sternberg EM. Neural regulation of innate immunity: a coordinated nonspecific host response to pathogens. Nature reviews Immunology. 2006;6(4):318-28. doi: 10.1038/nri1810. PubMed PMID: 16557263; PMCID: 1783839.
212. Taylor JM, Minter MR, Newman AG, Zhang M, Adlard PA, Crack PJ. Type-1 interferon signaling mediates neuro-inflammatory events in models of Alzheimer's disease. Neurobiology of aging. 2014;35(5):1012-23. doi: 10.1016/j.neurobiolaging.2013.10.089. PubMed PMID: 24262201.
213. Benveniste EN, Benos DJ. TNF-alpha- and IFN-gamma-mediated signal transduction pathways: effects on glial cell gene expression and function. FASEB journal : official publication of the Federation of American Societies for Experimental Biology. 1995;9(15):1577-84. PubMed PMID: 8529837.
214. Browne TC, McQuillan K, McManus RM, O'Reilly JA, Mills KH, Lynch MA. IFN-gamma Production by amyloid beta-specific Th1 cells promotes microglial activation and increases plaque burden in a mouse model of Alzheimer's disease. Journal of immunology. 2013;190(5):2241-51. doi: 10.4049/jimmunol.1200947. PubMed PMID: 23365075.
215. Chakrabarty P, Ceballos-Diaz C, Beccard A, Janus C, Dickson D, Golde TE, Das P. IFN-gamma promotes complement expression and attenuates amyloid plaque deposition in amyloid beta precursor protein transgenic mice. Journal of immunology. 2010;184(9):5333-43. doi: 10.4049/jimmunol.0903382. PubMed PMID: 20368278; PMCID: 3798002.
216. Chakrabarty P, Herring A, Ceballos-Diaz C, Das P, Golde TE. Hippocampal expression of murine TNFalpha results in attenuation of amyloid deposition in vivo. Molecular neurodegeneration. 2011;6:16. doi: 10.1186/1750-1326-6-16. PubMed PMID: 21324189; PMCID: 3050766.
217. DiCarlo G, Wilcock D, Henderson D, Gordon M, Morgan D. Intrahippocampal LPS injections reduce Abeta load in APP+PS1 transgenic mice. Neurobiology of aging. 2001;22(6):1007-12. PubMed PMID: 11755009.
218. Gordon MN, Schreier WA, Ou X, Holcomb LA, Morgan DG. Exaggerated astrocyte reactivity after nigrostriatal deafferentation in the aged rat. The Journal of comparative neurology. 1997;388(1):106-19. PubMed PMID: 9364241.
219. Livak KJ, Schmittgen TD. Analysis of relative gene expression data using real-time quantitative PCR and the 2(-Delta Delta C(T)) Method. Methods. 2001;25(4):402-8. doi: 10.1006/meth.2001.1262. PubMed PMID: 11846609.
220. Gordon MN, Holcomb LA, Jantzen PT, DiCarlo G, Wilcock D, Boyett KW, Connor K, Melachrino J, O'Callaghan JP, Morgan D. Time course of the development of Alzheimer-like pathology in the doubly transgenic PS1+APP mouse. Experimental neurology. 2002;173(2):183-95. doi: 10.1006/exnr.2001.7754. PubMed PMID: 11822882.

221. Ishizuka EK, Ferreira MJ, Grund LZ, Coutinho EM, Komegae EN, Cassado AA, Bortoluci KR, Lopes-Ferreira M, Lima C. Role of interplay between IL-4 and IFN-gamma in the in regulating M1 macrophage polarization induced by Nattectin. International immunopharmacology. 2012;14(4):513-22. doi: 10.1016/j.intimp.2012.08.009. PubMed PMID: 22940186.
222. Riquelme P, Tomiuk S, Kammler A, Fandrich F, Schlitt HJ, Geissler EK, Hutchinson JA. IFN-gamma-induced iNOS expression in mouse regulatory macrophages prolongs allograft survival in fully immunocompetent recipients. Molecular therapy : the journal of the American Society of Gene Therapy. 2013;21(2):409-22. doi: 10.1038/mt.2012.168. PubMed PMID: 22929659; PMCID: 3594012.
223. Frenkel D, Puckett L, Petrovic S, Xia W, Chen G, Vega J, Dembinsky-Vaknin A, Shen J, Plante M, Burt DS, Weiner HL. A nasal proteosome adjuvant activates microglia and prevents amyloid deposition. Annals of neurology. 2008;63(5):591-601. doi: 10.1002/ana.21340. PubMed PMID: 18360829; PMCID: 2747093.
224. Gonzalez-Scarano F, Baltuch G. Microglia as mediators of inflammatory and degenerative diseases. Annual review of neuroscience. 1999;22:219-40. doi: 10.1146/annurev.neuro.22.1.219. PubMed PMID: 10202538.
225. Lee JW, Lee YK, Yuk DY, Choi DY, Ban SB, Oh KW, Hong JT. Neuro-inflammation induced by lipopolysaccharide causes cognitive impairment through enhancement of beta-amyloid generation. Journal of neuroinflammation. 2008;5:37. doi: 10.1186/1742-2094-5-37. PubMed PMID: 18759972; PMCID: 2556656.
226. Mudd SH, Finkelstein JD, Irreverre F, Laster L. Homocystinuria: An Enzymatic Defect. Science. 1964;143(3613):1443-5. PubMed PMID: 14107447.
227. Rozen R. Genetic predisposition to hyperhomocysteinemia: deficiency of methylenetetrahydrofolate reductase (MTHFR). Thromb Haemost. 1997;78(1):523-6. PubMed PMID: 9198208.
228. Selhub J, Jacques PF, Wilson PW, Rush D, Rosenberg IH. Vitamin status and intake as primary determinants of homocysteinemia in an elderly population. JAMA. 1993;270(22):2693-8. PubMed PMID: 8133587.
229. Lentz SR, Erger RA, Dayal S, Maeda N, Malinow MR, Heistad DD, Faraci FM. Folate dependence of hyperhomocysteinemia and vascular dysfunction in cystathionine beta-synthase-deficient mice. Am J Physiol Heart Circ Physiol. 2000;279(3):H970-5. PubMed PMID: 10993757.
230. Van Dam F, Van Gool WA. Hyperhomocysteinemia and Alzheimer's disease: A systematic review. Arch Gerontol Geriatr. 2009;48(3):425-30. doi: 10.1016/j.archger.2008.03.009. PubMed PMID: 18479766.
231. Blasi E, Barluzzi R, Bocchini V, Mazzolla R, Bistoni F. Immortalization of murine microglial cells by a v-raf/v-myc carrying retrovirus. J Neuroimmunol. 1990;27(2-3):229-37. PubMed PMID: 2110186.
232. Olmsted JB, Witman GB, Carlson K, Rosenbaum JL. Comparison of the microtubule proteins of neuroblastoma cells, brain, and Chlamydomonas flagella. Proceedings of the National Academy of Sciences of the United States of America. 1971;68(9):2273-7. PubMed PMID: 5289385; PMCID: PMC389399.

233. Rosenberg GA. Inflammation and white matter damage in vascular cognitive impairment. Stroke; a journal of cerebral circulation. 2009;40(3 Suppl):S20-3. doi: 10.1161/STROKEAHA.108.533133. PubMed PMID: 19064797; PMCID: PMC2811584.
234. Dong Y, Benveniste EN. Immune function of astrocytes. Glia. 2001;36(2):180-90. PubMed PMID: 11596126.
235. Hanisch UK. Microglia as a source and target of cytokines. Glia. 2002;40(2):140-55. doi: 10.1002/glia.10161. PubMed PMID: 12379902.
236. Butt AM, Kalsi A. Inwardly rectifying potassium channels (Kir) in central nervous system glia: a special role for Kir4.1 in glial functions. J Cell Mol Med. 2006;10(1):33-44. PubMed PMID: 16563220; PMCID: PMC3933100.
237. Price DL, Ludwig JW, Mi H, Schwarz TL, Ellisman MH. Distribution of rSlo Ca2+-activated K+ channels in rat astrocyte perivascular endfeet. Brain research. 2002;956(2):183-93. PubMed PMID: 12445685.
238. Simard M, Nedergaard M. The neurobiology of glia in the context of water and ion homeostasis. Neuroscience. 2004;129(4):877-96. doi: 10.1016/j.neuroscience.2004.09.053. PubMed PMID: 15561405.
239. Alzheimer's A. 2015 Alzheimer's disease facts and figures. Alzheimer's & dementia : the journal of the Alzheimer's Association. 2015;11(3):332-84. PubMed PMID: 25984581.
240. Gorelick PB, Scuteri A, Black SE, Decarli C, Greenberg SM, Iadecola C, Launer LJ, Laurent S, Lopez OL, Nyenhuis D, Petersen RC, Schneider JA, Tzourio C, Arnett DK, Bennett DA, Chui HC, Higashida RT, Lindquist R, Nilsson PM, Roman GC, Sellke FW, Seshadri S, American Heart Association Stroke Council CoE, Prevention CoCNCoCR, Intervention, Council on Cardiovascular S, Anesthesia. Vascular contributions to cognitive impairment and dementia: a statement for healthcare professionals from the american heart association/american stroke association. Stroke; a journal of cerebral circulation. 2011;42(9):2672-713. doi: 10.1161/STR.0b013e3182299496. PubMed PMID: 21778438; PMCID: PMC3778669.
241. Snyder HM, Corriveau RA, Craft S, Faber JE, Greenberg SM, Knopman D, Lamb BT, Montine TJ, Nedergaard M, Schaffer CB, Schneider JA, Wellington C, Wilcock DM, Zipfel GJ, Zlokovic B, Bain LJ, Bosetti F, Galis ZS, Koroshetz W, Carrillo MC. Vascular contributions to cognitive impairment and dementia including Alzheimer's disease. Alzheimer's & dementia : the journal of the Alzheimer's Association. 2015;11(6):710-7. doi: 10.1016/j.jalz.2014.10.008. PubMed PMID: 25510382; PMCID: PMC4731036.
242. Bacskai BJ, Kajdasz ST, Christie RH, Carter C, Games D, Seubert P, Schenk D, Hyman BT. Imaging of amyloid-beta deposits in brains of living mice permits direct observation of clearance of plaques with immunotherapy. Nature medicine. 2001;7(3):369-72. doi: 10.1038/85525. PubMed PMID: 11231639.
243. Wilcock DM, Rojiani A, Rosenthal A, Levkowitz G, Subbarao S, Alamed J, Wilson D, Wilson N, Freeman MJ, Gordon MN, Morgan D. Passive amyloid immunotherapy clears amyloid and transiently activates microglia in a transgenic mouse model of amyloid deposition. The Journal of neuroscience : the official

journal of the Society for Neuroscience. 2004;24(27):6144-51. doi: 10.1523/JNEUROSCI.1090-04.2004. PubMed PMID: 15240806.
244. Siemers ER, Sundell KL, Carlson C, Case M, Sethuraman G, Liu-Seifert H, Dowsett SA, Pontecorvo MJ, Dean RA, Demattos R. Phase 3 solanezumab trials: Secondary outcomes in mild Alzheimer's disease patients. Alzheimer's & dementia : the journal of the Alzheimer's Association. 2016;12(2):110-20. doi: 10.1016/j.jalz.2015.06.1893. PubMed PMID: 26238576.
245. Demattos RB, Lu J, Tang Y, Racke MM, Delong CA, Tzaferis JA, Hole JT, Forster BM, McDonnell PC, Liu F, Kinley RD, Jordan WH, Hutton ML. A plaque-specific antibody clears existing beta-amyloid plaques in Alzheimer's disease mice. Neuron. 2012;76(5):908-20. doi: 10.1016/j.neuron.2012.10.029. PubMed PMID: 23217740.
246. Gessner JE, Heiken H, Tamm A, Schmidt RE. The IgG Fc receptor family. Ann Hematol. 1998;76(6):231-48. PubMed PMID: 9692811.
247. Alamed J, Wilcock DM, Diamond DM, Gordon MN, Morgan D. Two-day radial-arm water maze learning and memory task; robust resolution of amyloid-related memory deficits in transgenic mice. Nature protocols. 2006;1(4):1671-9. doi: 10.1038/nprot.2006.275. PubMed PMID: 17487150.
248. Wilcock DM, Lewis MR, Van Nostrand WE, Davis J, Previti ML, Gharkholonarehe N, Vitek MP, Colton CA. Progression of amyloid pathology to Alzheimer's disease pathology in an amyloid precursor protein transgenic mouse model by removal of nitric oxide synthase 2. The Journal of neuroscience : the official journal of the Society for Neuroscience. 2008;28(7):1537-45. doi: 10.1523/JNEUROSCI.5066-07.2008. PubMed PMID: 18272675; PMCID: PMC2621082.
249. Wilcock DM, Gordon MN, Morgan D. Quantification of cerebral amyloid angiopathy and parenchymal amyloid plaques with Congo red histochemical stain. Nature protocols. 2006;1(3):1591-5. doi: 10.1038/nprot.2006.277. PubMed PMID: 17406451.
250. Weekman EM, Sudduth TL, Abner EL, Popa GJ, Mendenhall MD, Brothers HM, Braun K, Greenstein A, Wilcock DM. Transition from an M1 to a mixed neuroinflammatory phenotype increases amyloid deposition in APP/PS1 transgenic mice. Journal of neuroinflammation. 2014;11:127. doi: 10.1186/1742-2094-11-127. PubMed PMID: 25062954; PMCID: PMC4128532.
251. Mantovani A, Sica A, Locati M. Macrophage polarization comes of age. Immunity. 2005;23(4):344-6. doi: 10.1016/j.immuni.2005.10.001. PubMed PMID: 16226499.
252. Walker DG, Lue LF. Immune phenotypes of microglia in human neurodegenerative disease: challenges to detecting microglial polarization in human brains. Alzheimer's research & therapy. 2015;7(1):56. doi: 10.1186/s13195-015-0139-9. PubMed PMID: 26286145; PMCID: PMC4543480.
253. Sperling RA, Jack CR, Jr., Black SE, Frosch MP, Greenberg SM, Hyman BT, Scheltens P, Carrillo MC, Thies W, Bednar MM, Black RS, Brashear HR, Grundman M, Siemers ER, Feldman HH, Schindler RJ. Amyloid-related imaging abnormalities in amyloid-modifying therapeutic trials: recommendations from the Alzheimer's Association Research Roundtable Workgroup. Alzheimer's &

dementia : the journal of the Alzheimer's Association. 2011;7(4):367-85. doi: 10.1016/j.jalz.2011.05.2351. PubMed PMID: 21784348; PMCID: PMC3693547.
254. Wilcock DM, Morgan D, Gordon MN, Taylor TL, Ridnour LA, Wink DA, Colton CA. Activation of matrix metalloproteinases following anti-Abeta immunotherapy; implications for microhemorrhage occurrence. Journal of neuroinflammation. 2011;8:115. doi: 10.1186/1742-2094-8-115. PubMed PMID: 21906275; PMCID: 3182918.
255. Frackowiak J, Wisniewski HM, Wegiel J, Merz GS, Iqbal K, Wang KC. Ultrastructure of the microglia that phagocytose amyloid and the microglia that produce beta-amyloid fibrils. Acta Neuropathol. 1992;84(3):225-33. PubMed PMID: 1414275.
256. Wisniewski HM, Barcikowska M, Kida E. Phagocytosis of beta/A4 amyloid fibrils of the neuritic neocortical plaques. Acta Neuropathol. 1991;81(5):588-90. PubMed PMID: 1858487.
257. Chakrabarty P, Tianbai L, Herring A, Ceballos-Diaz C, Das P, Golde TE. Hippocampal expression of murine IL-4 results in exacerbation of amyloid deposition. Molecular neurodegeneration. 2012;7:36. doi: 10.1186/1750-1326-7-36. PubMed PMID: 22838967; PMCID: PMC3441281.
258. Chakrabarty P, Li A, Ceballos-Diaz C, Eddy JA, Funk CC, Moore B, DiNunno N, Rosario AM, Cruz PE, Verbeeck C, Sacino A, Nix S, Janus C, Price ND, Das P, Golde TE. IL-10 alters immunoproteostasis in APP mice, increasing plaque burden and worsening cognitive behavior. Neuron. 2015;85(3):519-33. doi: 10.1016/j.neuron.2014.11.020. PubMed PMID: 25619653; PMCID: PMC4320003.
259. Hernandez-Guillamon M, Martinez-Saez E, Delgado P, Domingues-Montanari S, Boada C, Penalba A, Boada M, Pagola J, Maisterra O, Rodriguez-Luna D, Molina CA, Rovira A, Alvarez-Sabin J, Ortega-Aznar A, Montaner J. MMP-2/MMP-9 plasma level and brain expression in cerebral amyloid angiopathy-associated hemorrhagic stroke. Brain pathology. 2012;22(2):133-41. doi: 10.1111/j.1750-3639.2011.00512.x. PubMed PMID: 21707819.
260. Greenberg SM, Vonsattel JP. Diagnosis of cerebral amyloid angiopathy. Sensitivity and specificity of cortical biopsy. Stroke; a journal of cerebral circulation. 1997;28(7):1418-22. PubMed PMID: 9227694.
261. Hartz AM, Bauer B, Soldner EL, Wolf A, Boy S, Backhaus R, Mihaljevic I, Bogdahn U, Klunemann HH, Schuierer G, Schlachetzki F. Amyloid-beta contributes to blood-brain barrier leakage in transgenic human amyloid precursor protein mice and in humans with cerebral amyloid angiopathy. Stroke; a journal of cerebral circulation. 2012;43(2):514-23. doi: 10.1161/STROKEAHA.111.627562. PubMed PMID: 22116809.
262. Gonzalez-Velasquez FJ, Kotarek JA, Moss MA. Soluble aggregates of the amyloid-beta protein selectively stimulate permeability in human brain microvascular endothelial monolayers. J Neurochem. 2008;107(2):466-77. doi: 10.1111/j.1471-4159.2008.05618.x. PubMed PMID: 18702666; PMCID: PMC4406342.
263. Carrano A, Hoozemans JJ, van der Vies SM, Rozemuller AJ, van Horssen J, de Vries HE. Amyloid Beta induces oxidative stress-mediated blood-brain

barrier changes in capillary amyloid angiopathy. Antioxid Redox Signal. 2011;15(5):1167-78. doi: 10.1089/ars.2011.3895. PubMed PMID: 21294650.
264. Joosten E, van den Berg A, Riezler R, Naurath HJ, Lindenbaum J, Stabler SP, Allen RH. Metabolic evidence that deficiencies of vitamin B-12 (cobalamin), folate, and vitamin B-6 occur commonly in elderly people. Am J Clin Nutr. 1993;58(4):468-76. PubMed PMID: 8037789.
265. Pennypacker LC, Allen RH, Kelly JP, Matthews LM, Grigsby J, Kaye K, Lindenbaum J, Stabler SP. High prevalence of cobalamin deficiency in elderly outpatients. Journal of the American Geriatrics Society. 1992;40(12):1197-204. PubMed PMID: 1447433.
266. Wald DS, Kasturiratne A, Simmonds M. Effect of folic acid, with or without other B vitamins, on cognitive decline: meta-analysis of randomized trials. Am J Med. 2010;123(6):522-7 e2. doi: 10.1016/j.amjmed.2010.01.017. PubMed PMID: 20569758.
267. Durga J, van Boxtel MP, Schouten EG, Kok FJ, Jolles J, Katan MB, Verhoef P. Effect of 3-year folic acid supplementation on cognitive function in older adults in the FACIT trial: a randomised, double blind, controlled trial. Lancet. 2007;369(9557):208-16. doi: 10.1016/S0140-6736(07)60109-3. PubMed PMID: 17240287.
268. Smith AD, Smith SM, de Jager CA, Whitbread P, Johnston C, Agacinski G, Oulhaj A, Bradley KM, Jacoby R, Refsum H. Homocysteine-lowering by B vitamins slows the rate of accelerated brain atrophy in mild cognitive impairment: a randomized controlled trial. PloS one. 2010;5(9):e12244. doi: 10.1371/journal.pone.0012244. PubMed PMID: 20838622; PMCID: PMC2935890.
269. de Jager CA, Oulhaj A, Jacoby R, Refsum H, Smith AD. Cognitive and clinical outcomes of homocysteine-lowering B-vitamin treatment in mild cognitive impairment: a randomized controlled trial. Int J Geriatr Psychiatry. 2012;27(6):592-600. doi: 10.1002/gps.2758. PubMed PMID: 21780182.
270. Mishiro K, Ishiguro M, Suzuki Y, Tsuruma K, Shimazawa M, Hara H. A broad-spectrum matrix metalloproteinase inhibitor prevents hemorrhagic complications induced by tissue plasminogen activator in mice. Neuroscience. 2012;205:39-48. doi: 10.1016/j.neuroscience.2011.12.042. PubMed PMID: 22244977.
271. Chen W, Hartman R, Ayer R, Marcantonio S, Kamper J, Tang J, Zhang JH. Matrix metalloproteinases inhibition provides neuroprotection against hypoxia-ischemia in the developing brain. Journal of neurochemistry. 2009;111(3):726-36. doi: 10.1111/j.1471-4159.2009.06362.x. PubMed PMID: 19712057.
272. Cui J, Chen S, Zhang C, Meng F, Wu W, Hu R, Hadass O, Lehmidi T, Blair GJ, Lee M, Chang M, Mobashery S, Sun GY, Gu Z. Inhibition of MMP-9 by a selective gelatinase inhibitor protects neurovasculature from embolic focal cerebral ischemia. Molecular neurodegeneration. 2012;7:21. doi: 10.1186/1750-1326-7-21. PubMed PMID: 22587708; PMCID: PMC3500265.
273. Guo Z, Sun X, He Z, Jiang Y, Zhang X, Zhang JH. Matrix metalloproteinase-9 potentiates early brain injury after subarachnoid

hemorrhage. Neurol Res. 2010;32(7):715-20. doi: 10.1179/016164109X12478302362491. PubMed PMID: 19703360.
274. Yu F, Kamada H, Niizuma K, Endo H, Chan PH. Induction of mmp-9 expression and endothelial injury by oxidative stress after spinal cord injury. J Neurotrauma. 2008;25(3):184-95. doi: 10.1089/neu.2007.0438. PubMed PMID: 18352832; PMCID: PMC2365489.
275. Switzer JA, Hess DC, Ergul A, Waller JL, Machado LS, Portik-Dobos V, Pettigrew LC, Clark WM, Fagan SC. Matrix metalloproteinase-9 in an exploratory trial of intravenous minocycline for acute ischemic stroke. Stroke; a journal of cerebral circulation. 2011;42(9):2633-5. doi: 10.1161/STROKEAHA.111.618215. PubMed PMID: 21737808; PMCID: PMC3181080.
276. Lee SR, Kim HY, Rogowska J, Zhao BQ, Bhide P, Parent JM, Lo EH. Involvement of matrix metalloproteinase in neuroblast cell migration from the subventricular zone after stroke. The Journal of neuroscience : the official journal of the Society for Neuroscience. 2006;26(13):3491-5. doi: 10.1523/JNEUROSCI.4085-05.2006. PubMed PMID: 16571756.
277. Guerreiro R, Wojtas A, Bras J, Carrasquillo M, Rogaeva E, Majounie E, Cruchaga C, Sassi C, Kauwe JS, Younkin S, Hazrati L, Collinge J, Pocock J, Lashley T, Williams J, Lambert JC, Amouyel P, Goate A, Rademakers R, Morgan K, Powell J, St George-Hyslop P, Singleton A, Hardy J, Alzheimer Genetic Analysis G. TREM2 variants in Alzheimer's disease. The New England journal of medicine. 2013;368(2):117-27. doi: 10.1056/NEJMoa1211851. PubMed PMID: 23150934; PMCID: PMC3631573.
278. Jonsson T, Stefansson H, Steinberg S, Jonsdottir I, Jonsson PV, Snaedal J, Bjornsson S, Huttenlocher J, Levey AI, Lah JJ, Rujescu D, Hampel H, Giegling I, Andreassen OA, Engedal K, Ulstein I, Djurovic S, Ibrahim-Verbaas C, Hofman A, Ikram MA, van Duijn CM, Thorsteinsdottir U, Kong A, Stefansson K. Variant of TREM2 associated with the risk of Alzheimer's disease. The New England journal of medicine. 2013;368(2):107-16. doi: 10.1056/NEJMoa1211103. PubMed PMID: 23150908; PMCID: PMC3677583.
279. Hamerman JA, Jarjoura JR, Humphrey MB, Nakamura MC, Seaman WE, Lanier LL. Cutting edge: inhibition of TLR and FcR responses in macrophages by triggering receptor expressed on myeloid cells (TREM)-2 and DAP12. Journal of immunology. 2006;177(4):2051-5. PubMed PMID: 16887962.
280. Kleinberger G, Yamanishi Y, Suarez-Calvet M, Czirr E, Lohmann E, Cuyvers E, Struyfs H, Pettkus N, Wenninger-Weinzierl A, Mazaheri F, Tahirovic S, Lleo A, Alcolea D, Fortea J, Willem M, Lammich S, Molinuevo JL, Sanchez-Valle R, Antonell A, Ramirez A, Heneka MT, Sleegers K, van der Zee J, Martin JJ, Engelborghs S, Demirtas-Tatlidede A, Zetterberg H, Van Broeckhoven C, Gurvit H, Wyss-Coray T, Hardy J, Colonna M, Haass C. TREM2 mutations implicated in neurodegeneration impair cell surface transport and phagocytosis. Sci Transl Med. 2014;6(243):243ra86. doi: 10.1126/scitranslmed.3009093. PubMed PMID: 24990881.
281. Otero K, Shinohara M, Zhao H, Cella M, Gilfillan S, Colucci A, Faccio R, Ross FP, Teitelbaum SL, Takayanagi H, Colonna M. TREM2 and beta-catenin regulate bone homeostasis by controlling the rate of osteoclastogenesis. Journal

of immunology. 2012;188(6):2612-21. doi: 10.4049/jimmunol.1102836. PubMed PMID: 22312126; PMCID: PMC3732181.
282. Takahashi K, Rochford CD, Neumann H. Clearance of apoptotic neurons without inflammation by microglial triggering receptor expressed on myeloid cells-2. The Journal of experimental medicine. 2005;201(4):647-57. doi: 10.1084/jem.20041611. PubMed PMID: 15728241; PMCID: PMC2213053.
283. Wang Y, Cella M, Mallinson K, Ulrich JD, Young KL, Robinette ML, Gilfillan S, Krishnan GM, Sudhakar S, Zinselmeyer BH, Holtzman DM, Cirrito JR, Colonna M. TREM2 lipid sensing sustains the microglial response in an Alzheimer's disease model. Cell. 2015;160(6):1061-71. doi: 10.1016/j.cell.2015.01.049. PubMed PMID: 25728668; PMCID: PMC4477963.
284. Wu K, Byers DE, Jin X, Agapov E, Alexander-Brett J, Patel AC, Cella M, Gilfilan S, Colonna M, Kober DL, Brett TJ, Holtzman MJ. TREM-2 promotes macrophage survival and lung disease after respiratory viral infection. The Journal of experimental medicine. 2015;212(5):681-97. doi: 10.1084/jem.20141732. PubMed PMID: 25897174; PMCID: PMC4419356.
285. N'Diaye EN, Branda CS, Branda SS, Nevarez L, Colonna M, Lowell C, Hamerman JA, Seaman WE. TREM-2 (triggering receptor expressed on myeloid cells 2) is a phagocytic receptor for bacteria. J Cell Biol. 2009;184(2):215-23. doi: 10.1083/jcb.200808080. PubMed PMID: 19171755; PMCID: PMC2654305.
286. Frank S, Burbach GJ, Bonin M, Walter M, Streit W, Bechmann I, Deller T. TREM2 is upregulated in amyloid plaque-associated microglia in aged APP23 transgenic mice. Glia. 2008;56(13):1438-47. doi: 10.1002/glia.20710. PubMed PMID: 18551625.
287. Ulrich JD, Finn MB, Wang Y, Shen A, Mahan TE, Jiang H, Stewart FR, Piccio L, Colonna M, Holtzman DM. Altered microglial response to Abeta plaques in APPPS1-21 mice heterozygous for TREM2. Molecular neurodegeneration. 2014;9:20. doi: 10.1186/1750-1326-9-20. PubMed PMID: 24893973; PMCID: PMC4049806.
288. Jay TR, Miller CM, Cheng PJ, Graham LC, Bemiller S, Broihier ML, Xu G, Margevicius D, Karlo JC, Sousa GL, Cotleur AC, Butovsky O, Bekris L, Staugaitis SM, Leverenz JB, Pimplikar SW, Landreth GE, Howell GR, Ransohoff RM, Lamb BT. TREM2 deficiency eliminates TREM2+ inflammatory macrophages and ameliorates pathology in Alzheimer's disease mouse models. The Journal of experimental medicine. 2015;212(3):287-95. doi: 10.1084/jem.20142322. PubMed PMID: 25732305; PMCID: PMC4354365.
289. Beckmann N, Doelemeyer A, Zurbruegg S, Bigot K, Theil D, Frieauff W, Kolly C, Moulin P, Neddermann D, Kreutzer R, Perrot L, Brzak I, Jacobson LH, Staufenbiel M, Neumann U, Shimshek DR. Longitudinal noninvasive magnetic resonance imaging of brain microhemorrhages in BACE inhibitor-treated APP transgenic mice. Neurobiology of aging. 2016;45:50-60. doi: 10.1016/j.neurobiolaging.2016.05.009. PubMed PMID: 27459925.
290. Aisen PS, Schmeidler J, Pasinetti GM. Randomized pilot study of nimesulide treatment in Alzheimer's disease. Neurology. 2002;58(7):1050-4. PubMed PMID: 11940691.

291. Group AR, Lyketsos CG, Breitner JC, Green RC, Martin BK, Meinert C, Piantadosi S, Sabbagh M. Naproxen and celecoxib do not prevent AD in early results from a randomized controlled trial. Neurology. 2007;68(21):1800-8. doi: 10.1212/01.wnl.0000260269.93245.d2. PubMed PMID: 17460158.
292. Van Gool WA, Weinstein HC, Scheltens P, Walstra GJ. Effect of hydroxychloroquine on progression of dementia in early Alzheimer's disease: an 18-month randomised, double-blind, placebo-controlled study. Lancet. 2001;358(9280):455-60. PubMed PMID: 11513909.
293. Sudduth TL, Weekman EM, Price BR, Gooch JL, Woolums A, Norris CM, Wilcock DM. Time-course of glial changes in the hyperhomocysteinemia model of vascular cognitive impairment and dementia (VCID). Neuroscience. 2017;341:42-51. doi: 10.1016/j.neuroscience.2016.11.024. PubMed PMID: 27890830.
294. Wilcock DM, Vitek MP, Colton CA. Vascular amyloid alters astrocytic water and potassium channels in mouse models and humans with Alzheimer's disease. Neuroscience. 2009;159(3):1055-69. doi: 10.1016/j.neuroscience.2009.01.023. PubMed PMID: 19356689; PMCID: PMC2699894.

Vita
Erica Marie Weekman

Educational Institutions

University of Kentucky, Lexington, KY 2008-2012
Bachelor of Science in Biology
Magna Cum Laude
Minor in Anthropology

Research and Professional Experience

Graduate Student, University of Kentucky 2013-2017
Mentor: Donna Wilcock, Ph.D.

Undergraduate Research Assistant, University of Kentucky 2011-2012
Mentor: Karyn Esser, Ph.D.

Scholastic and Professional Honors

NRSA F31 Fellowship 2015-2017
B.Sc. Magna Cum Laude, University of Kentucky 2012
Physiology Scholars Program Travel Award 2012
Physiology Scholars Program 2012
Presidential Scholarship, University of Kentucky 2008-2012

Peer Reviewed Publications

Weekman, E., Woolums, A., Sudduth, T., Wilcock, D. Hyperhomocysteinemia induced gene expression changes in astrocytes, microglia, endothelial cells and neurons. 2017, In preparation

Sudduth, T., **Weekman, E.,** Gooch, J., Woolums, A., Norris, C., Wilcock, D. Neurovascular astrocyte degeneration in the hyperhomocysteinemia model of vascular cognitive impairment and dementia (VCID). Neuroscience. 2017. Jan 26;341:42-51. DOI: 10.1016/j.neuroscience.2016.11.024. PMID: 27890830.

Weekman, E., Sudduth, T., Caverly, C., Kopper, T., Phillips, O., Powell, D., Wilcock, D. Reduced efficacy of anti-Aβ immunotherapy in a mouse model of amyloid deposition and vascular cognitive impairment co-morbidity. Journal of Neuroscience. 2016 Sep 21;36(38):9896-907. DOI: 10.1523/JNEUROSCI.1762-16.2016. PMID: 27656027.

Hainsworth, A., Yeo, N., **Weekman, E.,** Wilcock, D. Homocysteine, hyperhomocysteinemia and vascular contributions to cognitive impairment and dementia (VCID). Biochim Biophys Acta. 2015, PMID: 26689889

Weekman, E., and Wilcock, D. Matrix metalloproteinase in blood brain barrier breakdown and dementia. Journal of Alzheimer's Disease. 2015, 49(4). DOI: 10.3233/JAD-150759. PMID: 26599057

Latta, CH., Sudduth, T., **Weekman, E.,** Brothers, H., Abner, E., Popa, G., Mendenhall, M., Gonzalez-Oregon, F., Braun, K., and Wilcock D. Determining the role of IL-4 induced neuroinflammation in microglial activity and amyloid-β using BV2 microglial cells and APP/PS1 transgenic mice. Journal of Neuroinflammation. 2015, 12:41. DOI: 10.1186/s12974-015-0243-6. PMID: 25885682

Weekman, E., Sudduth, T., Abner, E., Popa, G., Mendenhall, M., Brothers, H., Braun, K., Greenstein, A., and Wilcock, D. Transition from an M1 to a mixed neuroinflammatory phenotype increases amyloid deposition in APP/PS1 transgenic mice. Journal of Neuroinflammation. 2014, 11:127 DOI: 10.1186/1742-2094-11-127. PMID: 25062954

Sudduth, T., **Weekman, E.**, Brothers, H., Braun, K., and Wilcock, D. Beta-amyloid deposition is shifted to the vasculature and memory impairment is exacerbated when hyperhomocysteinemia is induced in APP/PS1 transgenic mice. Alzheimer's Research and Therapy. 2014, 6(3):32. DOI: 10.1186/alzrt262. PMID: 24991237

Abstracts

Weekman, E., Sudduth, T., Phillips, O., Powell, D., Wilcock. D. 2016. Cerebrovascular consequences of an anti-Aβ immunotherapy in a co-morbidity mouse model. Abstract for poster and oral presentation at the 2016 VasCog Conference (Amsterdam, The Netherlands) and the 2016 Society for Neuroscience Conference (San Diego, CA), respectively. ***Presented by E. Weekman***

Weekman, E., Caverly, C., Kopper, T., Sudduth, T., Wilcock, D. 2015. Reduced efficacy of anti-Aβ immunotherapy in a mouse model of amyloid deposition and vascular cognitive impairment co-morbidity. Abstract for oral presentation at the Alzheimer's Association International Conference (Washington, DC) and the Society for Neuroscience Conference (Chicago, IL). ***Presented by E. Weekman***

Brothers. H., Phillips. O., Latta. C., Sudduth. T., Braun. K., **Weekman. E.**, Wilcock. D. 2015. Amyloid and tau accumulations combined with chronic cerebrovascular hypoperfusion model the unique progression of impairment and

pathology in mixed dementia. Abstract for poster presentation at Alzheimer's disease/Parkinson's disease Conference, Nice, France. *Presented by H. Brothers*

Weekman. E., Sudduth. T., Wilcock. D., 2015. Anti-amyloid immunotherapy results in exacerbation of cerebrovascular disease through activation of matrix metalloproteinases. Abstract for poster presentation at the International Stroke Conference, Nashville, TN. ***Presented by E. Weekman***

Weekman. E., Sudduth. T., Brothers. H., Braun. K., Wilcock. D., 2014. Modeling the co-morbidity of vascular dementia and amyloid pathology of Alzheimer's disease. Abstract for poster presentation at Society for Neuroscience, Washington, D.C. ***Presented by E. Weekman***

Brothers, H., Latta, C., Sudduth, T., Braun, K., **Weekman, E.**, Wilcock, D., 2014. Cerebrovascular and Alzheimer's pathologies in mouse models of mixed dementia. Abstract for nanosymposium at Society for Neuroscience, Washington, D.C. *Presented by H. Brothers*

Latta, C., Sudduth, T., **Weekman, E.**, Brothers, H., Gonzalez-Oregon, F., Braun, K., Wilcock, D. 2014. Determining the role of an M2a phenotype on microglial activity and amyloid deposition using BV2 microglial cells and APP/PS1 transgenic mice. Abstract for poster presentation at ApoE, ApoE Receptors and Neurodegeneration Symposium, Lexington, KY. *Presented by C. Latta*

Brothers, H., Latta, C., Sudduth, T., **Weekman, E.**, Braun, K., Wilcock, D. 2014. Chronic hypoperfusion, Alzheimer's pathology and dementia. Abstract for poster presentation at ApoE, ApoE Receptors and Neurodegeneration Symposium, Lexington, KY. *Presented by H. Brothers*

Brothers, H., Sudduth, T., **Weekman, E.**, Braun, K., Latta, C., Wilcock, D. 2013. Developing models to study the impact of cerebrovascular disease on Alzheimer's pathology. Abstract for poster presentation at Markesbery Symposium on Aging, Lexington, KY. *Presented by H. Brothers*

Weekman, E., Sudduth, T., Greenstein, A., and Wilcock, D. 2013. Determining the effects of neuroinflammatory phenotypes on amyloid deposition in APP/PS1 transgenic mice. Abstract for poster presentation, Society for Neuroscience, San Diego, CA. ***Presented by E. Weekman***

Weekman, E., Zhang, X., and Esser, K. 2012. Comparison of clock gene expression across skeletal muscles of different origins and functions. Abstract for poster presentation, Experimental Biology, San Diego, CA. ***Presented by E. Weekman***